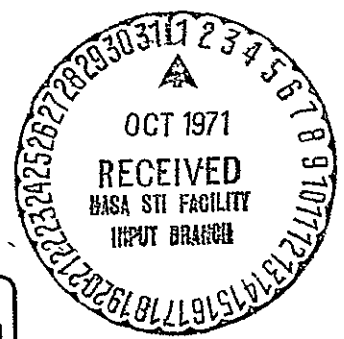
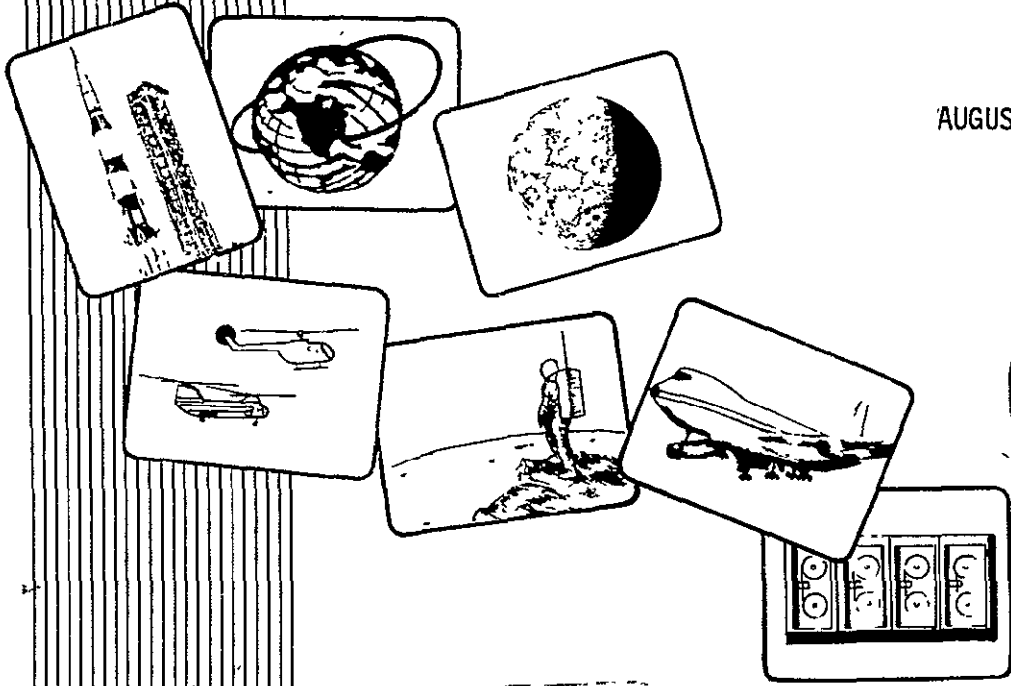


D2-118406-1

APOLLO OXYGEN TANK STRATIFICATION ANALYSIS
FINAL REPORT

VOLUME I OF II

AUGUST 31, 1971



FACILITY FORM 602

N71-36248
(ACCESSION NUMBER)

106

CR-115743
(NASA CR OR TMX OR AD NUMBER)

(THRU) NOV 63

(CODE) 31

(CATEGORY)

THE **BOEING** COMPANY
HOUSTON, TEXAS

Reproduced by
**NATIONAL TECHNICAL
INFORMATION SERVICE**
Springfield, Va 22151

CR-115143

DOCUMENT NO. D2-118406-1

TITLE APOLLO OXYGEN TANK STRATIFICATION ANALYSIS
FINAL REPORT
VOLUME I OF II
CONTRACT NO. NAS9-11576

Prepared by:
Propulsion and Power Systems
5-2940

Prepared for:
National Aeronautics and Space Administration
Manned Spacecraft Center
Houston, Texas

August 31, 1971

Prepared by: J. E. Barton
H. W. Patterson
D. D. Rule

Approved by: 
 R. K. Nuno (5-2940)
Program Manager

REVISIONS

REV. SYM	DESCRIPTION	DATE	APPROVED

ABSTRACT

An analysis of the Apollo oxygen tank stratified performance in the Apollo low "g" flight environment was conducted and the capability of the tank to satisfy mission requirements evaluated. The analysis used a stratification model which was available when the program was initiated November 1, 1970. The model solves the compressible viscous flow equations in a two dimensional region representing the interior of the tank. Model improvements made to improve the accuracy and efficiency of performance simulations are described. Conditions analyzed included attitude hold and passive thermal control flight modes and a range of tank quantities and flow rates. The analysis of one period investigated included the effects of fluid rotations caused by a change in the vehicle rotation rate. The tank performance and model accuracy were evaluated by comparing simulated tank pressure and heater temperature with observed data. The tank performance was found to be adequate for known mission requirements. The model accurately simulated tank performance for all conditions with the exception of the fluid rotations which were three dimensional and could not be adequately modeled.

KEY WORDS

Apollo
Convection
Cryogenic
Heat Transfer
Heater Cycles
Heater Temperatures
Oxygen
Pressure Decay
Pressurization
Radiation
Stratification
Thermodynamics

ACKNOWLEDGEMENTS

The stratification model used for the oxygen tank analysis was developed by Mr. C. K. Forester, Boeing - Seattle. He also analyzed the fluid rotations in the tank and made other major contributions to the program which were sincerely appreciated. The able assistance of Mr. J. B. Urquhart, Boeing-Huntsville, is also acknowledged for his analysis of transient fluid rotations in the tank which were used to check out the numerical model.

Special thanks are extended to Mr. R. R. Rice, NASA-MSD, for his many useful suggestions and help in acquiring and interpreting the flight data necessary for the analysis.

TABLE OF CONTENTS

Paragraph		Page
	Revisions	i
	Abstract	ii
	Key Words	ii
	Acknowledgements	iii
	Table of Contents	iv
	Illustrations	v
	Tables	vii
	Nomenclature	viii
	References	ix
SECTION 1		
1.0	Introduction	1-1
1.1	Purpose	1-1
1.2	Background	1-1
1.3	Scope	1-1
SECTION 2		
2.0	Summary	2-1
SECTION 3		
3.0	Program Tasks	3-1
3.1	Task 1 - Math Model Improvement	3-1
3.1.1	Variable Grid	3-1
3.1.2	Improved Computing Efficiency	3-2
3.1.3	Simulation Results	3-2
3.2	Task 2 - Apollo 12 GET 197-209	3-9
3.2.1	Simulation Results	3-9
3.3	Task 3 - Apollo 14 Predictions and Analysis	3-14
3.3.1	Preflight Predictions	3-14
3.3.2	Math Model Conversion	3-24
3.3.3	Apollo 14 Postflight Analysis	3-27
3.4	Task 4 - Fluid Rotation Analysis	3-53
3.4.1	Model Description	3-53
3.4.2	Rotation Effects Simulation	3-54
SECTION 4		
4.0	Conclusions	4-1
4.1	Recommendations	4-1
APPENDIX		
A	Stratification Math Model	A-1
B	Heater Temperature Correlations	B-1
C	Spin Transients for a Fluid in Thermodynamic Equilibrium	C-1

ILLUSTRATIONS

<u>FIGURE</u>	<u>TITLE</u>	<u>PAGE</u>
3-1	Apollo 12 Flight Data - Attitude Hold	3-4
3-2	Apollo 12 Simulation with Uniform Grid	3-5
3-3	Apollo 12 Simulation with Non-Uniform Grid	3-6
3-4	Profile of Y-Direction Velocity for the Apollo 12 Problem with Non-Uniform Grid	3-7
3-5	Profile of X-Direction Velocity for the Apollo 12 Problem with Non-Uniform Grid	3-8
3-6	Heater Cycle Simulation Without Heater Thermal Mass	3-11
3-7	Heater Cycle Simulation with Heater Thermal Mass	3-12
3-8	Comparison of Heater Cycle Simulation and Flight Data	3-13
3-9	Apollo 14 Oxygen Tank No. 1 Asymptotic Potential Pressure Decay EVA Test Prediction at Minimum Expected Acceleration	3-16
3-10	Apollo 14 Oxygen Tank No. 1 Asymptotic Potential Pressure Decay EVA Test Prediction at Maximum Expected Acceleration	3-17
3-11	Effect of Acceleration on Potential Pressure Decay	3-18
3-12	Apollo 14 Oxygen Tank No. 1 EVA Test Heater Temperature Prediction at 70% Quantity	3-19
3-13	Apollo 14 Oxygen Tank No. 3 EVA Test Heater Temperature Prediction at 20% Quantity	3-20
3-14	Apollo 14 Oxygen Tank No. 3 Test Heater Temperature Prediction at 5.5% Quantity	3-21

ILLUSTRATIONS (Continued)

<u>FIGURE</u>	<u>TITLE</u>	<u>PAGE</u>
3-15	Attitude Hold Heater Cycle - 0.95 Ft ² Heater Area	3-22
3-16	Real Time High Flow Test Simulation	3-23
3-17	Converted Math Model Results Verification	3-25
3-18	Improved Math Model Conversion Verification	3-26
3-19	PTC Heater Cycle Simulation	3-29
3-20	PTC Heater Cycle Convergence	3-30
3-21	Tank 1 Test Simulation - 0.95 Ft ² Heater Area	3-33
3-22	Tank 1 Transient Pressure and Flow Response	3-34
3-23	Plumbing System Pressure Response with High Flow Rates	3-35
3-24	Tank 1 Test Simulation with Pressure Dependent Flow Rate	3-36
3-25	Tank 3 Test Simulation	3-38
3-26	Tank 3 Test Convergence	3-39
3-27	Potential Pressure Decay, .95 Ft ² Heater Area	3-41
3-28	Convergence of Maximum Potential Pressure Decay at AET 5:44	3-42
3-29	Simulation of AET 10:30 to 12:00 Using 100 x 10 Grid	3-44
3-30	Effect of Stratification on Length of Heater Cycle	3-45
3-31	Convergence of Heater Sensor Temperature at AET 11:50	3-46
3-32	Low Density Heater Cycle Simulation	3-48

ILLUSTRATIONS (Continued)

<u>FIGURE</u>	<u>TITLE</u>	<u>PAGE</u>
3-33	Radiant Heat Transfer During Low Density Heater Cycle	3-49
3-34	Parametric Heater Response	3-51
3-35	Temperature Comparisons Summary	3-52
3-36	Transient Velocity Profiles in a Cylinder	3-56
3-37	Oxygen Tank Response After PTC Termination	3-57
3-38	Relative Rotation Effect	3-58
3-39	Rotation Simulation - Flight Data Comparison	3-59
A-1	Analytical Approach - Model Description	A-2
C-1	Transient Velocity Profiles in Couette Flow	C-4
C-2	Transient Velocity Profiles in a Sphere	C-7
C-3	Transient Velocity Profiles in a Cylinder	C-9
C-4	Transient Velocity Profiles in a Cylindrical Tank with a Heater	C-12
C-5	Transient Velocity Profiles Between Cylindrical Tank Quantity Probe and Heater	C-13
C-6	Estimated Transient Velocity Profiles Between Spherical Tank and Heater	C-14
C-7	Tank Wall Drag	C-18
C-8	Tank Wall Torque	C-19
C-9	Drag Coefficient for Flow Over Cylinder	C-21
C-10	Drag at Heater and Tank Wall	C-22
C-11	Torque at Heater and Tank Wall	C-23

TABLES

C-1	Quantity Versus Time for Dimensionless Time Variable	C-15
-----	--	------

NOMENCLATURE

Acronyms

AET	Apollo Elapsed Time
CSM	Command Service Module
DTO	Detailed Test Objectives
EVA	Extra-Vehicular Activity
GET	Ground Elapsed Time
LM	Lunar Module
MSC	Manned Spacecraft Center
PTC	Passive Thermal Control
SRU	Sperry Rand Univac

REFERENCES

1. C. K. Forester, D. D. Rule, and H. W. Patterson, Apollo Oxygen Tank Stratification Analysis, The Boeing Company, D2-118357-1, November 30, 1970.
2. NASA-MSC Contract No. NAS9-11576, Apollo Oxygen Tank Analysis, dated November 2, 1970.
3. Study Program Plan, Apollo Oxygen Tank Stratification Analysis, The Boeing Company, February 26, 1971, memo 5-2510-HOU-4-201.
4. Task Summary, Apollo 14 Oxygen Tank Tests (DT0) Predictions, The Boeing Company, January 29, 1971, memo 5-2940-HOU-1249.
5. Task Summary, Analysis of Apollo 12 for GET 197-209, The Boeing Company, February 22, 1971, memo 5-2510-HOU-4-198.
6. D. D. Rule, J. E. Barton, H. W. Patterson, Postflight Analysis of the Apollo 14 Cryogenic Oxygen System, The Boeing Company, D2-118405-1.
7. Task Summary, Math Model Improvement, The Boeing Company, July 30, 1971, memo 5-2510-HOU-4-323.
8. C. K. Forester, Pressurized Expulsion of Non-Isothermal Single Phase Cryogen, paper at the NASA-MSC Cryogenic Symposium, May 20 and 21, 1971.
9. H. W. Patterson, Correlation of Apollo Oxygen Tank Thermodynamic Performance Predictions, paper at the NASA-MSC Cryogenic Symposium May 20 and 21, 1971.
10. NASA-MSC Oxygen Tank Analysis Team Meeting, January 6, 1971.
11. J. E. Barton, G. I. Bultman, C. K. Forester, J. B. Urquhart, H. W. Patterson, Computer Program Manual - Apollo Oxygen Tank Stratification Analysis, D2-118407-1, August 31, 1971.
12. Apollo 14 Flight Data for Tank Accelerations and Miscellaneous Cryogenic System Variables.
13. Apollo Fuel Cell and Cryogenic Gas Storage System Flight Support Handbook, NASA-MSC Document, February 18, 1970.

SECTION 1

1.0 INTRODUCTION

1.1 Purpose

The primary purpose of the Apollo oxygen tank stratification analysis was to evaluate the effects of flow rates, accelerations and vehicle rotations on the oxygen tank flight performance. Program objectives derived from this primary purpose were:

1. Verify the existing stratification math model by comparison of model results with flight data.
2. Modify the stratification model to improve the simulation accuracy and reduce the computer time required for simulations.
3. Determine tank performance for a wide range of fluid conditions and flight environments.

1.2 Background

Comprehensive stratified performance analyses of the Apollo oxygen tanks were not conducted prior to the Apollo 13 mission, since mixing fans were available to reduce the effects of stratification on tank operation. After the Apollo 13 incident, an oxygen stratification model was developed (Reference 1)* and verified by analysis of one period on Apollo 12. This analysis verified the ability of the model to predict pressure collapses which could occur as a result of stratification. The ability to predict heater temperatures could not be verified since the Apollo 12 tanks did not contain heater temperature sensors. This basic model was used prior to initiation of the present contract to predict Apollo 14 oxygen tanks performance and verify that the Apollo 14 mission could be successfully performed. These early analyses were not, however, entirely adequate since "worst case" conditions were not included and the model was not completely verified. These analyses also identified model improvements needed to improve the simulation accuracy and reduce the required computer time.

1.3 Scope

The Apollo oxygen tank stratification analyses included detailed studies of the oxygen tank performance in flight. The analyses were not directed toward system performance and included only system and vehicle analyses necessary to define the tank flow rates and accelerations. The analytical effort was divided into four tasks:

*Conducted as part of NASA-MSC Contract NAS9-10364.

1.3 Scope (Continued)

Task 1 - Math Model Improvement

Model modifications to improve simulation accuracy and reduce computer time

Task 2 - Analysis of Apollo 12 for GET 197-209

Model verification for low tank quantities

Task 3 - Apollo 14 Predictions and Analysis

Worst case Apollo 14 pre-flight predictions, math model conversion to the NASA-MSD computers and Apollo 14 post-flight analysis

Task 4 - Fluid Rotation Analysis

Rotation model development and investigation of the effects of vehicle rotation on tank performance

These four tasks are the complete effort initiated November 1, 1970 as defined in Contract NAS9-11576, Apollo Oxygen Tank Stratification Analysis (References 2 and 3). The detailed results of each task were included in task reports (References 4 to 7) and delivered to NASA-MSD immediately after task completion. Preliminary task results were also presented at NASA-MSD meetings and conferences (References 8 to 10) to support the overall NASA oxygen tank analysis objectives.

A Supplemental Agreement has been executed to extend the contract period of performance through January 1972. The extended effort will include a postflight analysis of Apollo 15 and modifications of the math model to improve its utility. The results of these efforts will be summarized by an addendum delivered as Volume II of this final report at the end of the contract period.

SECTION 2

2.0 SUMMARY

The Apollo oxygen tanks were redesigned and the mixing fans removed after the Apollo 13 incident. This modification resulted in a requirement for the oxygen tanks to supply future mission flow requirements under stratified fluid conditions caused by the low "g" flight environment. Analyses completed prior to the initiation of this current contract predicted the stratified tank performance with a stratification model validated by analysis at one Apollo 12 condition. These predictions provided confidence that Apollo 14 mission could be accomplished, but did not adequately evaluate tank performance for conditions such as EVA expected during later missions. The Apollo Oxygen Tank Stratification Analysis Program (Contract NAS9-11576) was initiated to determine the tank performance for a wider range of fluid conditions and flight environments and to improve the efficiency and accuracy of the math model.

The stratification math model simulates the tank performance by a finite difference solution of the two dimensional equations for the convection flow field in the tank. The model accuracy and efficiency were improved by optimizing the arithmetic equations and equations sequence and by developing a variable grid capability. The variable grid permits refinement of the flow field in the region of the heater without unnecessary refinement in the remainder of the field. These model improvements reduced the computer time to one hour for a simulation that previously required three hours to obtain equivalent accuracy with the original model. Optimum use of the variable grid should reduce computer time to 10% - 20% of that previously required.

The basic stratification model was used for Apollo 14 preflight predictions, real-time flight support and postflight analysis. The preflight predictions for the high flow tests (DTO) simulating EVA conditions confirmed that heater temperatures and pressure decays would be within acceptable limits. The postflight analysis confirmed that heater temperature predictions were within 12°F at flight data for four attitude hold and PTC conditions investigated. The maximum temperature error during the high flow DTO was 60°F. This error was attributed to unusual acceleration conditions caused by oxygen venting during the test. Pressure decay predictions were verified by the postflight analysis. A simplified method for heater temperature predictions was also developed using a modified Rayleigh Number convection equation. The simplified method predicted heater temperatures within 50°F of flight data.

The effects of fluid rotation induced in the tank by changes in vehicle

2.0 SUMMARY (Continued)

rotation rate were analyzed with the math model modified to include rotating boundary conditions. The simulated heater temperature for an Apollo 14 heater cycle which exhibited a strong influence of rotation was in substantial disagreement with flight data. The simulated peak heater temperature was 136°F higher than the observed temperature at the flight maximum heater on time. The temperature error was caused by three-dimensional flows in the tank which could not be adequately analyzed with the two-dimensional model. The three-dimensional effect resulted from a vehicle yaw of more than 45° following the termination of PTC. The yaw maneuver placed the heater axis transverse to the rotating flow and caused the heater temperature to be lower than that expected without the yaw maneuver. The analysis did confirm that yaw or pitch maneuvers associated with initiation or termination of PTC will significantly reduce heater temperature.

It was concluded from the analyses conducted that the redesigned tanks are adequate for all known Apollo mission requirements; pressure decays are tolerable and heater temperature can be maintained within acceptable limits; and the stratification model provides accurate predictions. Analyses are recommended for the Apollo 15 mission EVA to completely confirm the capability for later missions since the Apollo 14 EVA simulation test was not fully representative of EVA requirements.

SECTION 3

3.0 PROGRAM TASKS

The program tasks were designed to support the Apollo 14 mission, to provide NASA-MSD an efficient and verified accurate stratification model, to evaluate the effects of fluid rotation on tank performance, and to assess tank capability for future missions. The program tasks directed toward these objectives were:

Task 1 - Math Model Improvement

Task 2 - Analysis of Apollo 12 for GET 197-209

Task 3 - Apollo 14 Predictions and Analysis

Task 4 - Fluid Rotation Analysis

The significant results of each task are summarized in this section. Detailed results, methods of analysis, conclusions and recommendations for each task are included in References 4 to 7.

3.1 Task 1 - Math Model Improvement

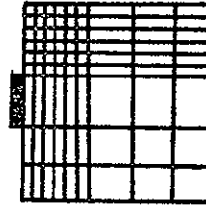
The stratification model (Reference 1 and Appendix A), available when this contract was initiated, provided generally good tank performance simulations; but the simulation accuracy was limited by computer core storage and time requirements. This basic model was modified to improve the simulation accuracy obtainable with existing computer core limits and with reasonable computer time requirements. The modifications included the addition of a variable grid capability and revision of the program calculation sequences. The variable grid was utilized for the purpose of obtaining improved boundary layer resolution, thereby improving the simulation accuracy. The program calculations were optimized to minimize the computer time required for each simulation with the variable grid model. The improved math model and its application are discussed by Reference 7. The model is operational on the NASA-MSD SRU-1108 computers and is completely described in Reference 11.

3.1.1 Variable Grid

The improved model divides the two-dimensional region representing the tank into one to seven sub-regions in each of the coordinate

3.1.1 Variable Grid (Continued)

directions (Figure). The dimension of each sub-region and the number of cells in each sub-region is arbitrary. The sub-regions can be arranged to provide good resolution of the boundary layer at the heater surface without the excessive number of cells required by the constant grid model. The program solves the complete compressible viscous flow equations in the entire region. The form of the equations used for each cell is selected on the basis of the cell location on the boundary or interior of a sub-region. The equations are considerably simplified, when adjacent cells are geometrically identical; and this selection reduces the number of calculations performed.



3.1.2 Improved Computing Efficiency

The model calculation routines which use a significant fraction of the computer time were modified and rearranged to minimize the total computer time required. Calculations requiring table searches for the same data are combined so that searches are not repeated. Logic tests based on cell location and geometry are used to select the simplest equation which can adequately describe the stresses on the cell. The algebraic equations in the iteration loops were formulated to require the least number of total calculations.

The efficiency improvements resulted in computer time savings of 7% to 26%. The time reduction depends on the number of grid sub-regions, because the equations used in the vicinity of the sub-region boundaries are more complex than those used in the interior of the sub-regions.

3.1.3 Simulation Results

The improved model capabilities were explored and demonstrated by simulation of an Apollo 12 period which had been analyzed with the original stratification model. The pressure cycles during the Apollo 12 period from GET 4:30 to 7:30 were of primary interest (Figure 3-1). The accuracy of simulation of the short pressure cycles at GET 5:30 depended primarily on the accuracy of the simulated heater boundary layer.

Simulations of this Apollo 12 period were made with the original model and with the improved model to evaluate the program improvements. The simulations were run for sufficient time (one hour) to obtain "steady state" heater cycles. The uniform grid simulation with 80 cells in the X direction and 20 cells in the Y direction (80 x 20 grid) produced

3.1.3 Simulation Results (Continued)

steady state heater cycles in good agreement with flight data (Figure 3-2) and required 4300 seconds computing time. The improved model with a variable grid arranged to provide the same boundary layer cell density duplicated these results with a 24 x 20 grid and required about one-third the computing time. The same period was also simulated with the improved model with a 22 x 20 grid arranged to provide resolution comparable to a 140 x 20 uniform grid. This simulation provided more accurate pressure rise times (Figure 3-3) and required 3000 seconds computing time. The major computer time savings with the improved model result from the reduction in the total number of cells required with the variable grid. The computer time is proportional to the total number of cells. Simulations with the improved model can be accomplished with 10-30% of the computer time previously required if the variable grids are properly selected.

The heater boundary layer resolution achievable with the variable grid is shown by Figures 3-4 and 3-5. The velocity component in the X direction (Figure 3-5) is more sensitive to the grid than the Y direction velocity (Figure 3-4). The velocity in the X direction is directly related to the fluid expansion. The pressure rise rates are closely related to the fluid expansion and resolution of the X direction velocity is indicative of the accuracy of the heater cycle simulations. These boundary layer data indicate that the resolution required for accurate simulations can be achieved with the improved math model.

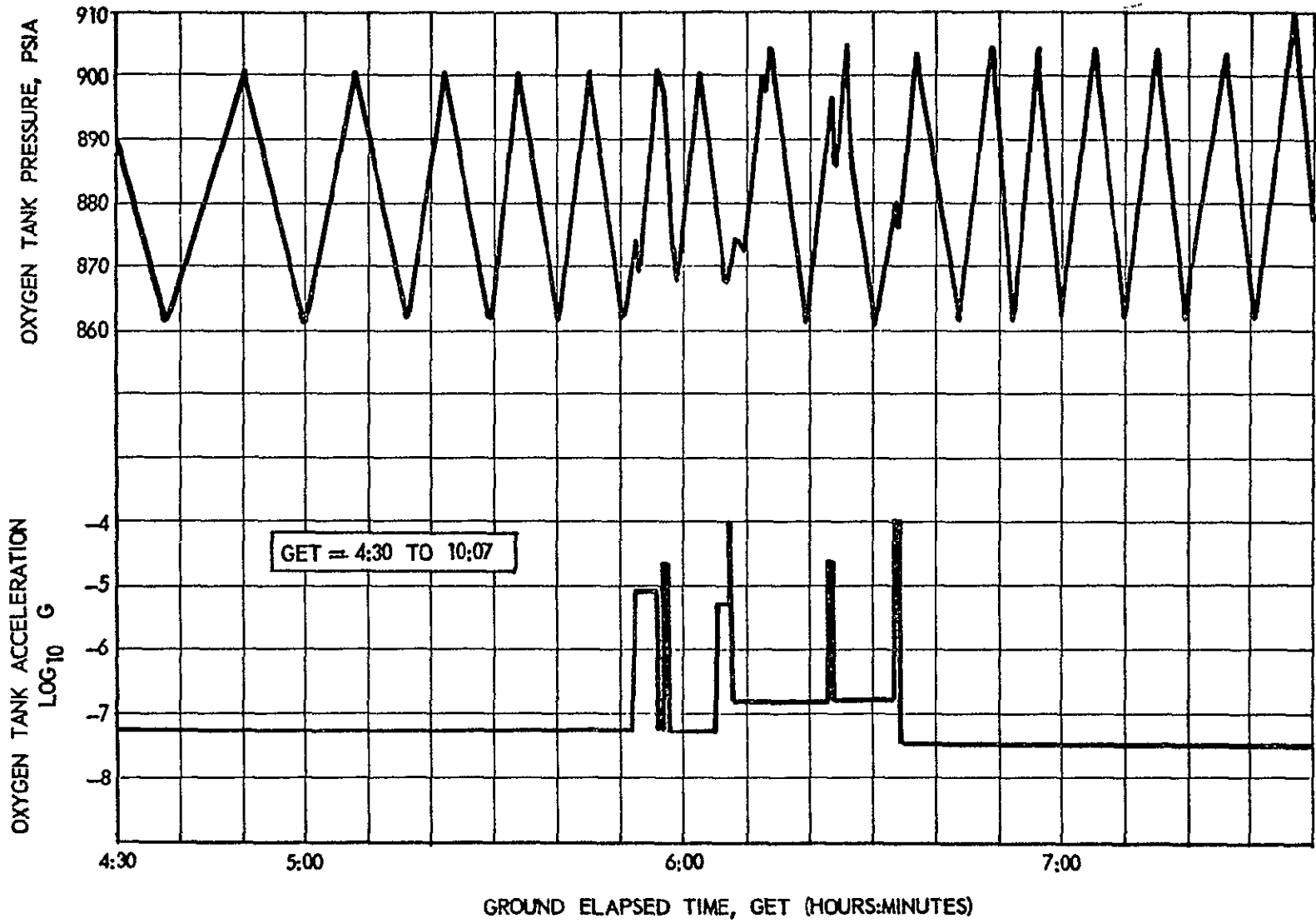


FIGURE 3-1 APOLLO 12 FLIGHT DATA - ATTITUDE HOLD

QUANTITY 95.0 PERCENT
ACCELERATION $2.0 \times 10^{-7} G$
GRID SIZE 80 X 20

HEATER POWER 114.00 WATTS
HEATER AREA 0.95 FT SQ
THERMAL MASS 0.07 BTU/DEG R

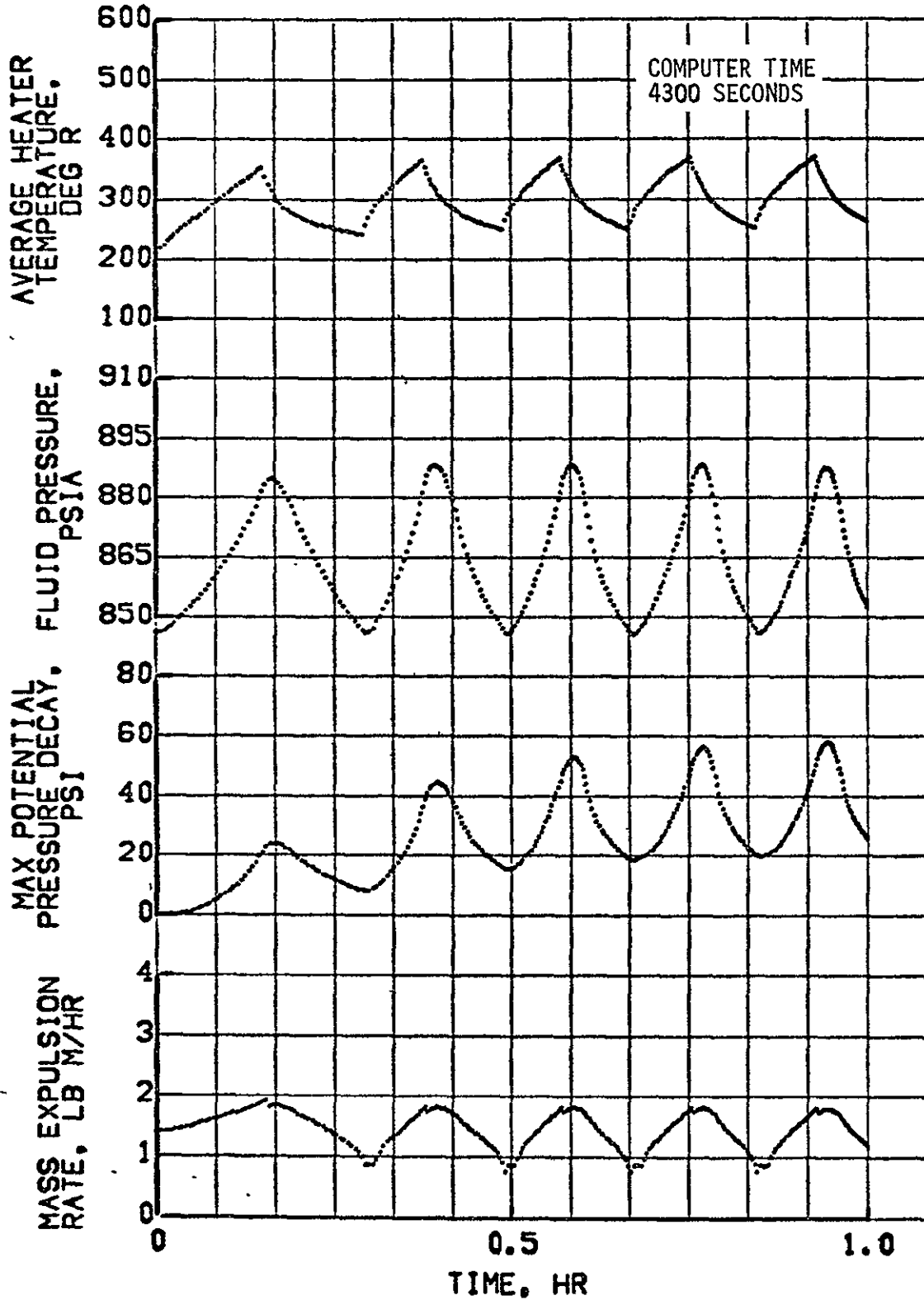


FIGURE 3-2 APOLLO 12 SIMULATION WITH UNIFORM GRID

QUANTITY 96.4 PERCENT
ACCELERATION $2.0 \times 10^{-7}G$
GRID SIZE 22 X 20

HEATER POWER 113.78 WATTS
HEATER AREA 0.95 FT SQ
THERMAL MASS 0.07 BTU/DEG R

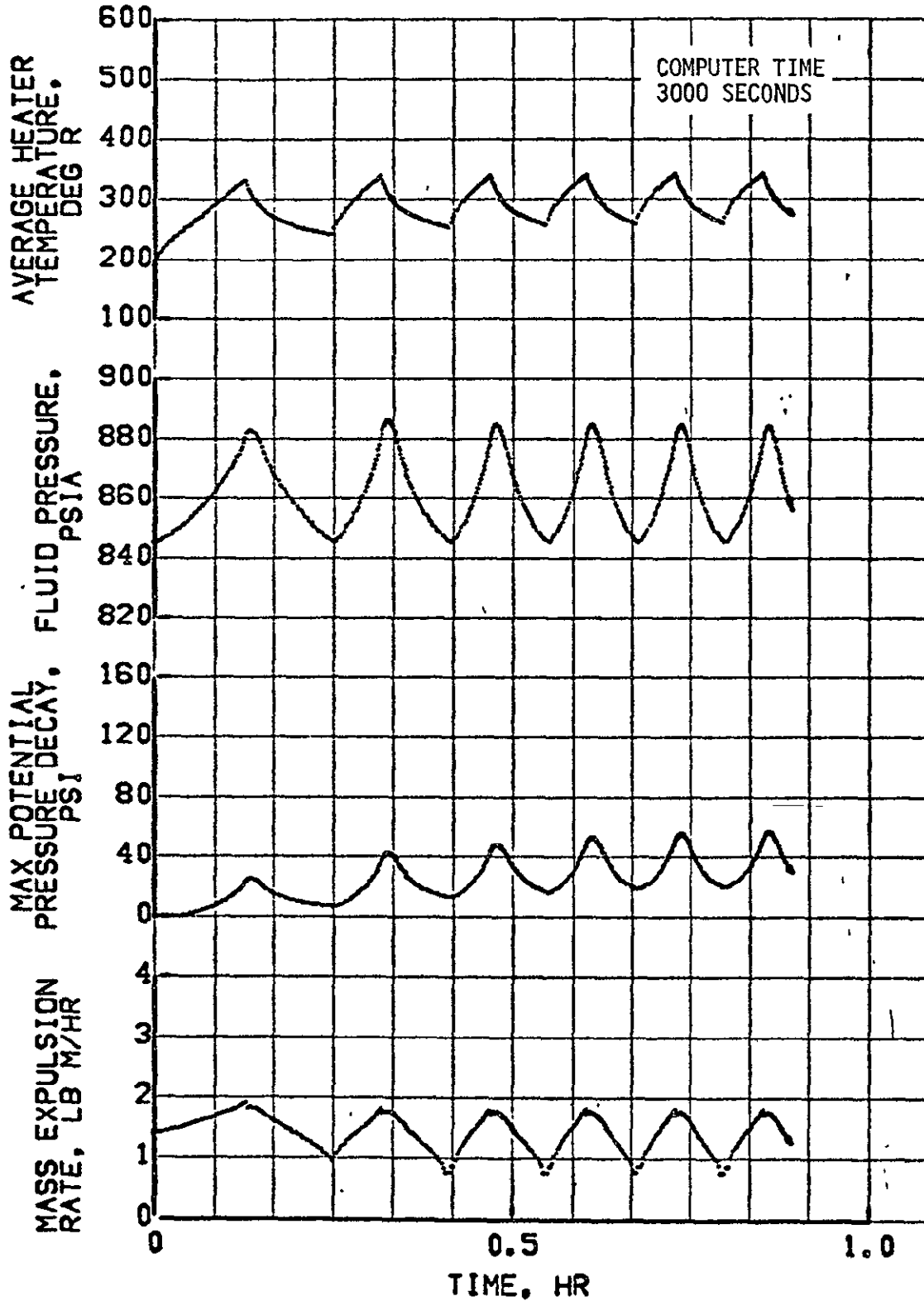


FIGURE 3-3 APOLLO 12 SIMULATION WITH NON-UNIFORM GRID

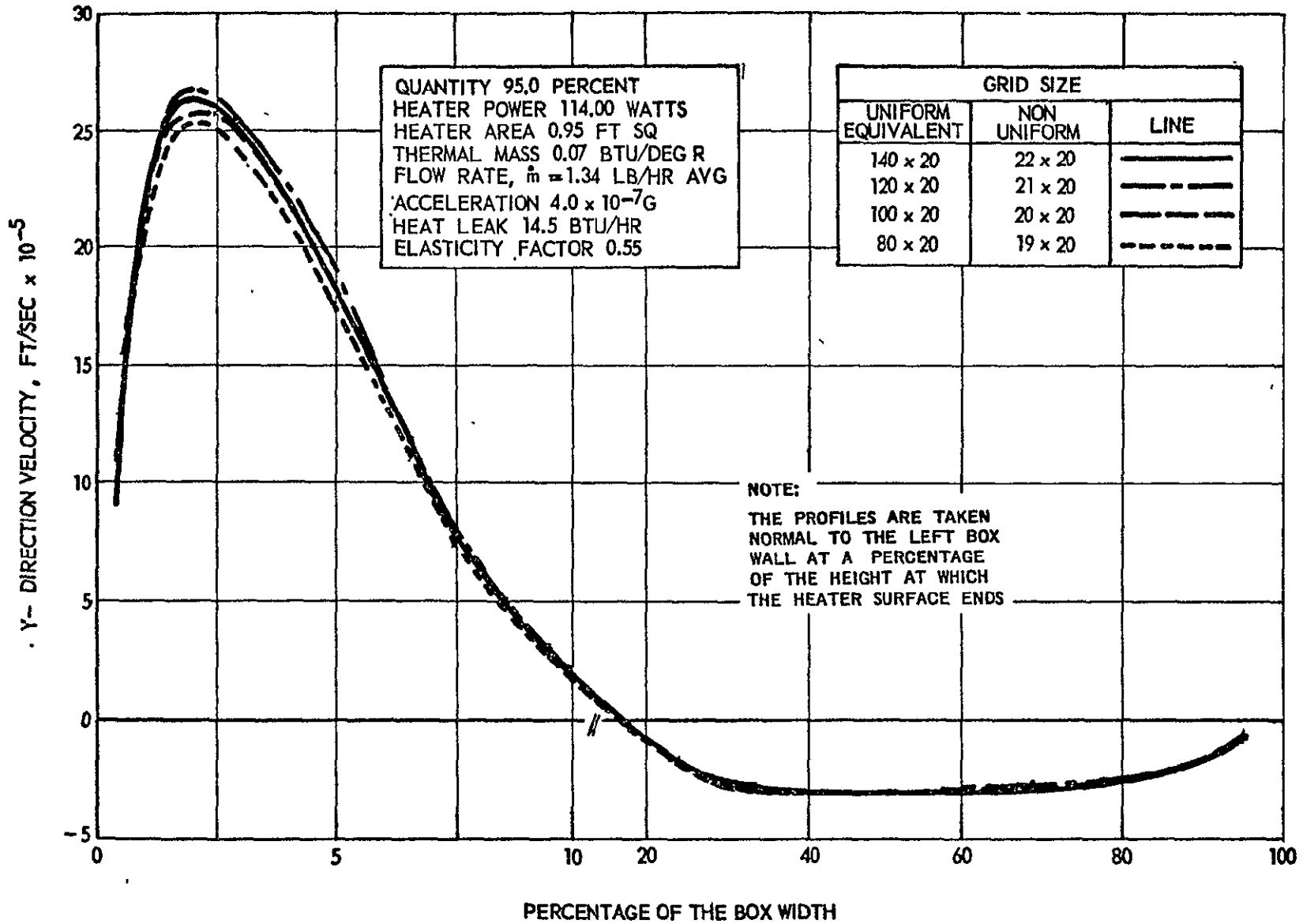


FIGURE 3-4 PROFILE OF Y-DIRECTION VELOCITY FOR THE APOLLO 12 PROBLEM WITH NON-UNIFORM GRID

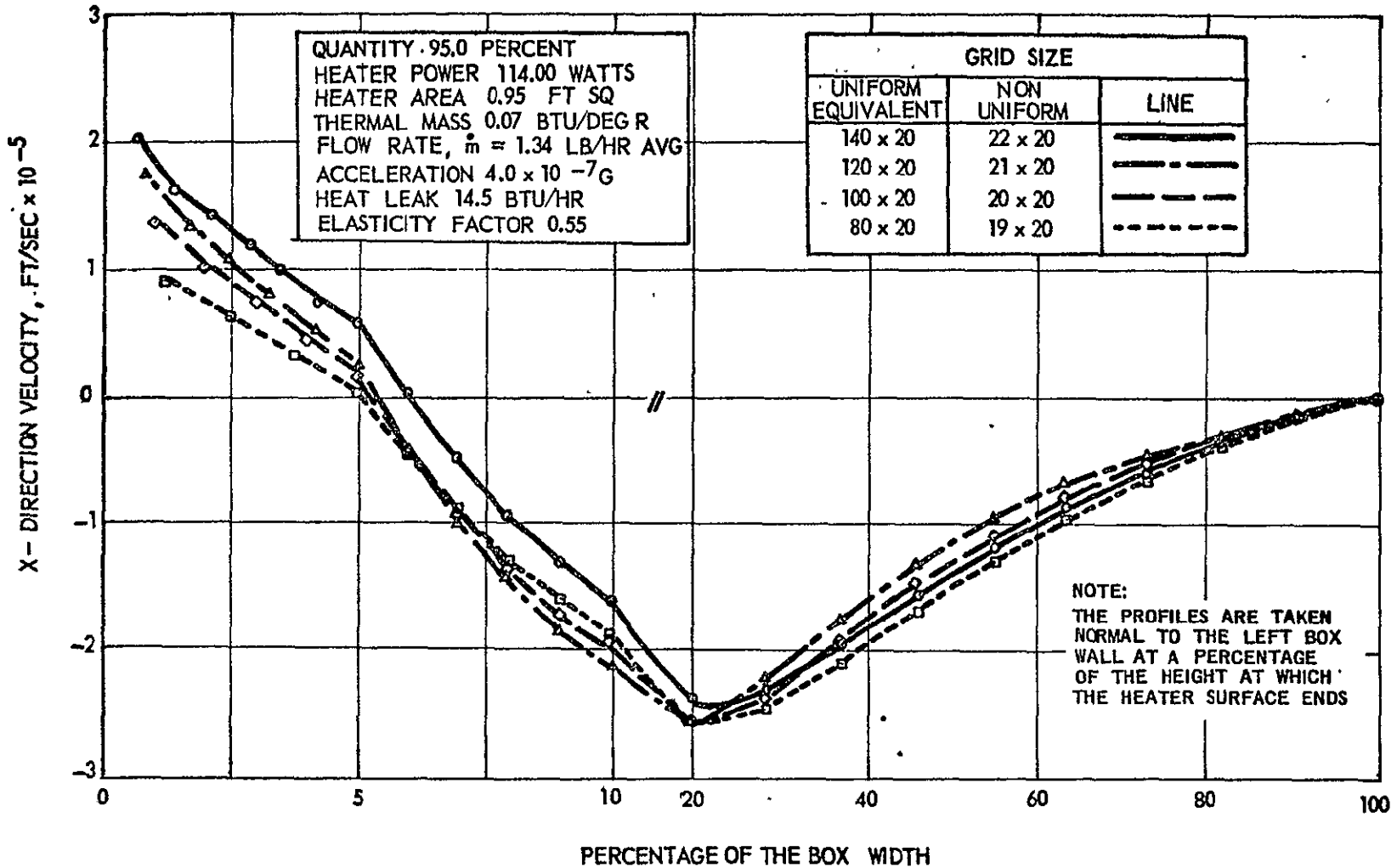


FIGURE 3-5 PROFILE OF X-DIRECTION VELOCITY FOR THE APOLLO 12 PROBLEM WITH NON-UNIFORM GRID

3.2 Task 2 - Apollo 12 GET 197-209

Analysis of Apollo post flight pressure data indicated that at quantities less than 40%, the oxygen tank heaters remained on longer than predicted by equilibrium thermodynamics. It was concluded that these longer cycles were due to either stratification, or other thermodynamic and heat transfer processes in the tanks. Previous Boeing stratification studies concentrated on the near full tank quantity range. These validated the stratification computer program by comparison with Apollo 12 flight data at near full quantities, but no comparisons had been made between flight data and program results at low quantities. An analysis of one low quantity heater cycle was initiated to determine the cause of the long on-time and to validate the stratification program for low tank quantities.

3.2.1 Simulation Results

The heater cycle selected from the Apollo 12 data for analysis occurred between GET 198 and 209 at 35% quantity. During this period the heater remained on for 12 minutes and 42 seconds and raised the pressure 33 psi. The on-time expected for this pressure rise is approximately 10 minutes and 45 seconds based on equilibrium calculations at the observed flow rates. The average flow rate to the fuel cells and through the ECS flow meters during the on-period was 1.0 lb/hr. The flow into the ECS surge tank was added to the 1.0 lb/hr usage rate and was taken as linear with the pressure rise during the cycle. The pressure rise of 33 psi from 866 to 899 psi resulted in an additional flow rate of 0.5 lb/hr at the top (899 psia) of the heater cycle. The analysis assumed an acceleration level of 2.0×10^{-6} "g" which is typical for the inboard tank during passive thermal control.

The simulation of the pressure rise during the on-cycle without thermal mass produced the results of Figure 3-6. These data show that the time for the 33 psi rise is less than the equilibrium rise time of 10 minutes and 45 seconds due to stratification effects. The heater temperature response shown by Figure 3-6 is typical of the response of the basic model without heater thermal mass and exhibits some temperature overshoot as the boundary layer flow is being established.

The tank pressures and heater temperatures resulting from simulations including a heater thermal mass of 0.07 BTU/°F are shown by Figure 3-7. The pressure data show a pressure rise of 33 psi in slightly over 12 minutes for the 60 x 10 grid simulation. The estimated asymptotic value of the time required for the 33 psi rise is 12 minutes and 10 seconds which is 32 seconds or 4.2% less than indicated by the flight data.

3.2.1 Low Quantity Modeling Requirements (Continued)

The results of the stratification program simulation of the heater cycle pressure rise are in good agreement with the flight data (Figure 3-8). The curvature of the simulated pressure-time curve during the first 3 minutes of on-time is caused by energy being stored in the heater and not transmitted to the fluid. The flight data similarly shows no pressure increase for the first four minutes. The simulated pressure-time curve is generally in agreement with the flight data within the accuracy of the telemetry data. The heater cycle pressure rise was accurately simulated by including the heater thermal mass during the heater on period; therefore, simulation of the pressure decay period was not necessary and was not done.

It was concluded that the heater thermal mass caused the heater cycles to be longer than equilibrium cycles at low quantities. The heater thermal mass was therefore permanently added to the stratification math model. The model was validated by this minor change producing good heater cycle simulation at the 35% tank quantity.

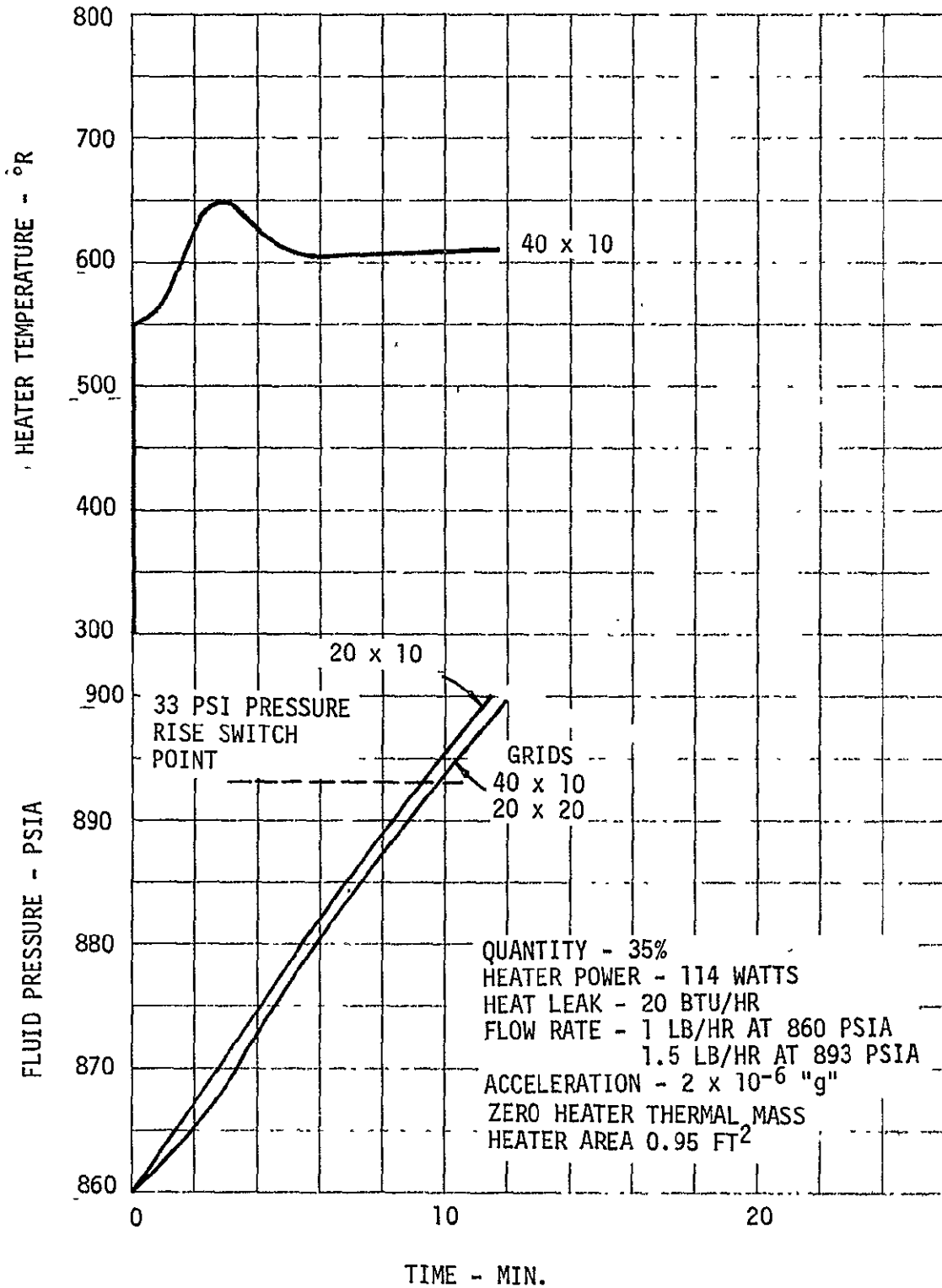


FIGURE 3-6 HEATER CYCLE SIMULATION WITHOUT HEATER THERMAL MASS

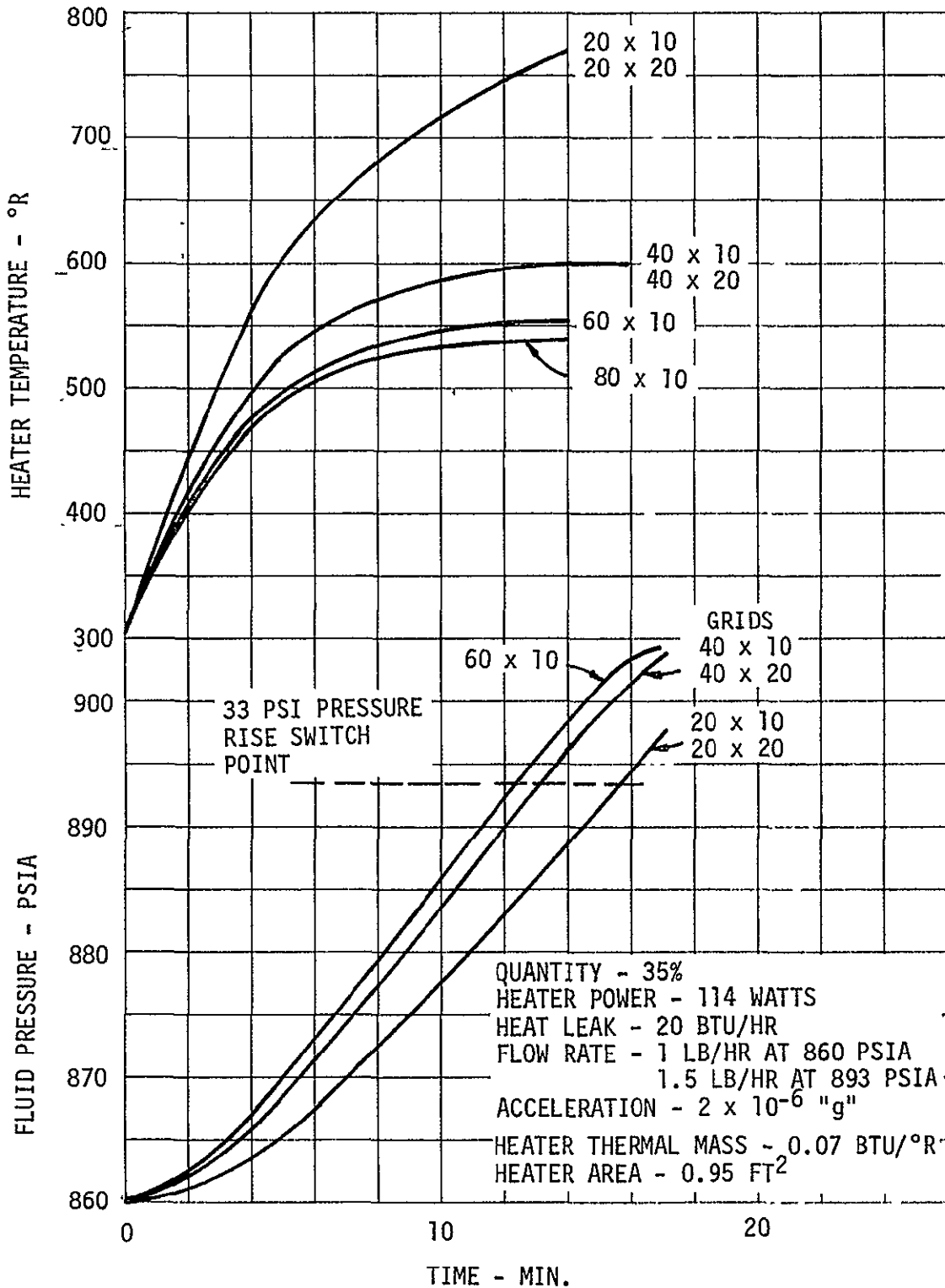


FIGURE 3-7 HEATER CYCLE SIMULATION WITH HEATER THERMAL MASS

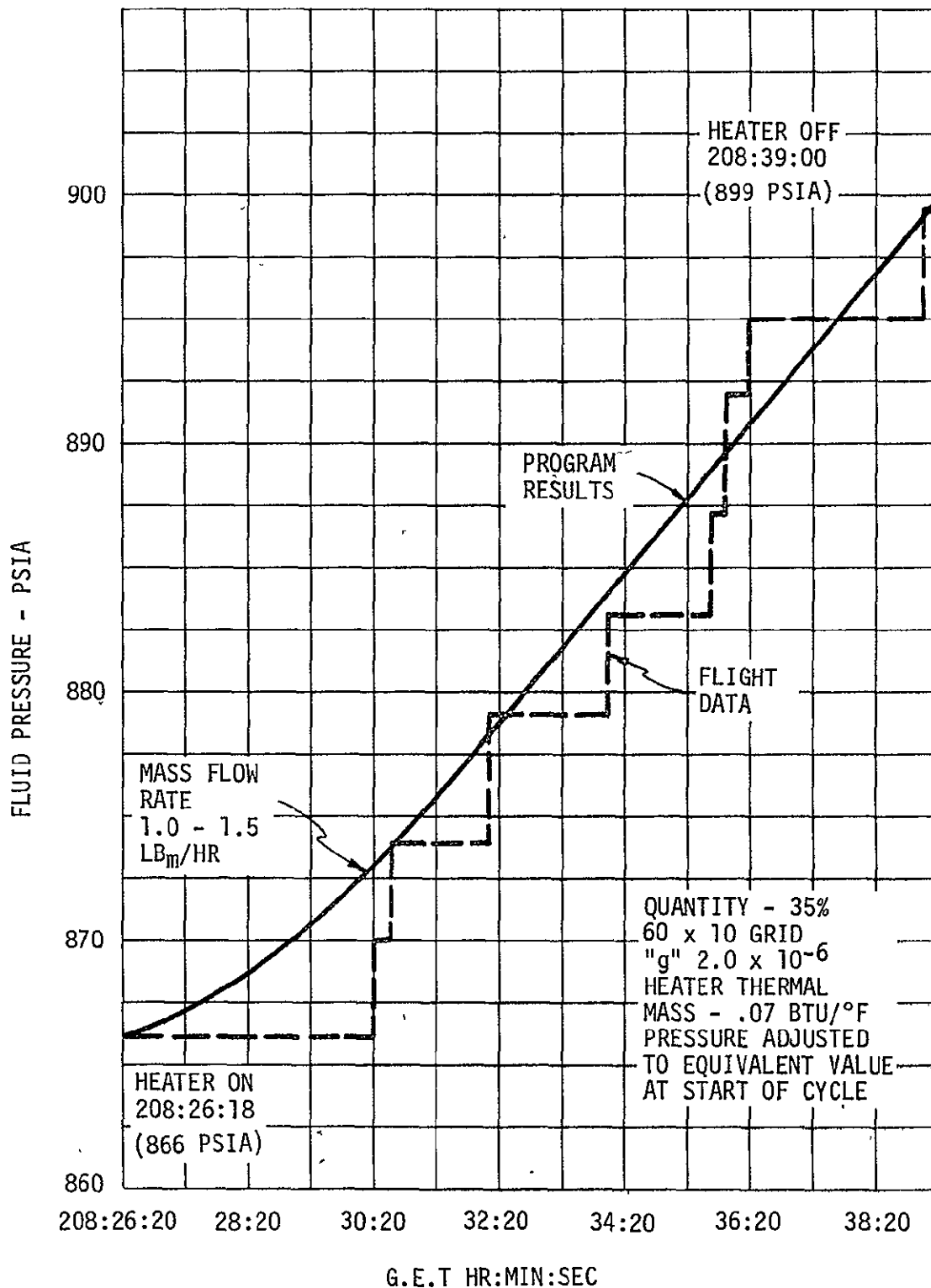


FIGURE 3-8 COMPARISON OF HEATER CYCLE SIMULATION AND FLIGHT DATA

3.3 Task 3 - Apollo 14 Predictions and Analysis

This task included pre-flight predictions of the Apollo 14 high flow (DTO) tests, conversion of the stratification math model from the CDC-6600 to the SRU-1108 for use at NASA/MSC, and post-flight analysis of the Apollo 14 mission. The pre-flight predictions for the high flow tests were revised during the mission to reflect changes in the test plans.

3.3.1 Pre-Flight Predictions

Predictions of the planned Apollo 14 oxygen tank functional tests were made to determine whether all test objectives could be satisfied, and if test procedures were adequate. Significant parameters predicted were the maximum potential pressure decays, and heater temperatures for the three planned test conditions.

The predictions (Ref. 4) were made with the basic stratification model not including heater thermal mass. Oxygen flow rates to the ECS were determined from the functional test plans. Fuel cell flow rates were based on expected power levels for the EVA simulation tests. The high flow EVA simulation test included overboard oxygen venting which produced significant vehicle and tank accelerations. The vent configuration was not firmly established when the analyses were initiated; therefore, two accelerations were used for tank 1 pressure decay predictions, 3.0×10^{-6} "g" and 3.3×10^{-7} "g". Subsequent analyses of the final vent configuration estimated an acceleration of 4.7×10^{-6} "g" for tank 1 and 4.9×10^{-6} "g" for tank 3.

The maximum potential pressure decay for the tank 1 EVA test at 70% quantity was estimated by extrapolation of simulation results with different grid sizes (Figures 3-9 and 3-10) to asymptotic limits. The effect of acceleration on the predicted potential pressure decay for the high quantity DTO is shown by Figure 3-11. At the expected acceleration level of 4.7×10^{-6} "g", the maximum pressure decay was predicted to be less than 7.5 psi. The "worst case" pressure decay of 145 psi at the lowest acceleration was tolerable and would not significantly reduce the tank flow rate. No significant pressure decay was predicted for the tank 3 EVA test at 20% tank quantity.

Maximum heater temperature predictions were also made for the two high flow EVA tests and the emergency return simulation. (Figures 3-12, 3-13, and 3-14). For three heater elements at the lowest possible "g" level the predicted maximum heater temperature during the 20% quantity tank 3 test was 320°F. Analysis of the emergency return test condition determined that the heater temperature would approach but not exceed 500°F for three element operation.

3.3.1 Pre-Flight Predictions (Continued)

The heater temperature red-line was set at 350°F during the Apollo 14 mission. To avoid exceeding this red-line the low quantity high flow test and the emergency return test were conducted with two heater elements. The original predictions for three heater elements were therefore invalidated and predictions of the tank 3 DTO were revised during the mission. The stratification model was modified prior to the mission to include the heater thermal mass which was neglected in the first predictions. Analyses were performed during the mission to verify the modified model heater temperature predictions and to provide realistic predictions of the tank 3 test before the test was started. Analysis of the heater cycle at AET 78:20 verified that a heater area of 0.95 ft² predicted the peak heater temperature within 30°F (Figure 3-15). Revised predictions for the tank 3 high flow test were, therefore, made with 0.95 ft² effective heater area. The predicted peak heater temperature for the first heater cycle was in excellent agreement with flight data (Figure 3-16). The predicted heater temperatures and tank pressures remained in good agreement with flight data until the test was terminated at GET 169:38:57. Deviations between predicted temperatures and flight data immediately after the start of the heater cycle were caused by the temperature sensor lag which was not included in the model used for these analyses.

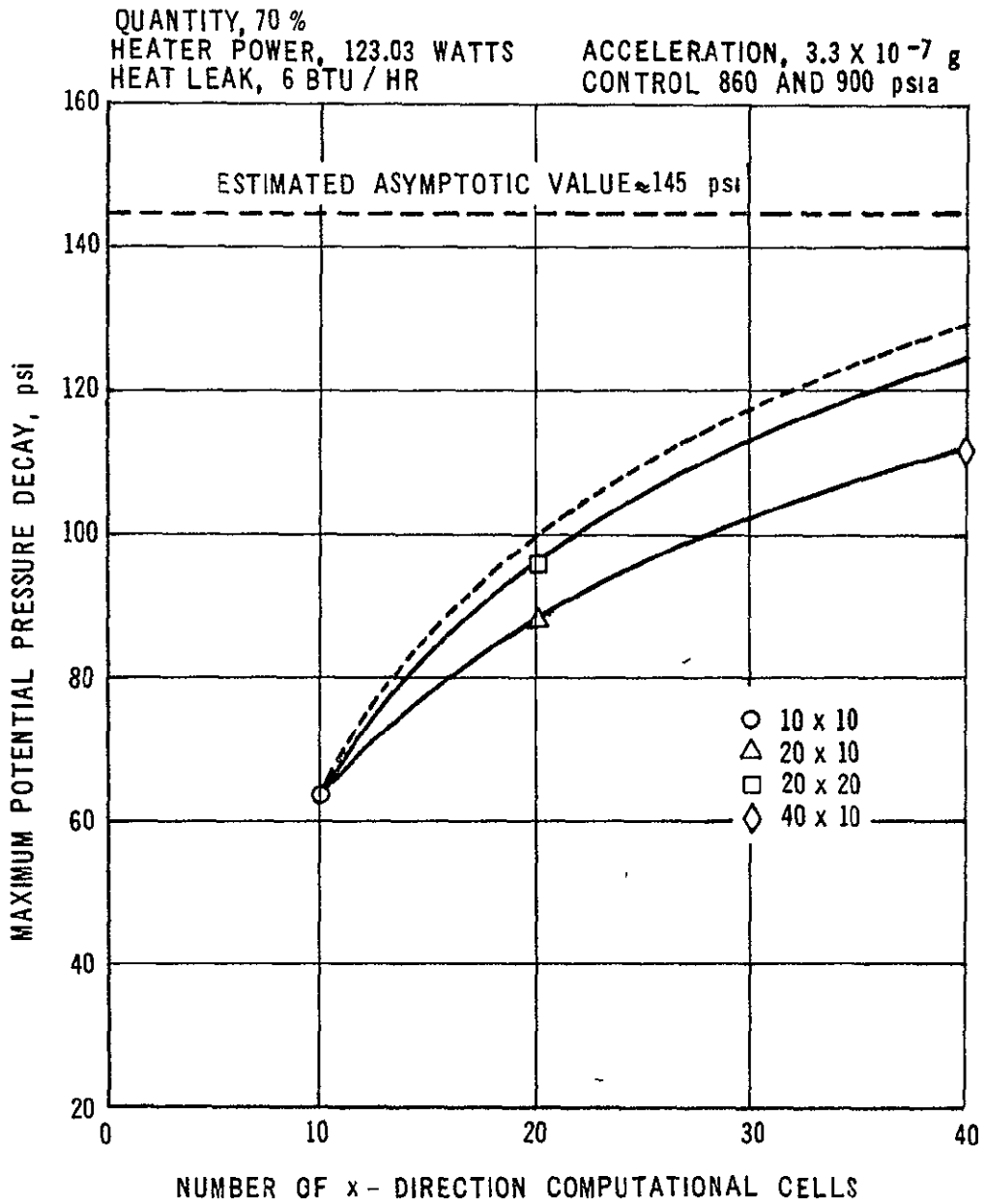


FIGURE 3-9 APOLLO 14 OXYGEN TANK NO. 1 ASYMPTOTIC POTENTIAL PRESSURE DECAY EVA TEST PREDICTION AT MINIMUM EXPECTED ACCELERATION

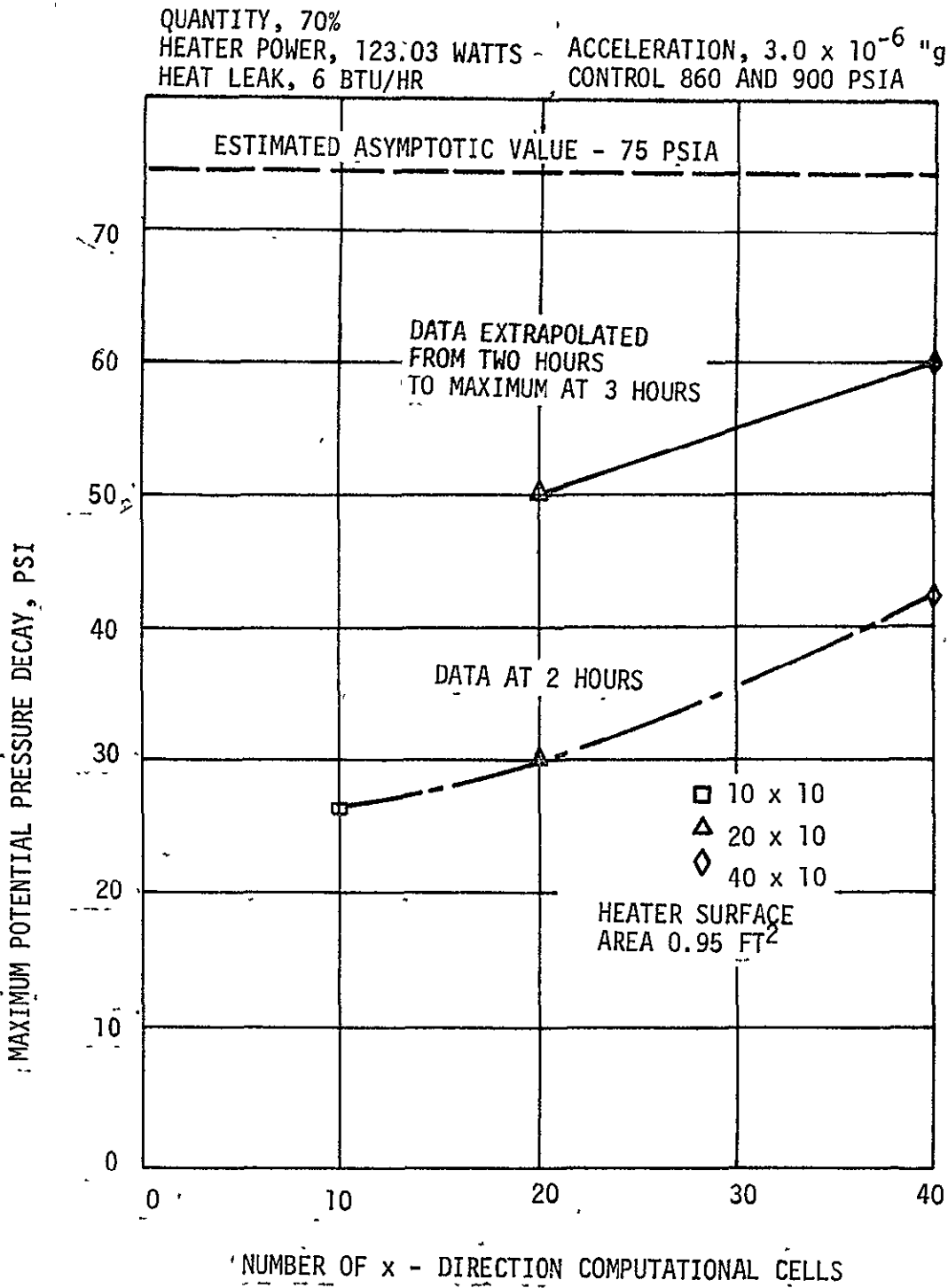


FIGURE 3-10 APOLLO 14 OXYGEN TANK NO. 1 ASYMPTOTIC POTENTIAL PRESSURE DECAY EVA TEST PREDICTION AT MAXIMUM EXPECTED ACCELERATION

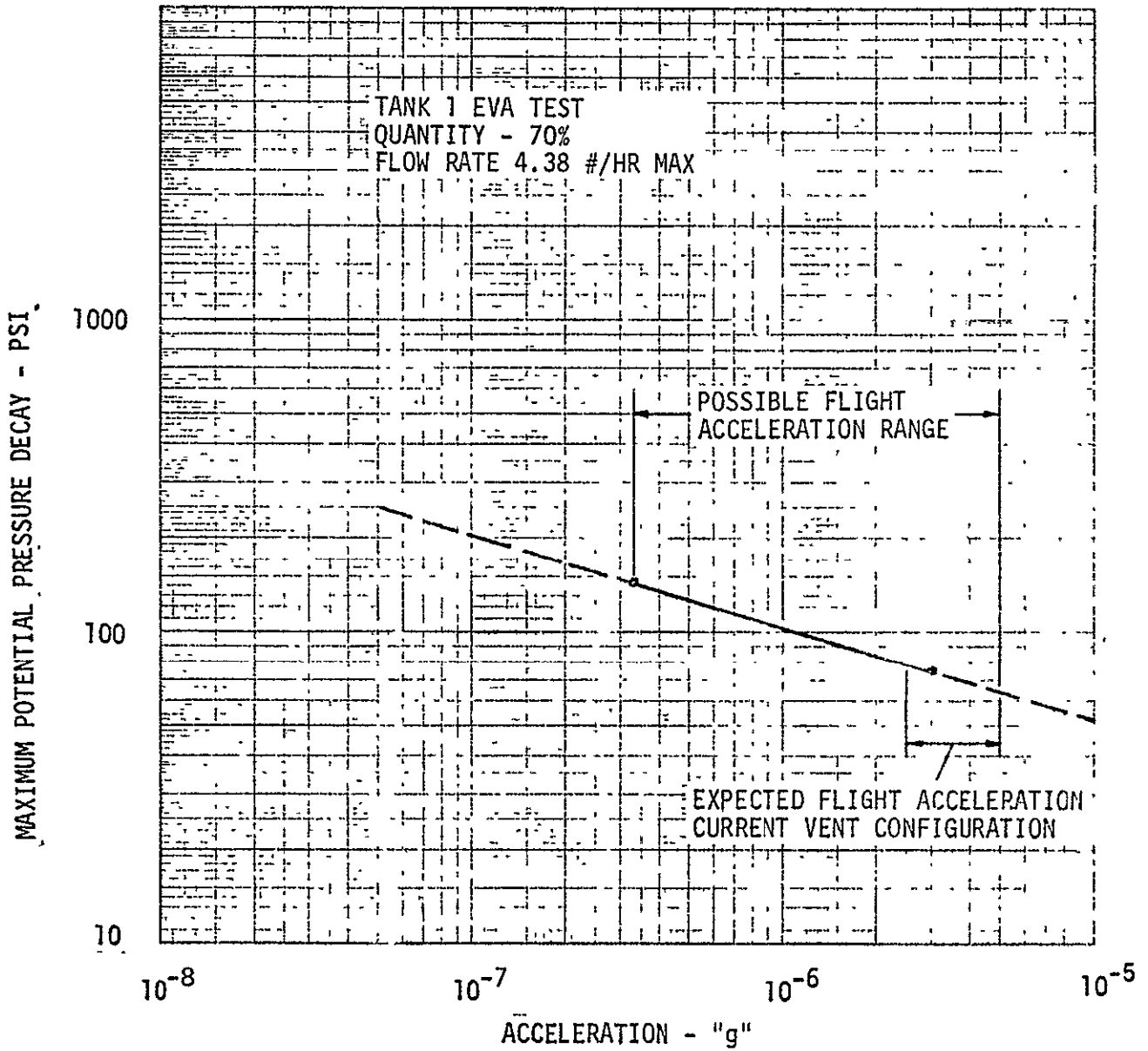


FIGURE 3-11 EFFECT OF ACCELERATION ON POTENTIAL PRESSURE DECAY

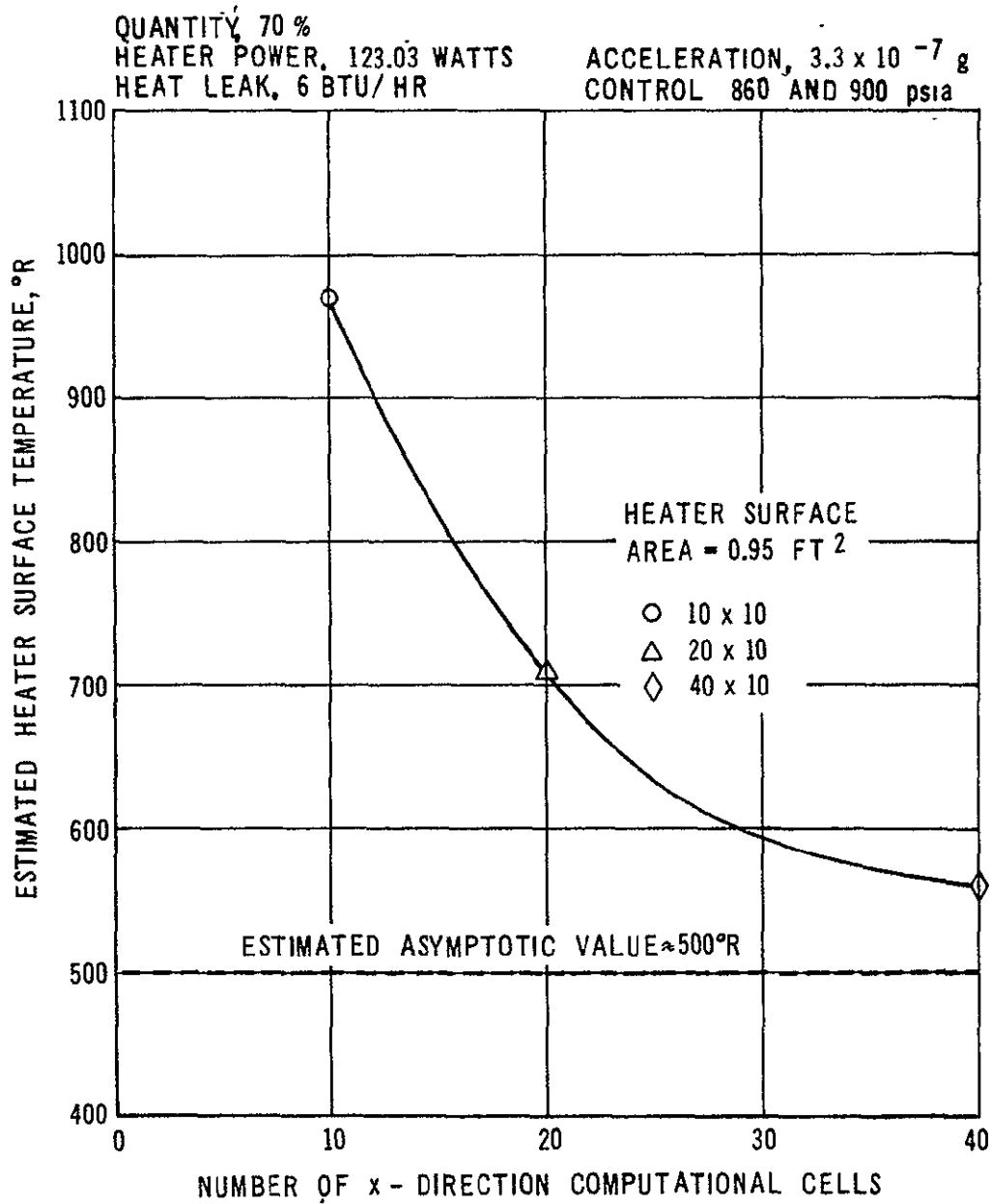


FIGURE 3-12 APOLLO 14 OXYGEN TANK NO. 1 EVA TEST HEATER TEMPERATURE PREDICTION AT 70% QUANTITY

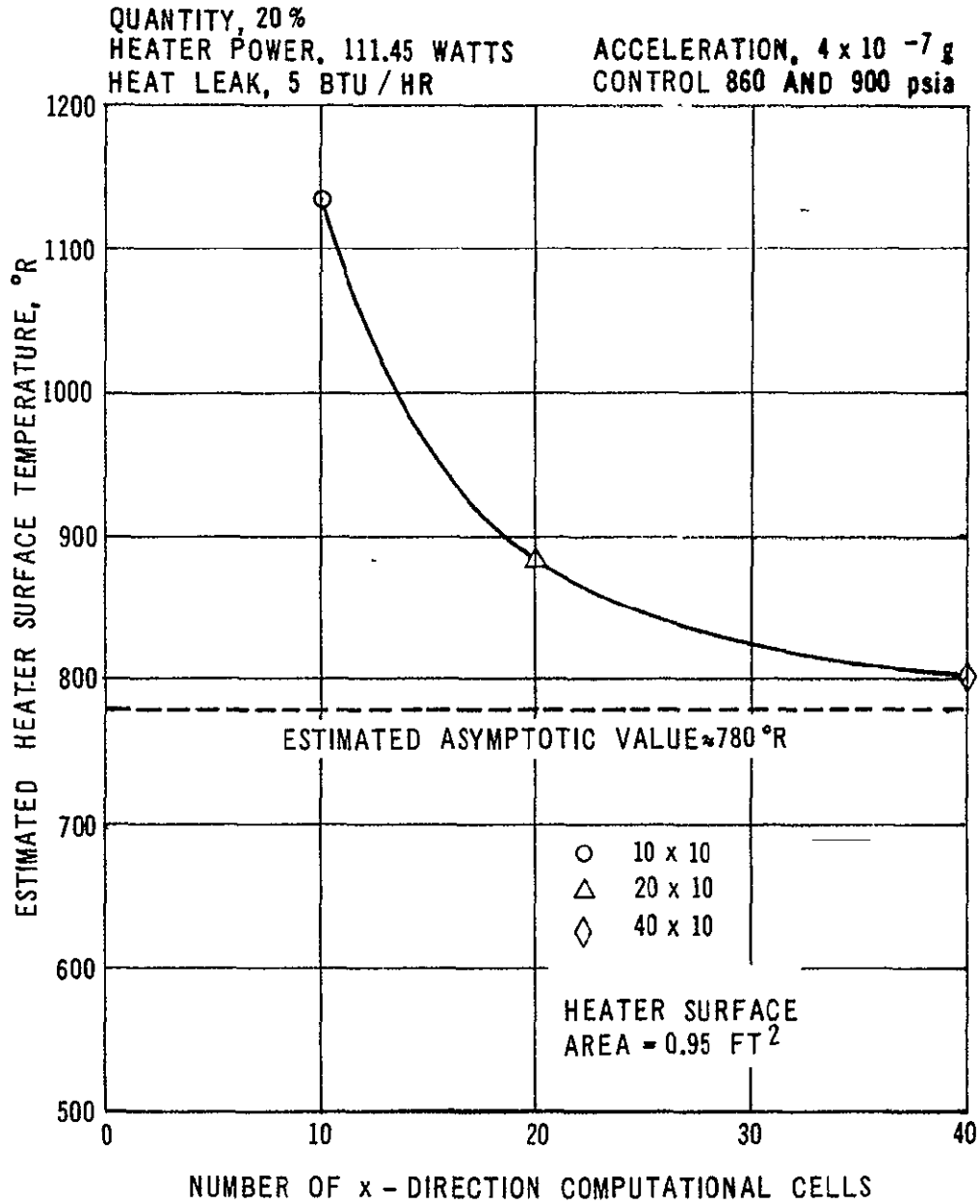


FIGURE 3-13 APOLLO 14 OXYGEN TANK NO. 3 EVA TEST HEATER TEMPERATURE PREDICTION AT 20% QUANTITY

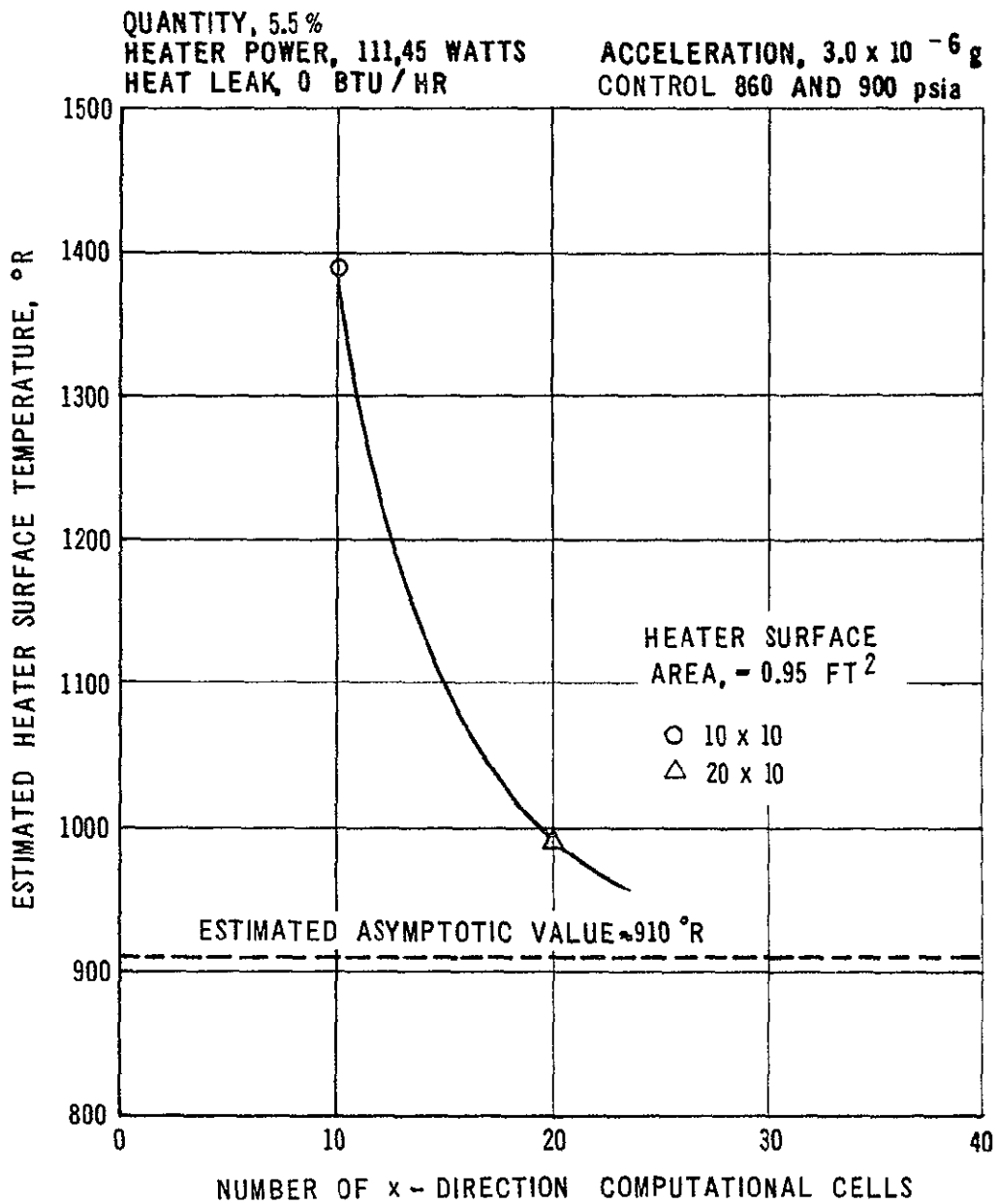


FIGURE 3-14 APOLLO 14 OXYGEN TANK NO. 3 TEST HEATER TEMPERATURE PREDICTION AT 5.5% QUANTITY

QUANTITY 35 PERCENT
 ACCELERATION $7 \times 10^{-8}G$
 GRID SIZE 60 X 10

HEATER POWER 70.5 WATTS
 HEATER AREA 0.95 FT. SQ.
 THERMAL MASS 0.10 BTU/DEG R

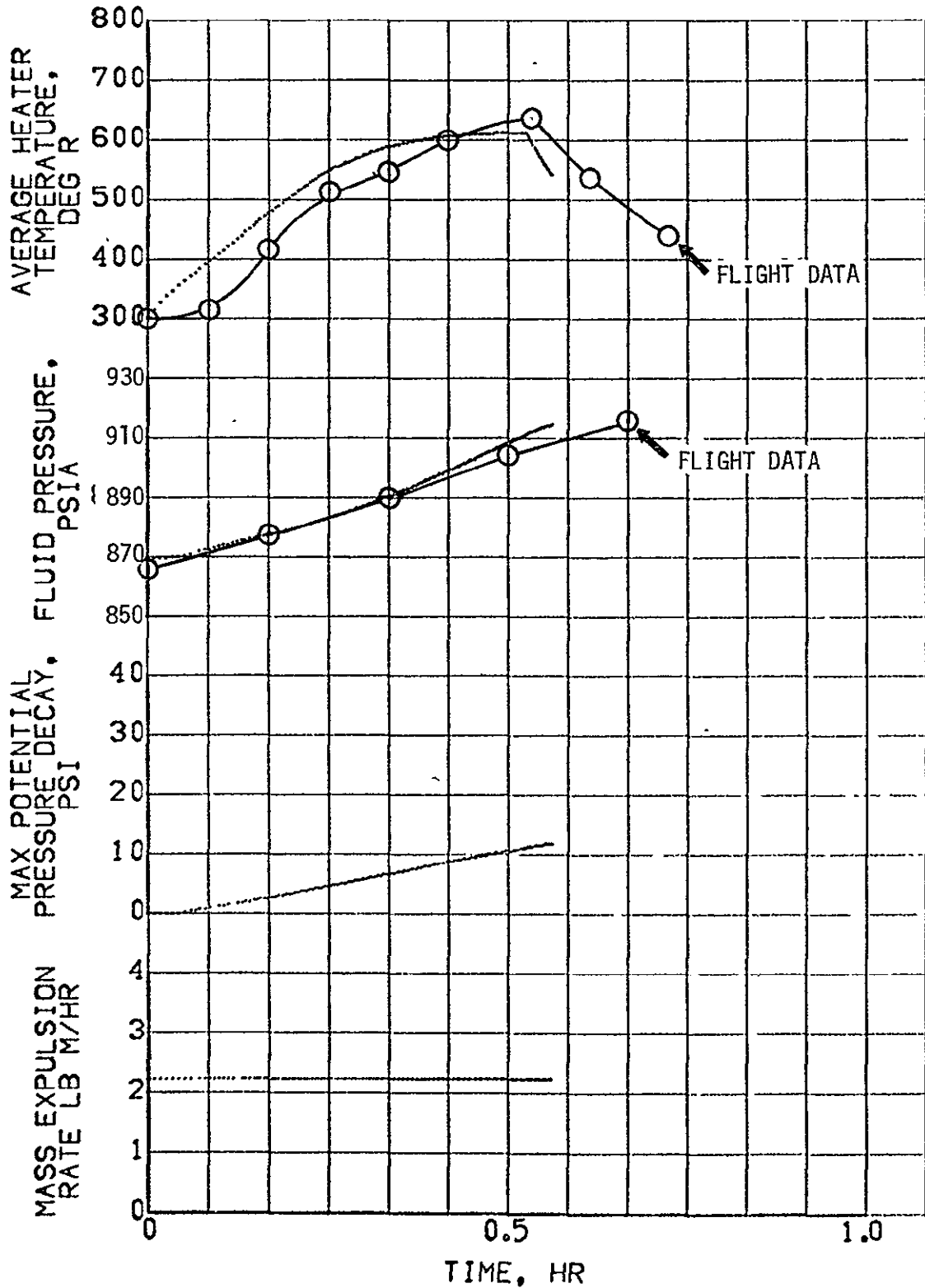


FIGURE 3-15 ATTITUDE HOLD HEATER CYCLE - 0.95 FT² HEATER AREA

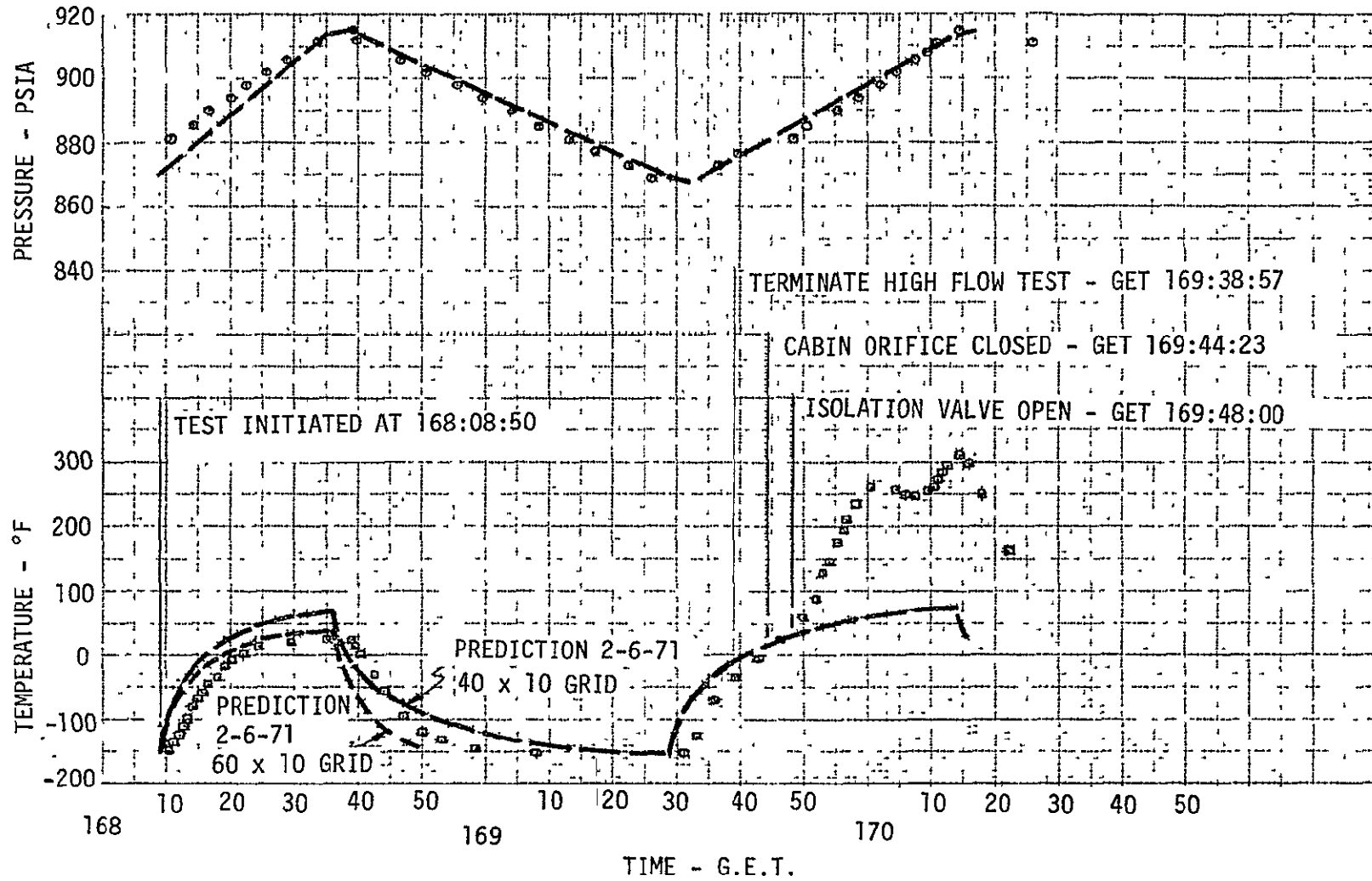


FIGURE 3-16 REAL TIME HIGH FLOW TEST SIMULATION

3.3.2 Math Model Conversion

The basic oxygen stratification math model developed under NASA-MSC contract NAS9-10364 was converted to FORTRAN V for operation on the NASA-MSC SRU-1108 computers. The converted model produced results in satisfactory agreement with the CDC-6600 results (Figure 3-17). This model was modified to include the effect of heater thermal mass and heater temperature sensor lag and was used exclusively to conduct the Apollo 14 Postflight Analysis. Comparisons of simulations with Apollo 14 flight data provided additional verification of the model prediction capability. The improved math model, including the variable grid, was converted to the SRU-1108 computer. Its prediction capability was evaluated by simulation of an Apollo 14 typical PTC heater cycle previously analyzed with the constant grid model. Comparison of results produced by the basic and improved math models (Figure 3-18) confirmed the satisfactory conversion and capability of the new model. The improved math model operation on the NASA-MSC SRU 1108 computers is described by Reference 11.

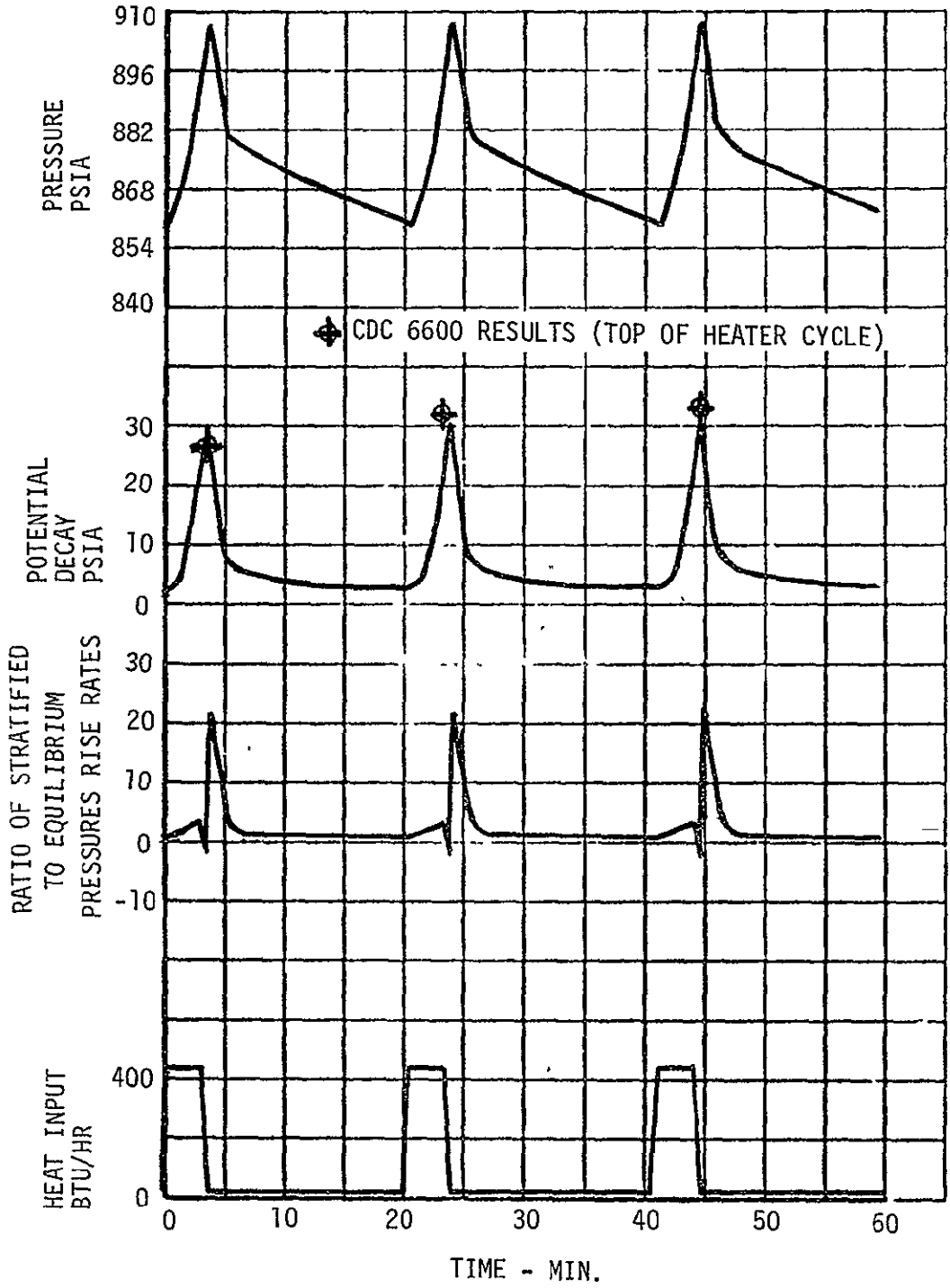


FIGURE 3-17 CONVERTED MATH MODEL RESULTS VERIFICATION

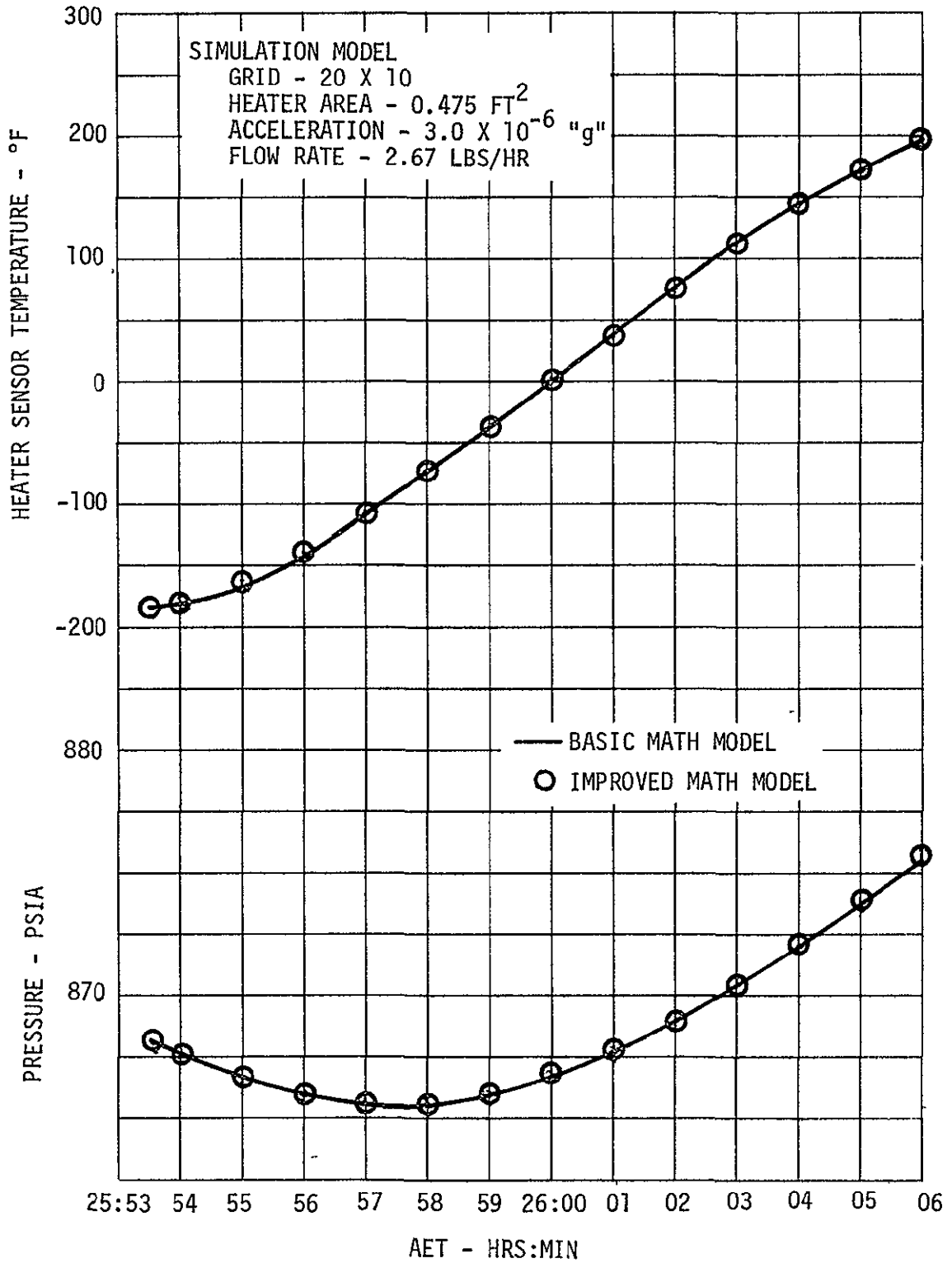


FIGURE 3-18 IMPROVED MATH MODEL CONVERSION VERIFICATION

3.3.3 Apollo 14 Postflight Analysis

Flight periods for simulation were selected with the concurrence of the technical monitor in order to demonstrate prediction capabilities for important tank performance parameters. The selected periods included the most critical flight conditions, flow rates and tank quantities. The bases for selecting the six flight periods analyzed are summarized by the table below.

<u>BASIS FOR PERIOD SELECTION</u>	<u>FLIGHT CONDITION</u>	<u>TANK QUANTITY</u>	<u>AET</u>
Nominal Heater Cycle	PTC	54%	26:00
Maximum Quantity for EVA Flow Rates	DTO	72%	167:00
Minimum Quantity for EVA Flow Rates	DTO	20%	167:00
Maximum Pressure Decay	Attitude Hold	97%	5:00
Short Heater Cycles	Attitude Hold	92%	11:00
Heater Temperature at Low Quantity	PTC	15%	186:00

These flight periods were simulated on the NASA-MSD SRU-1108 computers using the stratification math model. The simulations used input parameters, either measured or computed from flight data. These included acceleration levels, initial tank pressures, initial heater temperatures, percent quantity of fluid, and fluid flow rates. The simulations resulted in heater cycles, potential pressure decay and heater temperature; these were then compared to actual values of these parameters demonstrated in flight. The comparison showed that the Apollo 14 cryogenic oxygen system operated satisfactorily. In addition, this effort showed that the stratification math model could accurately predict system performance with certain limitations. The results of the simulation and discussions of math model adequacy are presented in the following paragraphs.

NOMINAL HEATER CYCLE

A PTC heater cycle at AET 26:00 was simulated to verify nominal system operation. The results of this analysis established a baseline for selecting model parameters for other flight periods simulated. This analysis was initiated before postflight "g" data were available, and an acceleration of 3.0×10^{-6} "g" was estimated from available data for guidance rotation rates. The flight acceleration data (Reference 12) confirmed that the average acceleration was within about 10% of the estimate. The average tank flow rate during the pressurization cycle was 2.67 lbs per hour including ECS and fuel cell flow rates of .94 and 1.45 lbs/hour, respectively, and .28 lbs/hour into the surge tank.

NOMINAL HEATER CYCLE (Continued)

Simulation results for heater sensor temperature for two different heater areas bracketed flight data (Figure 3-19). The small area simulation was made with a heater area of 0.475 ft^2 , which is the flat plate area equivalent to the 0.59 ft^2 outer surface of the cylindrical heater tube. Since the heater tube is perforated, flow through the tube could provide a flat plate area equal to the areas of the inner and outer tube surfaces, a total of 0.95 ft^2 . Analyses were conducted for both heater areas to determine which provided the most accurate simulation of sensor temperature and pressurization time. The large heater area reduced the heater sensor temperature, and the time required to pressurize was also reduced; because the small heater at higher temperature stored more thermal energy. Simulated pressure results lag behind flight data early in the stroke due to averaging the flow into the surge tank over the cycle.

The asymptotic limit for the heater temperature with the 0.475 ft^2 area is within 9°F of the flight data, while the heater on time for the same area is within 40 seconds of the flight data (Figure 3-20). These results are within the accuracy of the data itself. The asymptotic sensor temperature and heater on time with the larger heater area are not in good agreement with flight data, which implies that the inside of the heater tube was not an effective heat transfer surface. At this 54% tank quantity, nominal tank performance was closely simulated with a heater area of 0.475 ft^2 . Satisfactory convergence in this quantity range was obtained with maximum grid sizes of 60×10 .

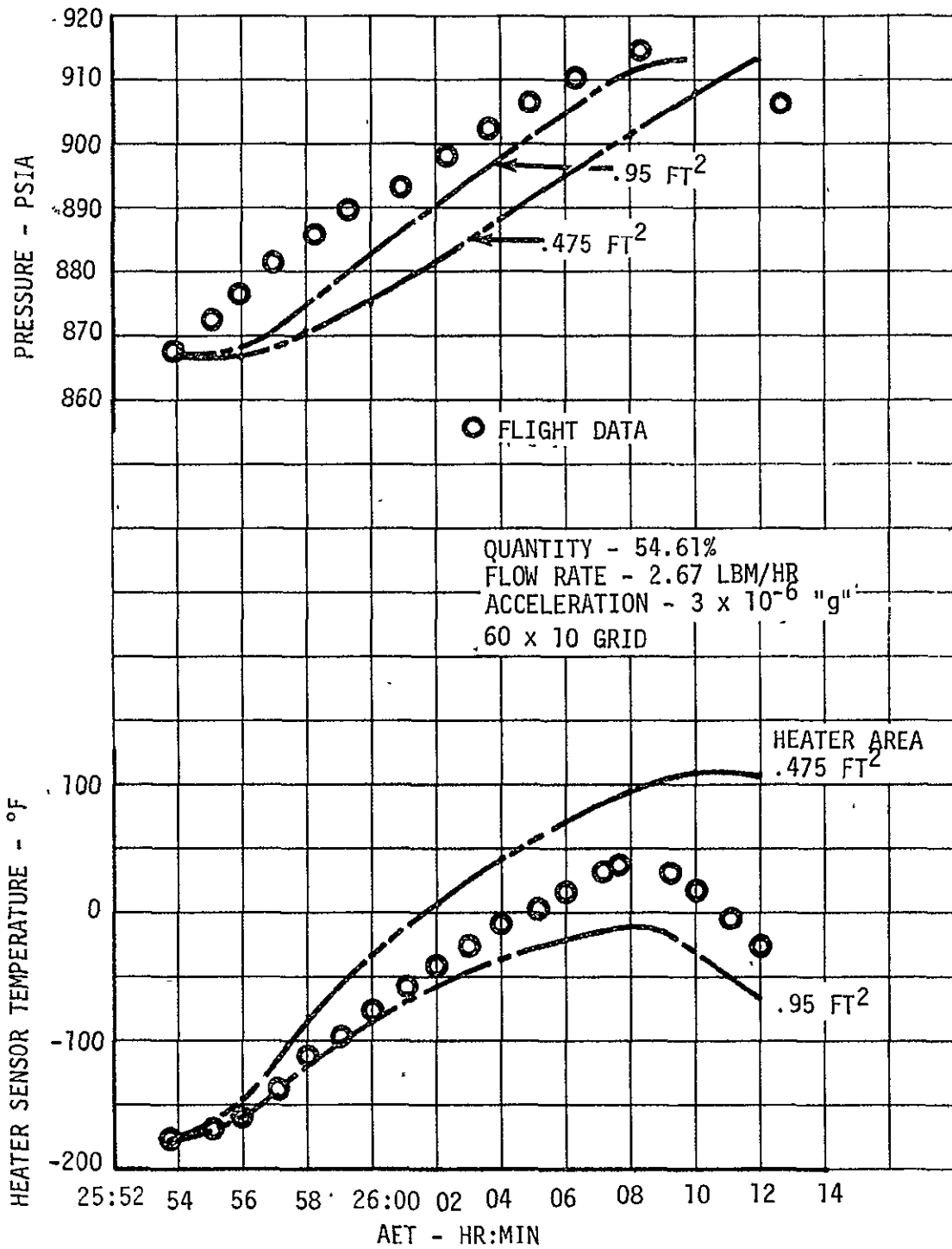


FIGURE 3-19 PTC HEATER CYCLE SIMULATION

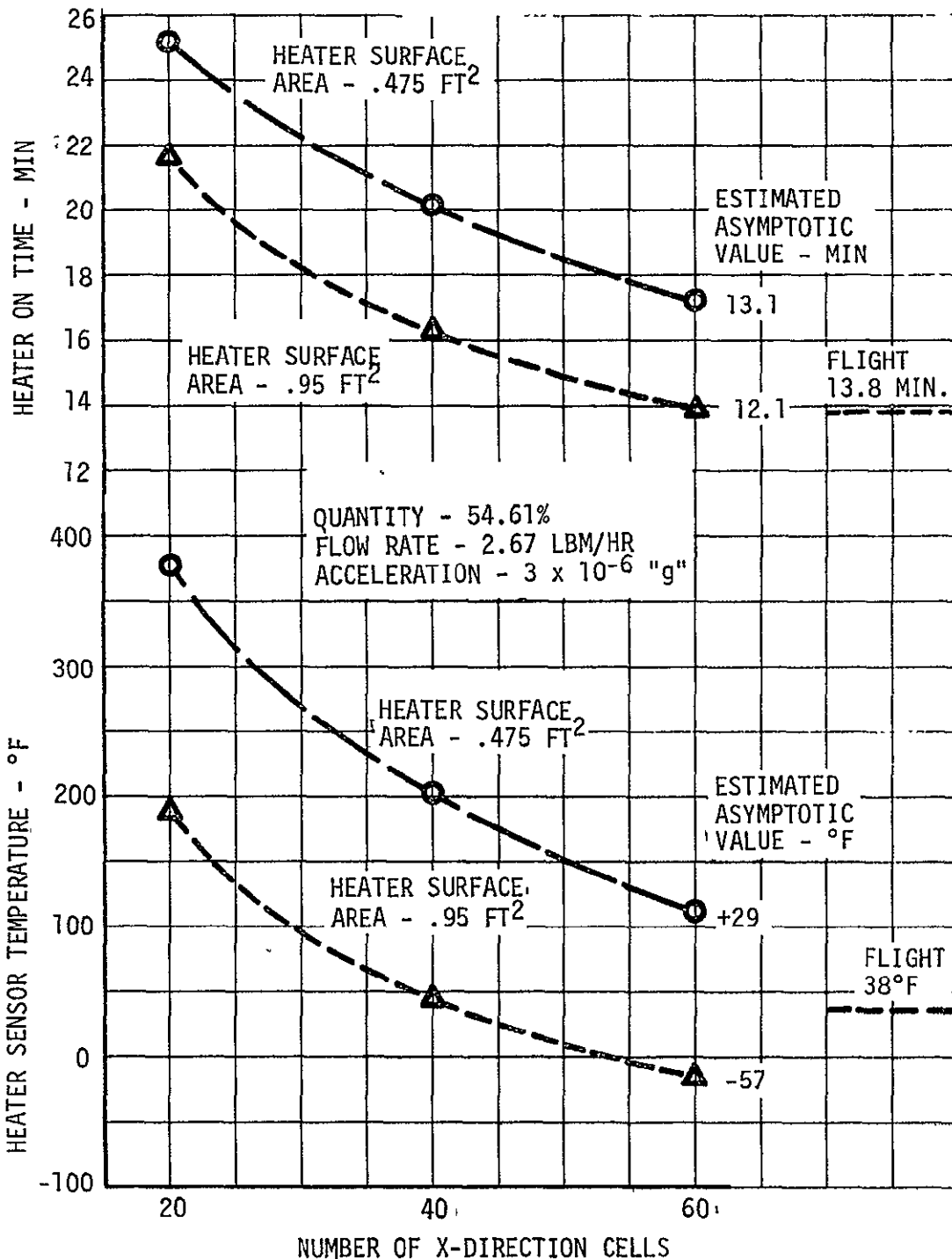


FIGURE 3-20 PTC HEATER CYCLE CONVERGENCE

MAXIMUM QUANTITY FOR EVA FLOW RATES

Simulations of the tank 1 high flow test at AET 167:00 were performed with time dependent flow rates calculated from ECS and fuel cell demands. The tank acceleration of $4.7 \times 10^{-6}g$ used for the simulation was calculated from the oxygen vent thrust. Abrupt changes in tank flow rates (Figure 3-21) occurred during the test period because tank 1 and tank 2 alternately supplied fuel cell flow rates. The heater cycles simulated with a 40×10 grid and heater area of 0.95 ft^2 are in poor agreement with flight data early in the simulation (Figure 3-21). The tank flow rates were investigated to determine if they could differ from the fixed demands used to perform the simulation enough to cause the error in heater cycles. Flow rates calculated from the actual tank pressure change rates by equilibrium thermodynamics indicated negative flow rates (flow into the tank) during part of the period (Figure 3-22). The large differences between flow rates based on demands and flow rates based on tank pressures indicated that flow rate errors caused the simulation inaccuracy.

The plumbing system thermodynamic behavior was investigated as a possible source of flow rate errors. When the demand flow rapidly increases, a cold, dense slug of fluid is drawn from the tank into the warm tubing. The density of the fluid inside the tank is approximately ten times the density of the fluid at the ambient temperature in the system plumbing. If no heat transfer is assumed between the hot and cold fluid, then to maintain pressure in the lines an equal volume of cold fluid must replace the volume of hot fluid. The tank flow rates will exceed the average system demand for some period of time to fill the lines with cryogenic fluid after the demand increases. This phenomena was investigated by using the existing math model to simulate the plumbing response to sudden high flow demands. The simulation outflow rate was 2.5 lbs/hour at 60°F and the inflow rate was 25 lbs/hour at the tank temperature of -195°F .

The simulated line pressure decreased for the first 15 seconds even though the inflow was an order of magnitude higher than the outflow (Figure 3-23). The pressure decrease with the high flow into the line confirms that the plumbing system could cause gross variations in tank outflow. After the lines were initially filled with cold cryogenic fluid the thermal capacitance of the system could cause sufficient pressure rise in the line to cause flow back into the tank. No attempt was made to analyze this effect for the duration of the high flow test, because computer time requirements are prohibitive with the existing model. The simulation of the line response for 18 seconds required more than one hour of computer time. It was concluded that large variations in the tank 1 flow rates occurred during the first few heater cycles of the high flow test as a result of plumbing system thermodynamics.

MAXIMUM QUANTITY FOR EVA FLOW RATES (Continued)

The tank flow rates could be adequately established for simulations for only the last heater cycle during the high flow test when the plumbing was near thermal equilibrium. Simulations of the last heater cycle were made with the model flow rate adjusted on the basis of pressure to properly include the fuel cell flow demands. Under these conditions, fair agreement was obtained with the flight pressure response for the 80 x 10 grid with a heater area of 0.95 ft² (Figure 3-24). The heater-on time however, did not converge, indicating that the heater boundary layer was not adequately resolved.

The maximum potential pressure decay immediately preceding termination of the high flow test was 32.3 psi. A pressure decay was not observed in flight because the tank 1 heater was turned off at 169:34 and no significant vehicle maneuver occurred to abruptly mix the fluid before the potential pressure decay had dissipated. The maximum decay potential could have been substantially greater if the test had continued for the full three hours or if the acceleration level had been lower.

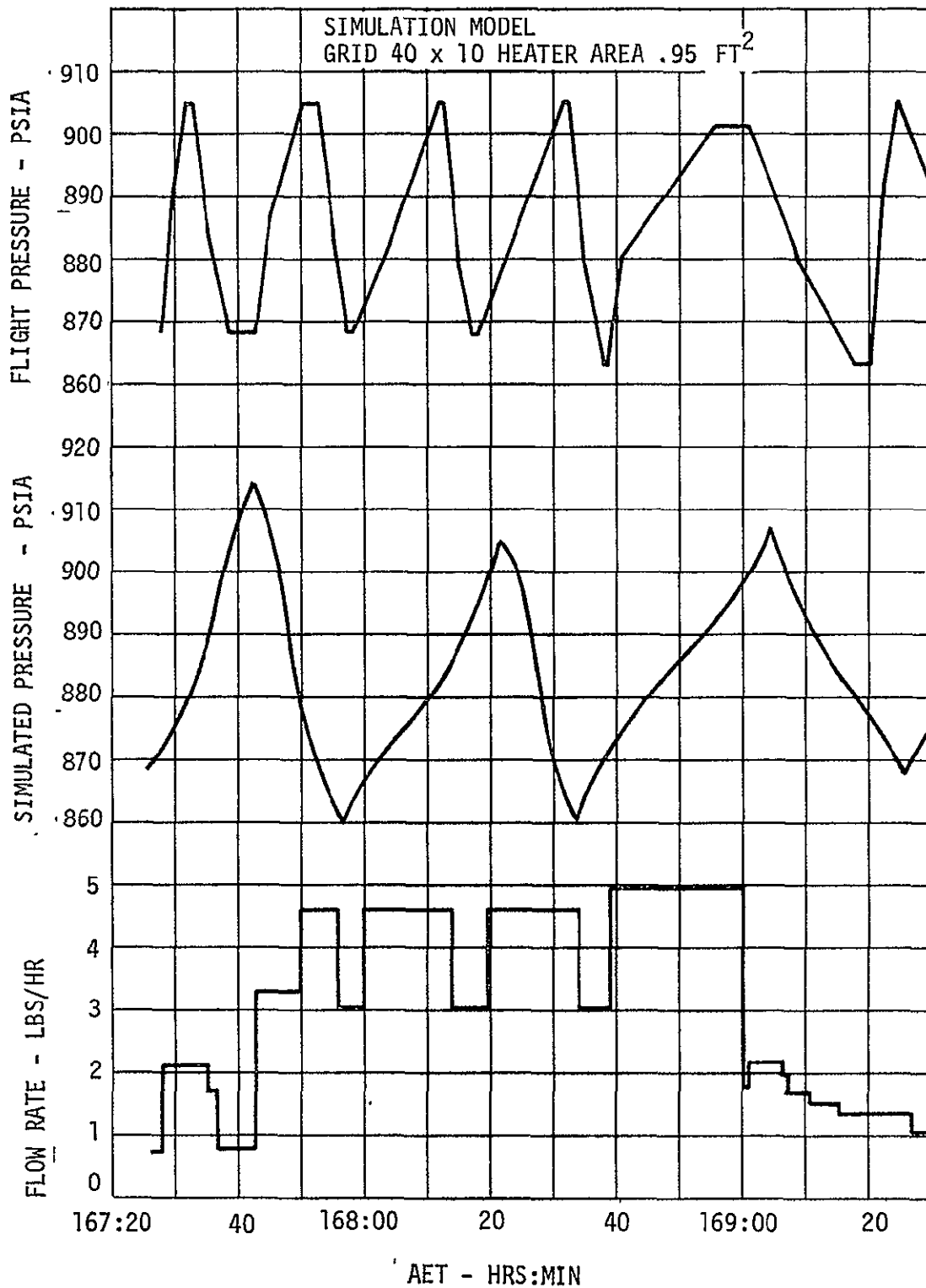


FIGURE 3-21 TANK 1 TEST SIMULATION - 0.95 FT² HEATER AREA

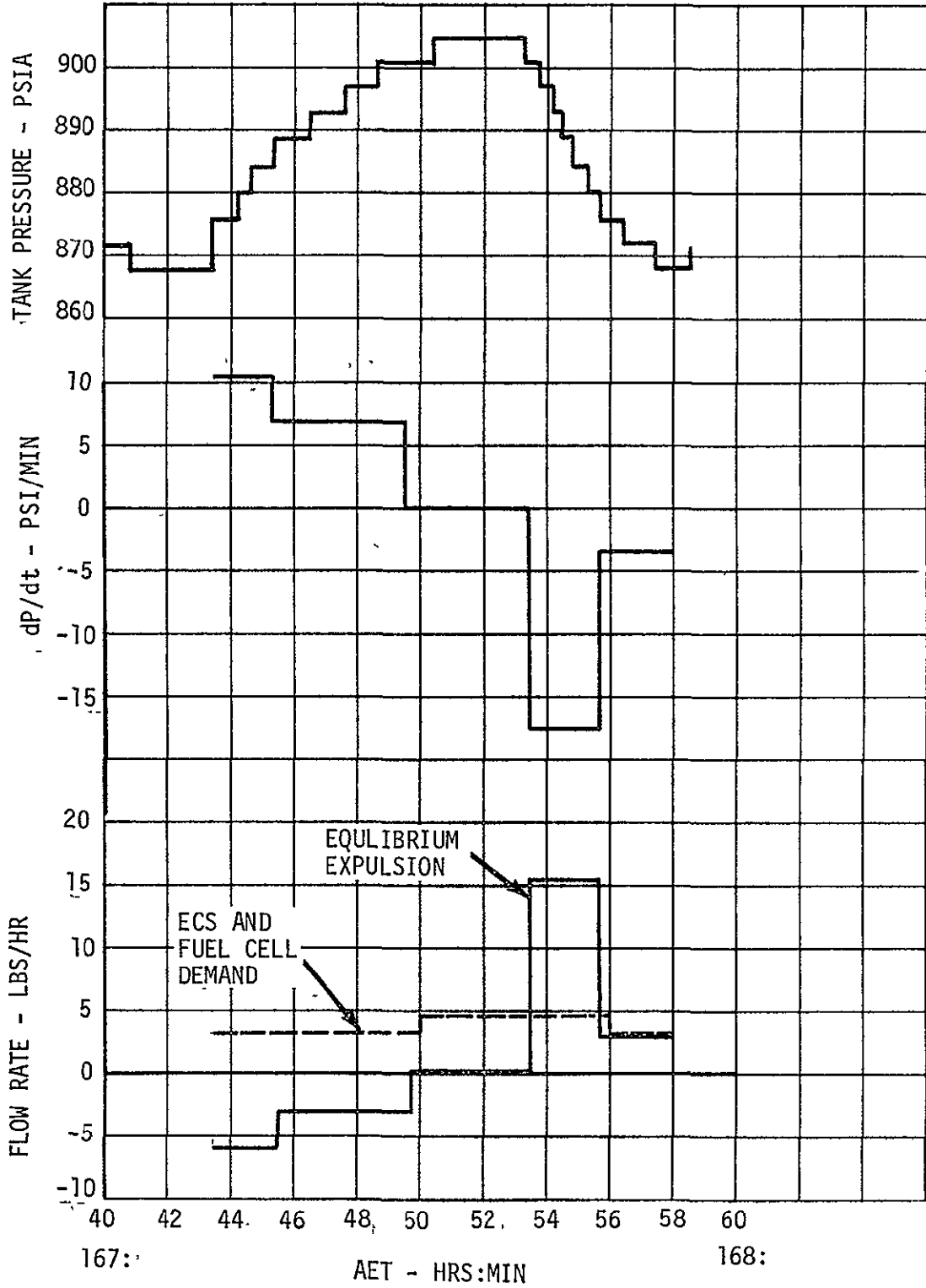


FIGURE 3-22 TANK 1 TRANSIENT PRESSURE AND FLOW RESPONSE

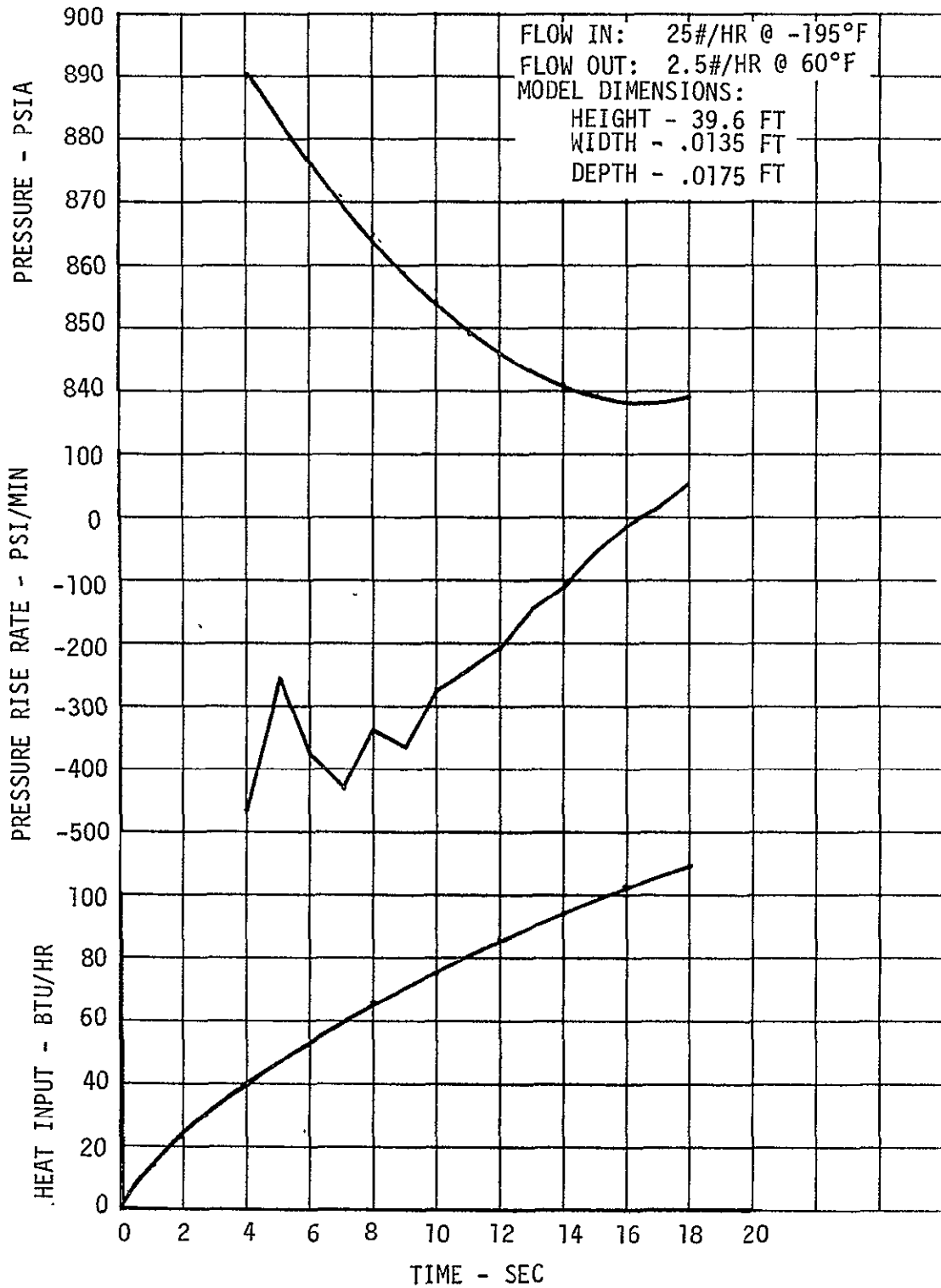


FIGURE 3-23 PLUMBING SYSTEM PRESSURE RESPONSE WITH HIGH FLOW RATES

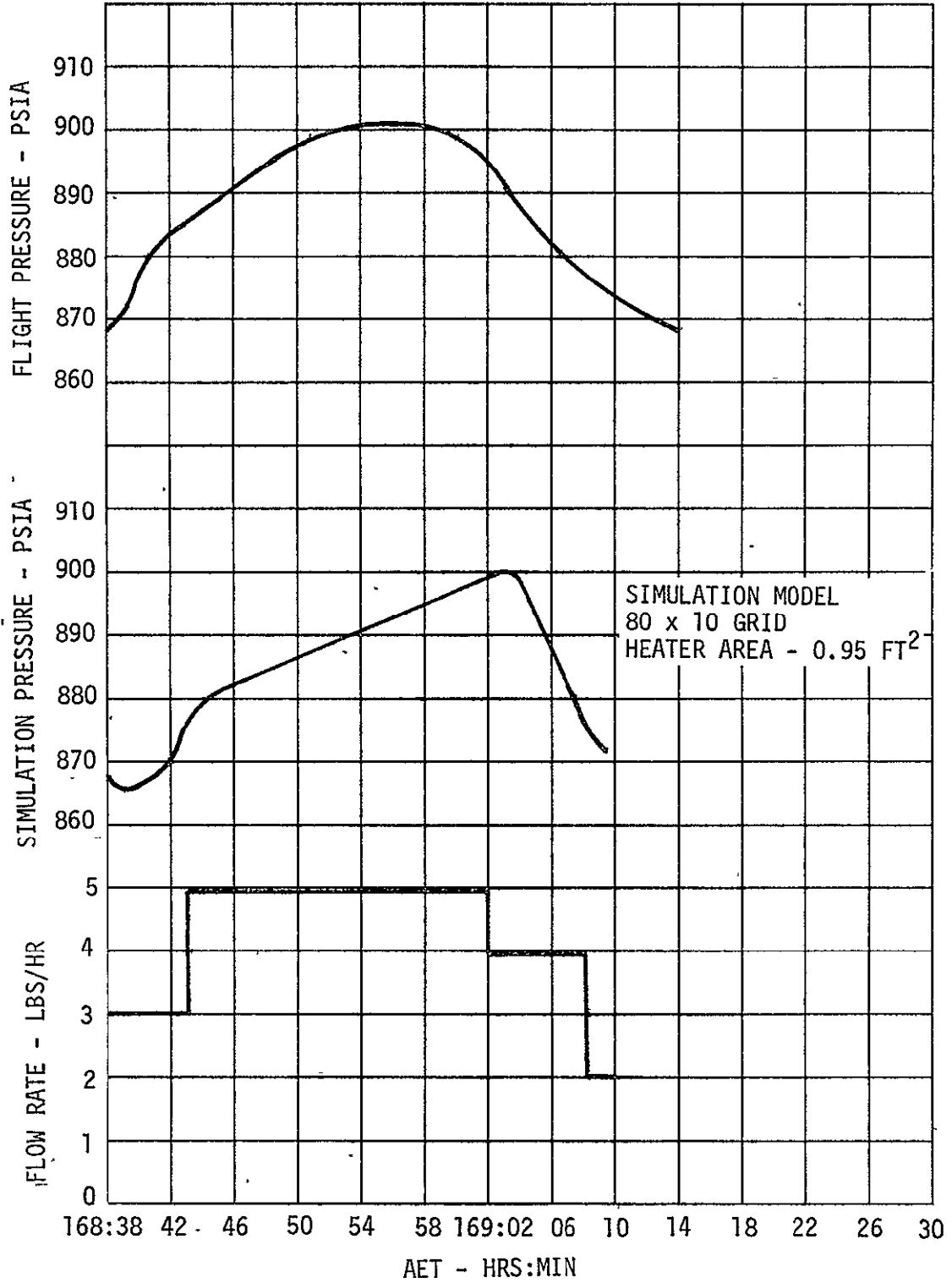


FIGURE 3-24 TANK 1 TEST SIMULATION WITH PRESSURE DEPENDENT FLOW RATE

MINIMUM QUANTITY FOR EVA FLOW RATES

Simulations of the tank 3 high flow tests at AET 167:00 were performed with heater areas of 0.95 and 0.475 ft². Expulsion rates were based upon ECS and fuel cell demands and the acceleration level of 4.9×10^{-6} "g" during the first part of the test was calculated from the thrust produced by the oxygen being vented overboard during the test. The acceleration near the end of the simulation period was assumed to be 7×10^{-8} "g", which is typical of the attitude hold condition. The DTO was terminated at the end of one and one-half hours instead of the planned three hours. The heater power was manually changed from 70 watts (2 elements) to 110 watts (3 elements) near AET 169:09. The results of a simulation with a heater area of 0.95 ft² and a grid of 40 x 10 are in good agreement with flight data for the entire period simulated (Figure 3-25). This particular combination of grid size and heater area predicted a heater sensor temperature of 23°F, above the observed temperature at end of the first heater cycle. During the second pressurization cycle, the test was terminated and the cabin orifice closed. The simulation tank acceleration dropped almost two orders of magnitude. Instead of saturating at a temperature comparable to the first cycle, the heater sensor continued to rise. When the heater power was stepped up from 70 to 110 watts, the temperature rise rate increased even more. The sensor continued to rise to 310°F showing no tendency to saturate, when the heater was turned off by the pressure switch at 169:34.

By comparing the results of combinations of grid and heater area with flight data (Figure 3-25), the 40 x 10 grid and larger heater simulates the high flow test pressure and temperature response better than any other combination. However, the asymptotic heater temperature with the 0.95 ft² heater area converged 45°F below flight data while the temperature with 0.475 ft² area converged 60°F above flight data (Figure 3-26). The asymptotic estimates of time to pressurize also span flight data. Previous analyses of a PTC heater cycle at GET 26:00 indicated that a low quantity, a heater tube area of 0.475 ft² produced better agreement with flight data when the external variables of "g" level and flow rate were accurately defined. This discrepancy between the simulation results for the two periods may have been caused by the abnormal "g" vector during the DTO test. The tank acceleration caused by the oxygen vented during the test was not perpendicular to the heater tube as it was during the PTC period. The two-dimensional math model simulations necessarily assumed the acceleration perpendicular to the heater.

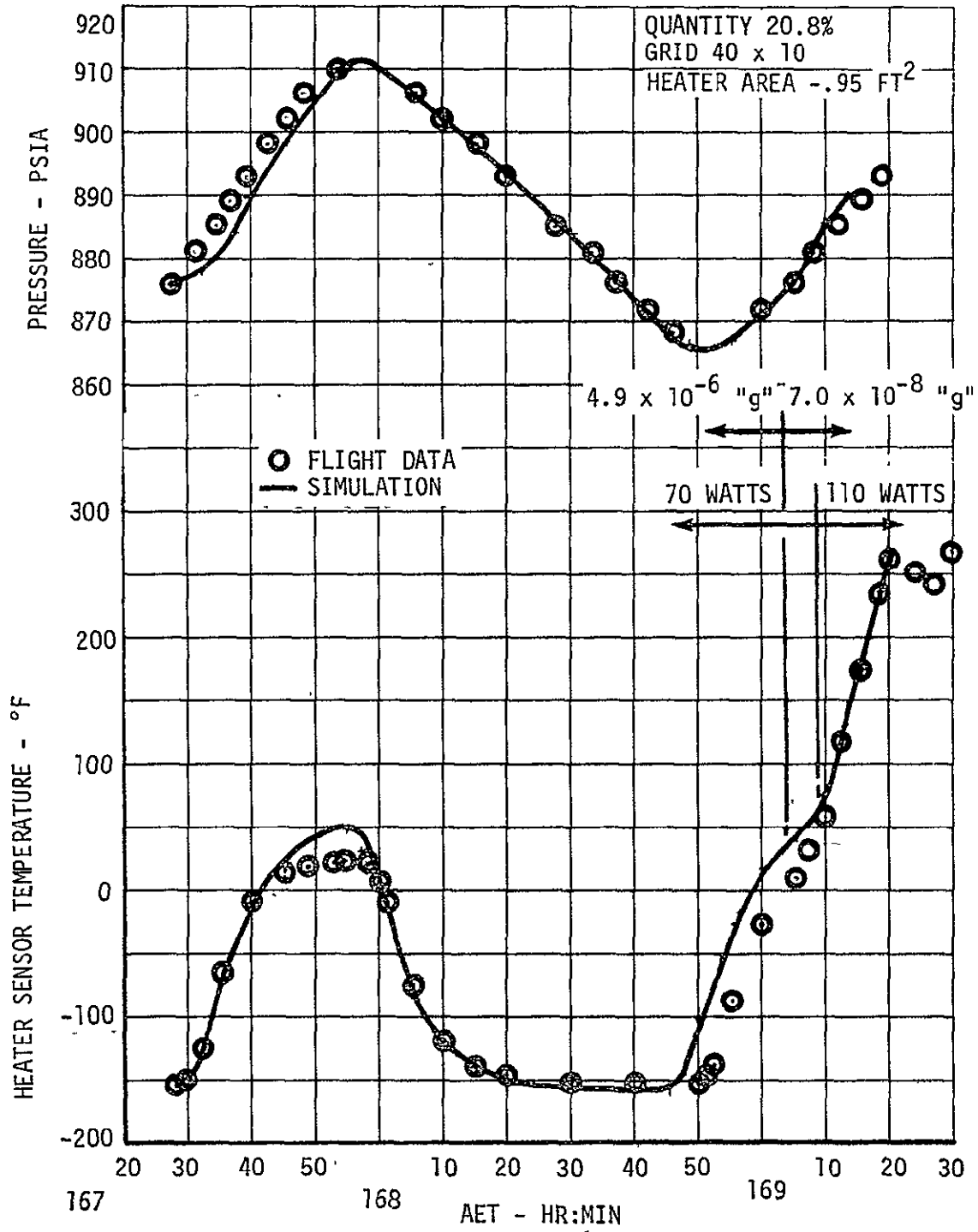


FIGURE 3-25 TANK 3 TEST SIMULATION

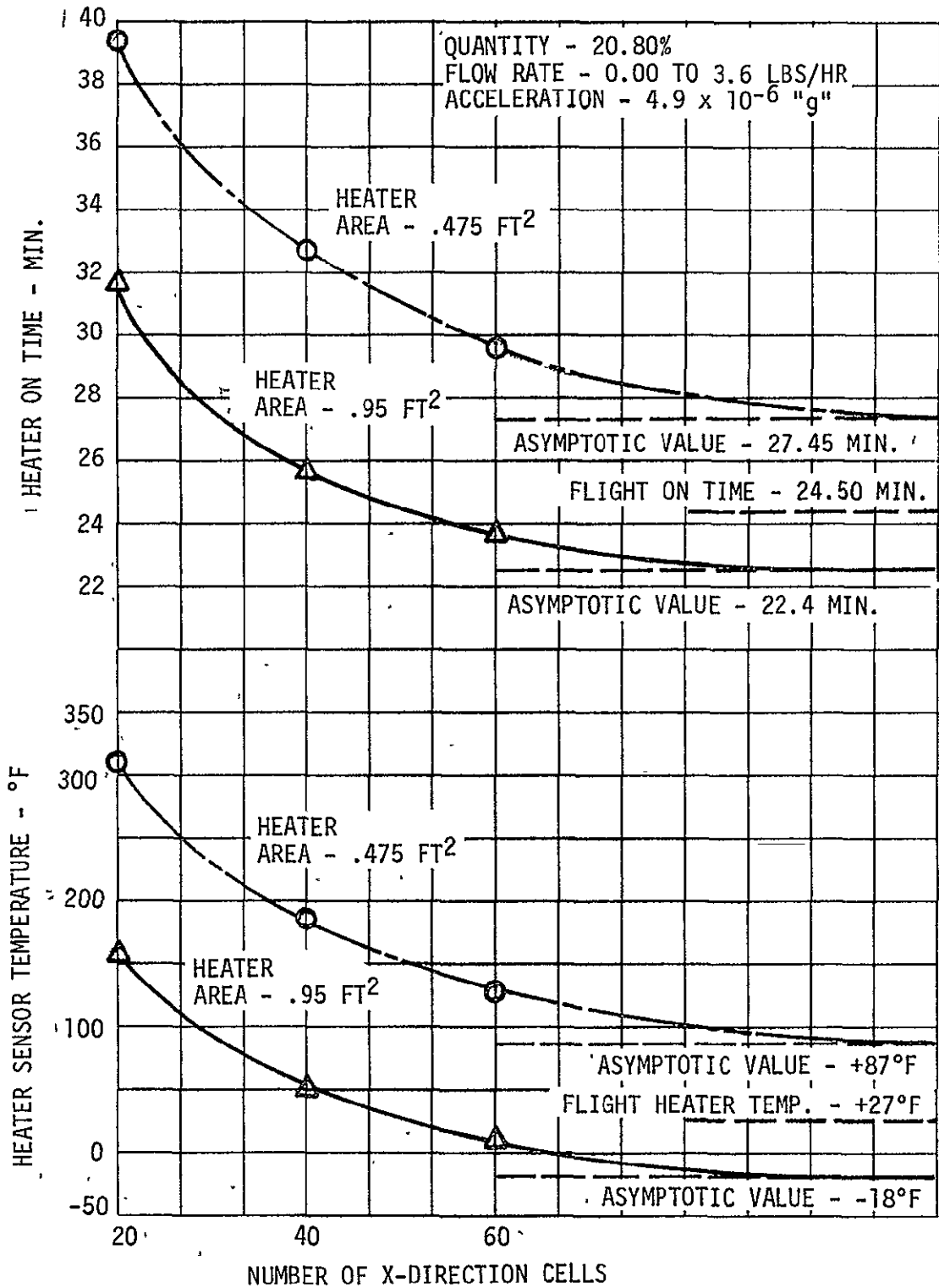


FIGURE 3-26 TANK 3 TEST CONVERGENCE

MAXIMUM PRESSURE DECAY

The only significant pressure drop during the flight of Apollo 14 due to stratification occurred during LM/CSM separation from the launch vehicle at AET 5:47. The tank 1 pressure dropped to 804 psia from an initial pressure in the control band of 868 to 905 psia. Prior to this at AET 4:57, docking caused the oxygen tanks to assume an equilibrium state which was maintained until the beginning of the next heater cycle at AET 5:14. The purpose of the simulation of this period was to predict the potential pressure decay at the time of separation from the launch vehicle.

The only available data for oxygen tank pressure and temperature during this period was manually recorded during the Apollo 14 flight. Thus, it was difficult to determine the exact starting conditions of the period to be simulated, the exact length of the heater on cycle, and the pressure in the tanks at separation.

Some difficulty with the stratification model stability was encountered during the simulation of this heater cycle. The instability was caused by a step down in acceleration level that occurred during the upstroke of the heater cycle. Because of a lack of sufficient computer core in the NASA-MSC SRU 1108 computers, a fine enough grid could not be utilized to avoid oscillation in the predicted potential decay after the step down in "g" level. The simulation instability caused the rise in the potential decay to be invalid after the acceleration change. The residual flows from the high "g" period during the first part of the period should cause the growth in potential pressure decay to be constant through the low "g" period. Therefore, since potential decay is a linear function of heater on time, the decay just before the "g" change was extrapolated to predict the later potential decay for each grid size (Figure 3-27). These predictions were extrapolated to an asymptotic value (Figure 3-28).

The pressure drop in flight could not be exactly determined due to the limitations of the available data, but was estimated to be between 59 and 100 psi. The maximum potential decay predicted by the simulation using the larger (0.95 ft²) heater size was 86 psia which agrees well with the flight data (Figure 3-28).

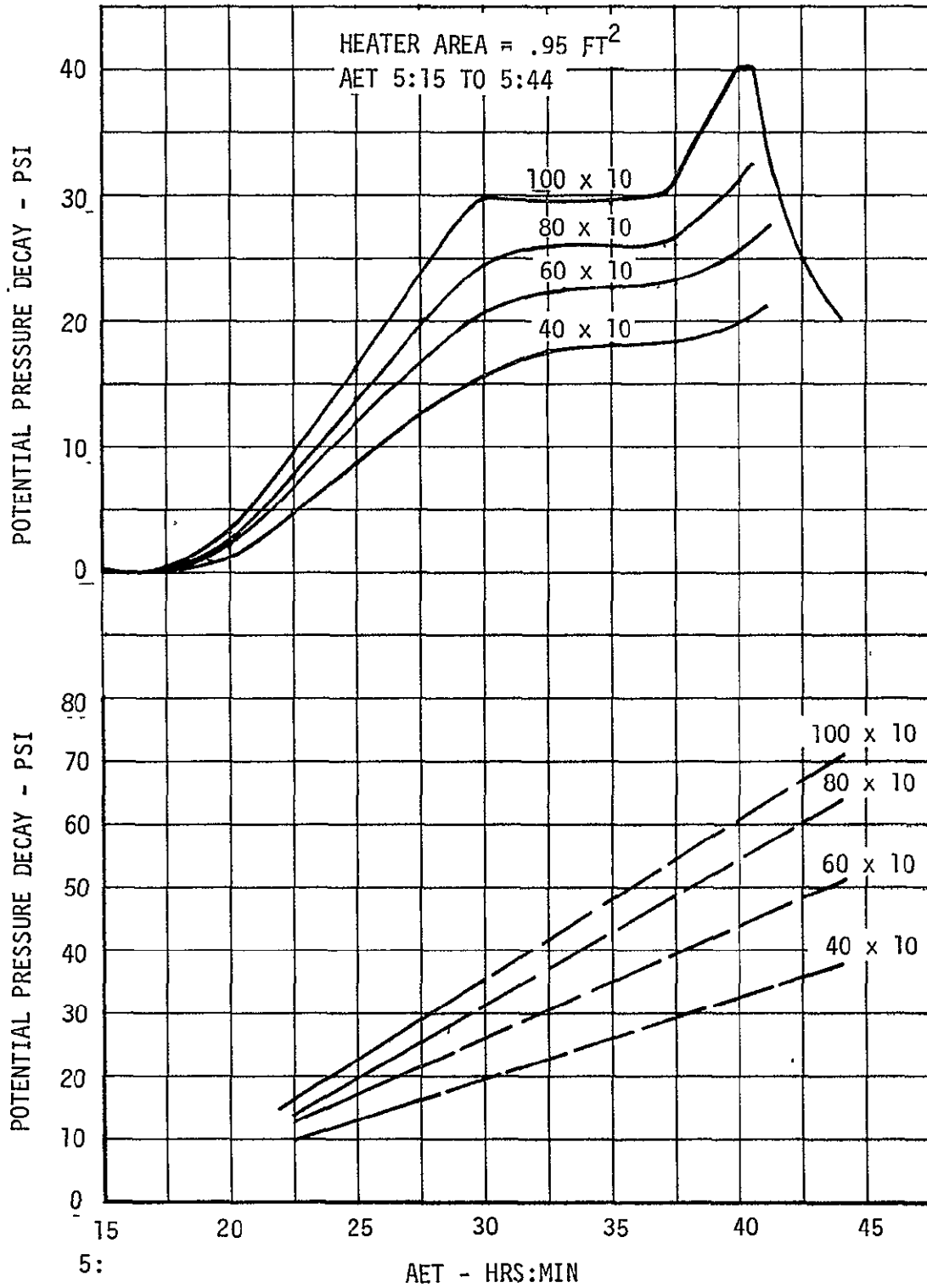


FIGURE 3-27 POTENTIAL PRESSURE DECAY, .95 FT² HEATER AREA

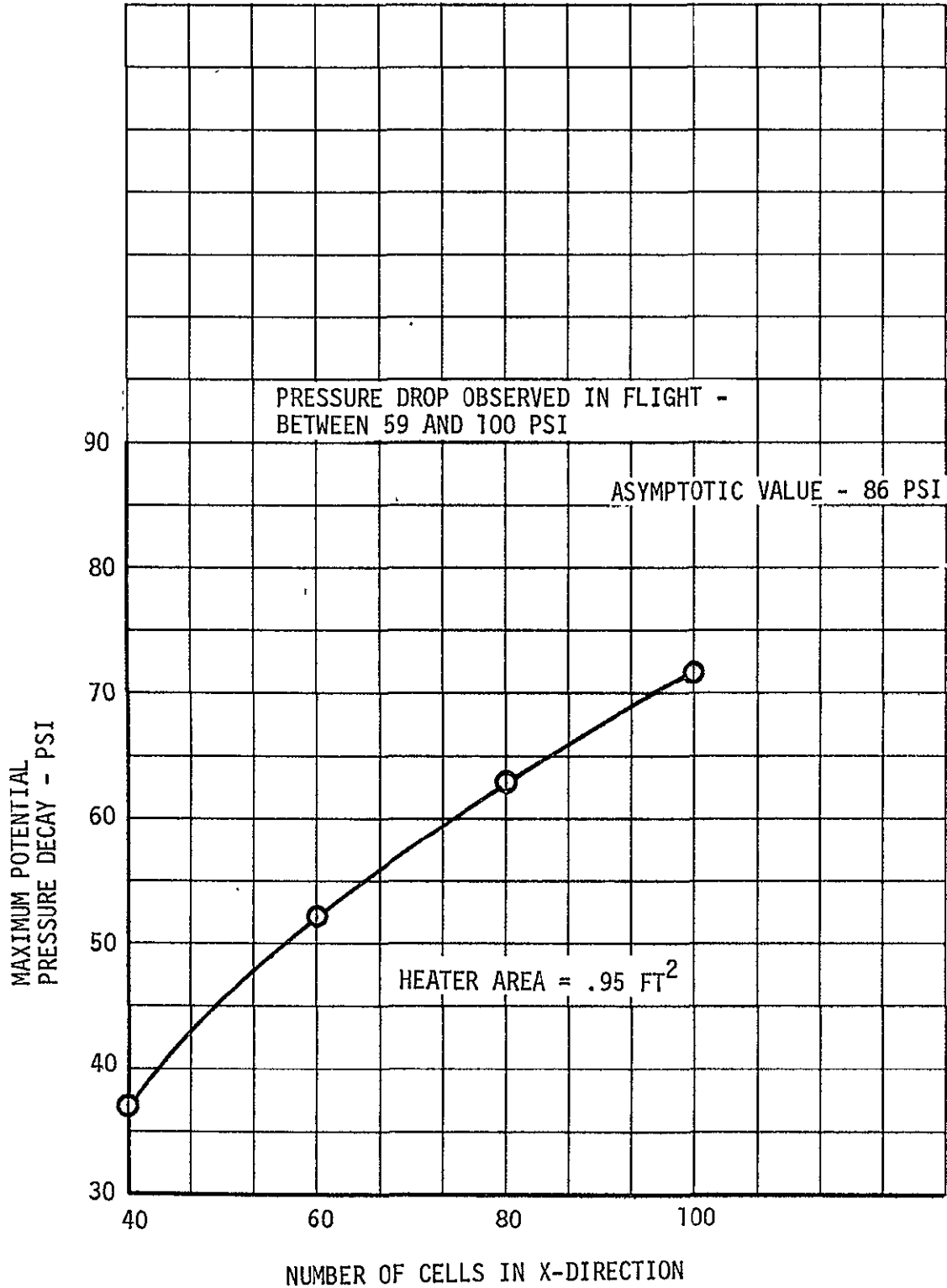


FIGURE 3-28 CONVERGENCE OF MAXIMUM POTENTIAL PRESSURE DECAY AT AET 5:44

SHORT HEATER CYCLES

During the period AET 10:30 to 12:30, oxygen tanks 1 and 2 were cycling in the automatic mode in attitude hold. At the start of this period, the total cycle time was approximately ten minutes, but by AET 11:30 the cycle time had shortened to six minutes. The minimum cycle time derived from equilibrium thermodynamics is 12.3 minutes. Because these unusually short cycle times were felt to be due to the effects of stratification, this period was chosen for analysis.

The simulation results of the 100 x 10 grid with the 0.95 ft² heater area are presented in Figure 3-29. The results of the simulation of total cycle time was not in good agreement with flight data. The trend of the pressure rise and fall times with grid size (Figure 3-30) indicate that if sufficient core were available on the computer to adequately resolve the boundary layer, an asymptotic value near flight data would be observed. Minimum heater temperature extrapolated to an infinite grid asymptote were within 1°F of the flight data (Figure 3-31). The maximum heater temperature (Figure 3-31) asymptotic value after one and one-half hours was within 12°F of the flight. The good heater temperature simulation confirms that the 0.95 ft² heater provides accurate results at high tank quantities.

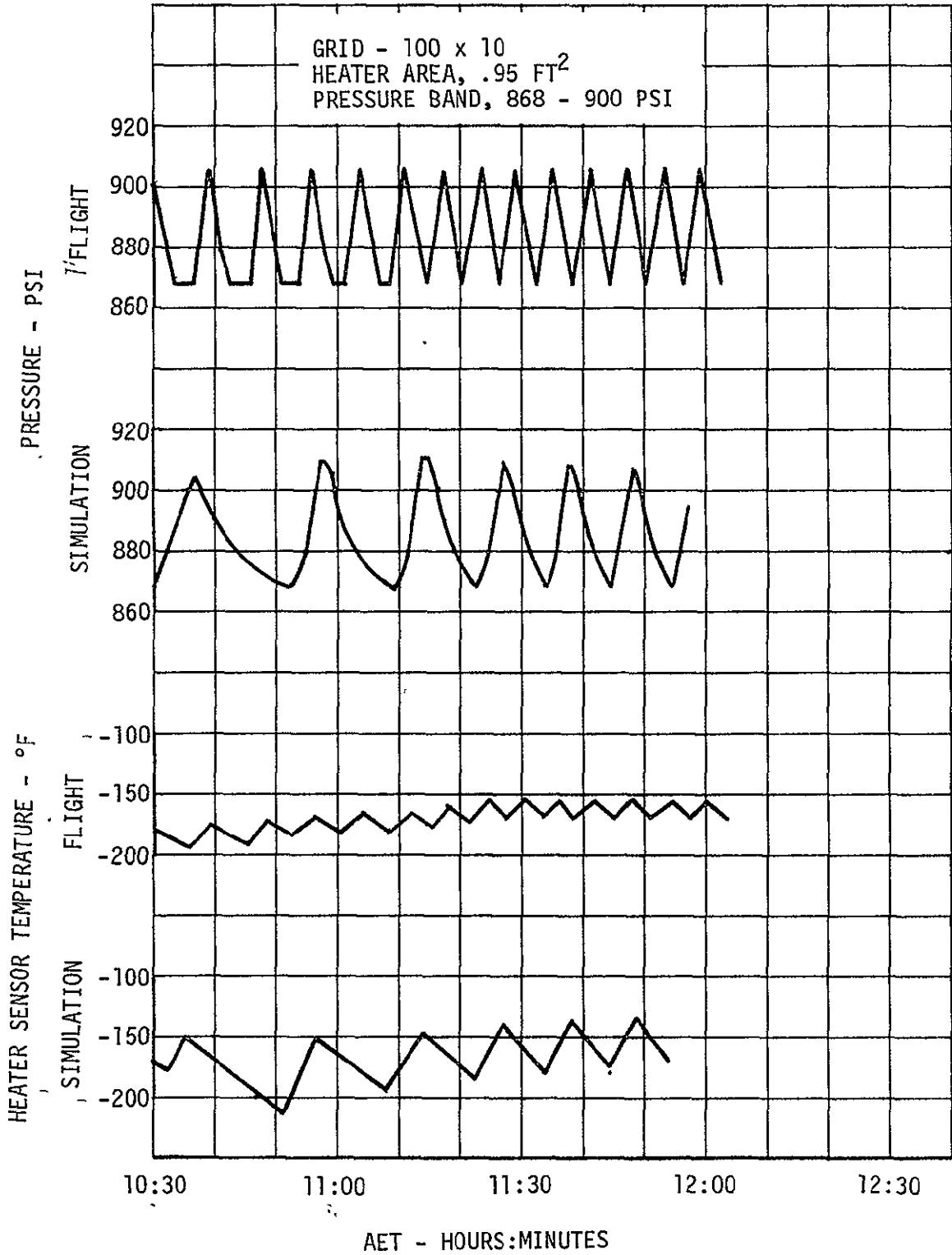


FIGURE 3-29 SIMULATION OF AET 10:30 TO 12:00 USING 100 x 10 GRID

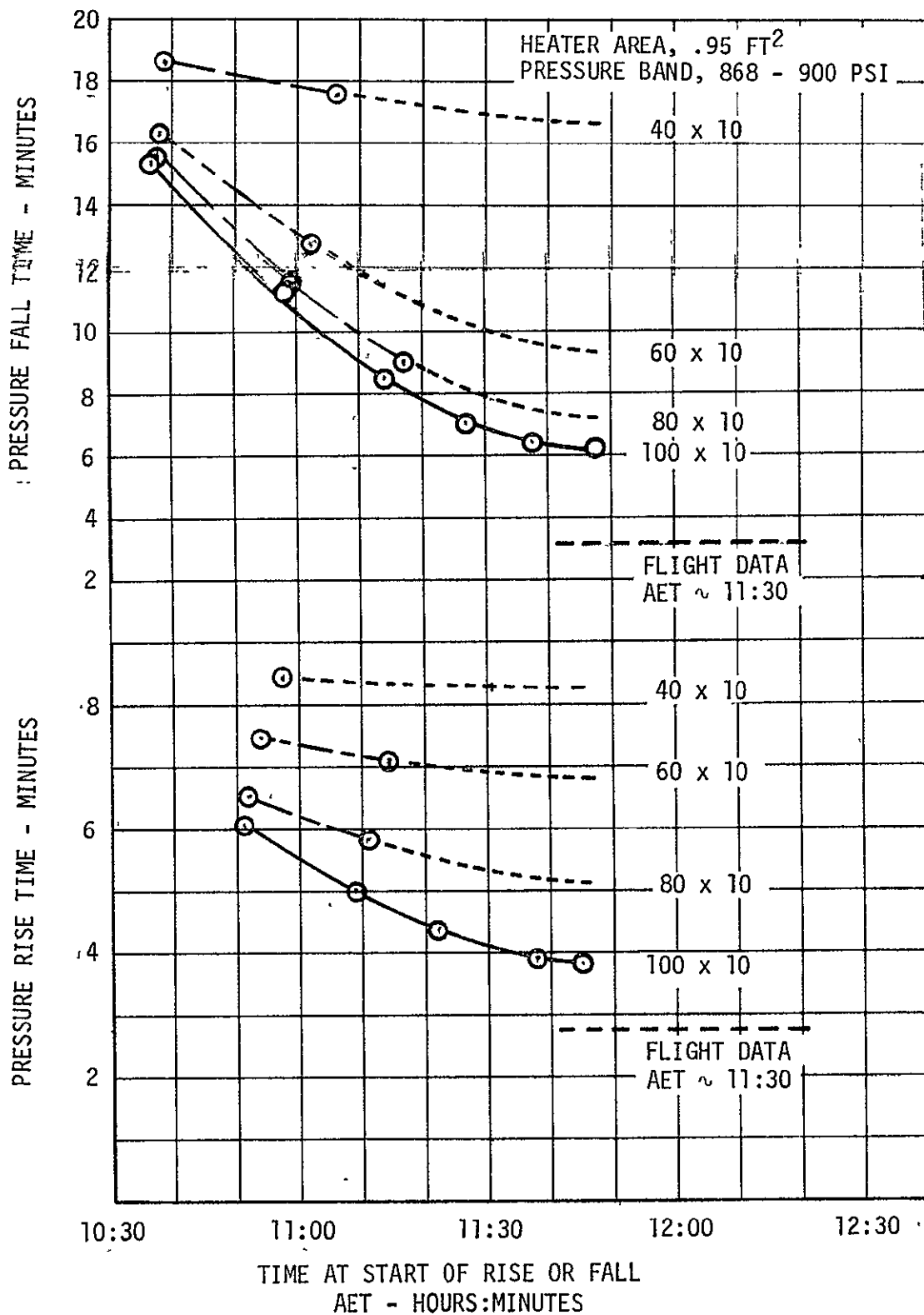


FIGURE 3-30 EFFECT OF STRATIFICATION ON LENGTH OF HEATER CYCLE

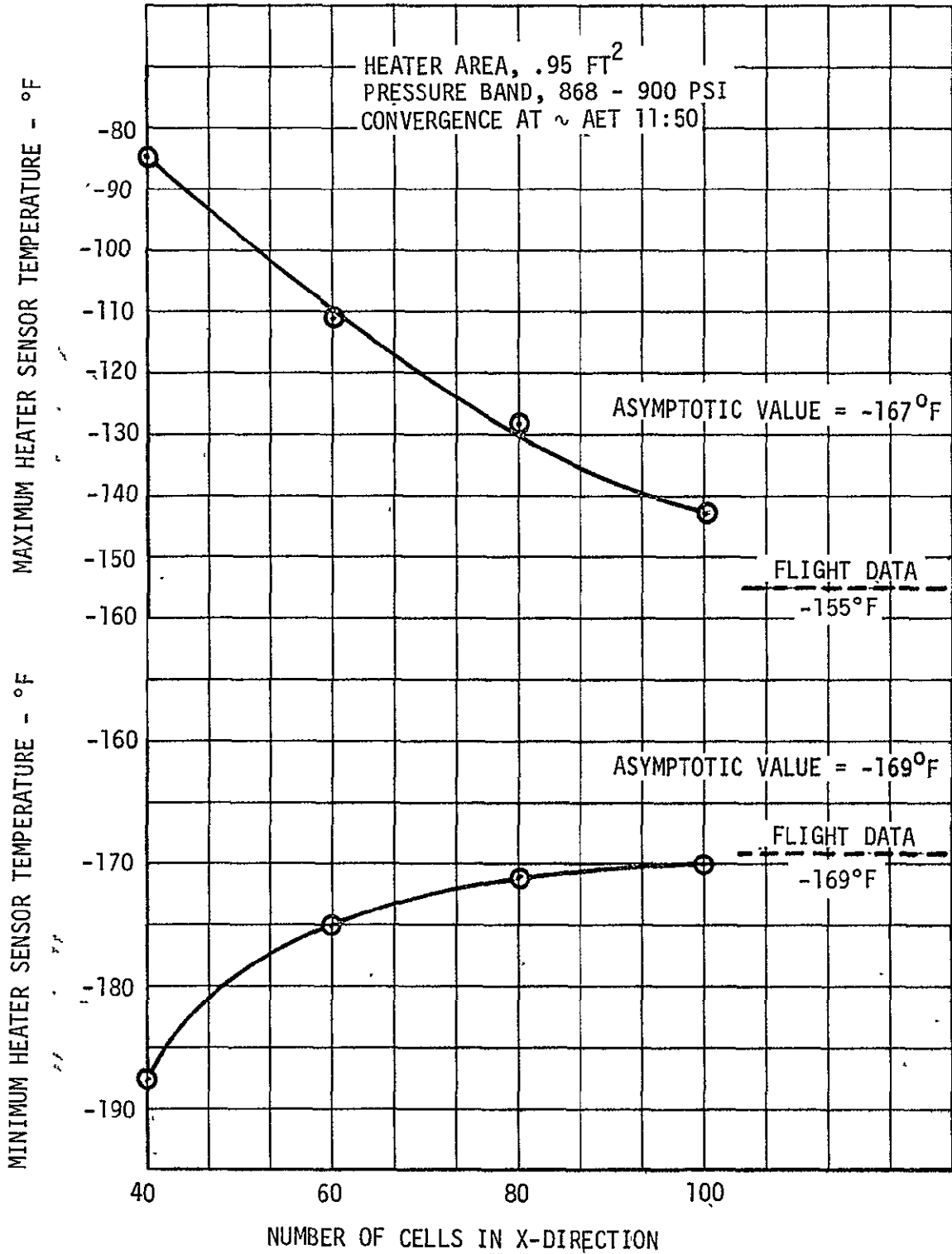


FIGURE 3-31 CONVERGENCE OF HEATER SENSOR TEMPERATURE AT AET 11:50

HEATER TEMPERATURE AT LOW QUANTITY

A heater cycle at AET 186:00 with 15% quantity was chosen for analysis to verify satisfactory heater-tank performance and the capability of the model to simulate performance at very low density. During this period, the vehicle was in a very weak PTC maneuver. Flight data show the acceleration on tank 3 to be 3.3×10^{-7} "g" (Reference 12). Fuel cell oxygen demands were calculated from postflight current data, while ECS and surge tank flows were calculated during this period with the flow distribution subroutine. The total tank 3 flow rate was approximately 2.0 lbs/hour. Heat input was set at 70 watts to match the two heater element configuration.

The sensor temperature response for the 40 x 10 and 60 x 10 grids (Figure 3-31) are almost identical, indicating satisfactory convergence of the 60 x 10 grid at this low quantity. The heater sensor temperature results for the 0.475 ft² heater area converged to within 10°F of the observed flight maximum temperature of 325°F.

The total pressurization time predicted by the 60 x 10 grid was thirteen minutes shorter than the observed fifty-three minutes. This discrepancy resulted from the manner in which the stratification model treats radiant heat transfer. To calculate pressure rise rates, it is assumed that the total heat to the fluid includes radiation. The heater convects energy into the fluid while it is simultaneously radiating energy to the tank wall. This radiated energy raises the wall temperature and is convected back into the fluid. An alternate way of modeling the radiant energy would be to have it totally absorbed by the tank wall and not available to raise the fluid pressure. For a heater temperature of 300°F, radiation accounts for 60 BTU/hour or 35% of the total two element heater power (Figure 3-33). By reducing the fluid heat input by this 60 BTU/hour, the pressurization time is lengthened to the observed fifty-three minutes (Figure 3-32). The results imply that for simulations where radiation is important, the radiant energy is absorbed by the tank wall and is not convected into the fluid for some length of time. The error in calculating pressurization times can be no greater than the fraction of radiant energy to total heater power. This discrepancy in the treatment of radiant energy does not affect the heater temperature sensor time response. Furthermore, these effects are negligible for the problems of interest at lower heater temperatures. For example, for the two element heater cycle during the tank 3 DTO at 20% quantity, the heater reached a maximum temperature of 27°F and radiated less than 10 BTU/hour. Radiation loss was not significant for the other simulations conducted during the postflight analysis and did not affect other results or conclusions.

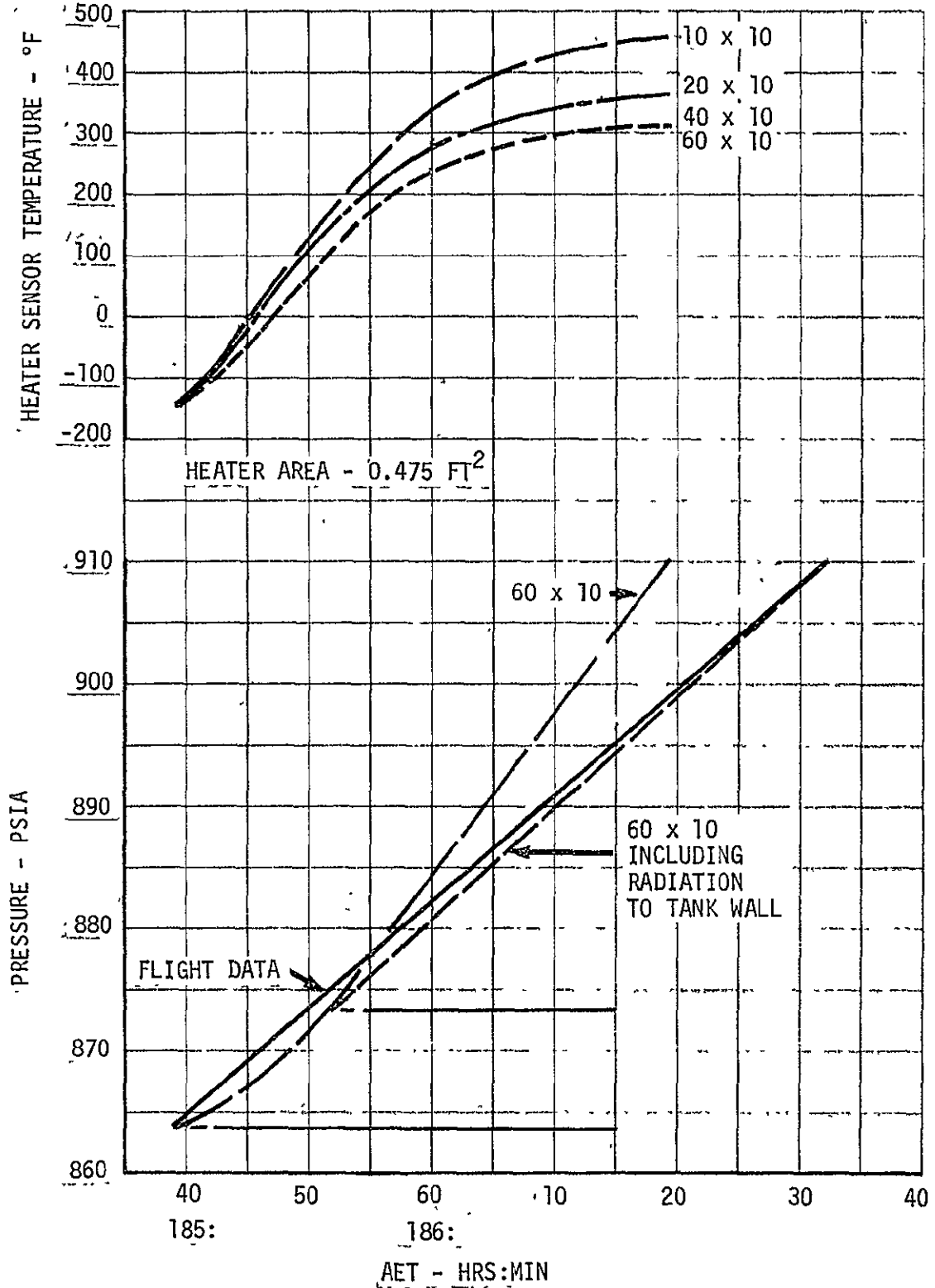


FIGURE 3-32 LOW DENSITY HEATER CYCLE SIMULATION

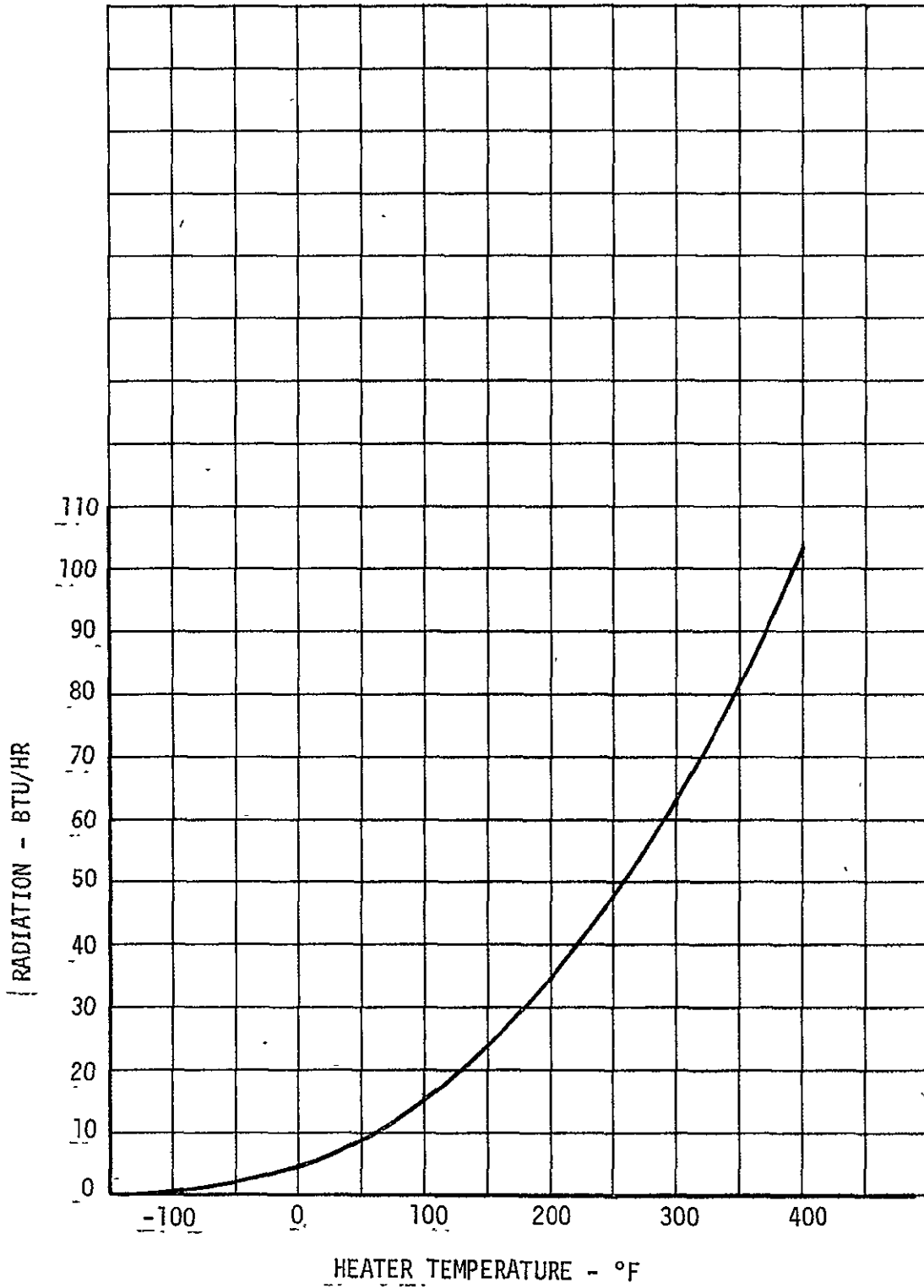


FIGURE 3-33 RADIANT HEAT TRANSFER DURING LOW DENSITY HEATER CYCLE

HEATER TEMPERATURE PREDICTIONS

The simulations previously discussed included correlations of heater temperature results from the stratification model with flight data. These correlations included a range of quantities from 15% to 97% and accelerations from 7×10^{-8} to 4.9×10^{-6} "g". The simulated maximum heater temperatures were in excellent agreement with flight data for the attitude hold and PTC periods.

<u>QUANTITY, CONDITION</u>	<u>ASSUMED HEATER AREA</u>	<u>TEMPERATURE ERROR</u>
97%, Attitude Hold	0.95 Ft ²	+ 2°F
92%, Attitude Hold	0.95 Ft ²	-12°F
70%, (DTO)	0.95 Ft ²	+31°F
54%, PTC	0.475 Ft ²	- 9°F
20%, (DTO)	0.95 Ft ² 0.475 Ft ²	-45°F +60°F
15%, PTC	0.475 Ft ²	-10°F

The best temperature simulation accuracy obtained by using the larger heater area for high quantities. The heater area parameter for the best temperature accuracy did not depend on the flight condition. The reduced accuracy of the DTO simulated temperatures may have been caused by abnormal accelerations which were not perpendicular to the heater as assumed by the model. The heater temperature is the tank variable most strongly affected by the low "g" flight environment. The good agreement between the simulated heater temperatures and the flight data verified the stratification math model prediction capability for the full range of quantities and accelerations from 3.3×10^{-7} "g" to 5×10^{-7} "g". These simulations, based on nominal performance of the tank heaters, confirmed that the tank performance was nominal and satisfactory during the entire Apollo 14 mission.

An empirical correlation using a Rayleigh Number convection heat transfer equation was developed to supplement the stratification model predictions for heater temperatures (Appendix B). This simplified model was used to develop heater temperature predictions as a function of tank quantity and heater on time (Figure 3-34). These predictions were compared to flight data from 20 Apollo 14 heater cycles (Figure 3-35). The average temperature deviation between the simplified model prediction and the flight data was 18.5°F and the standard deviation was 21.9°F. The individual predicted temperatures were within 50°F of flight data except for the data point taken from the tank 3 DTO (Figure 3-35). Parametric heater temperature predictions for the full range of flight conditions were based on this simplified model and are included in Reference 6.

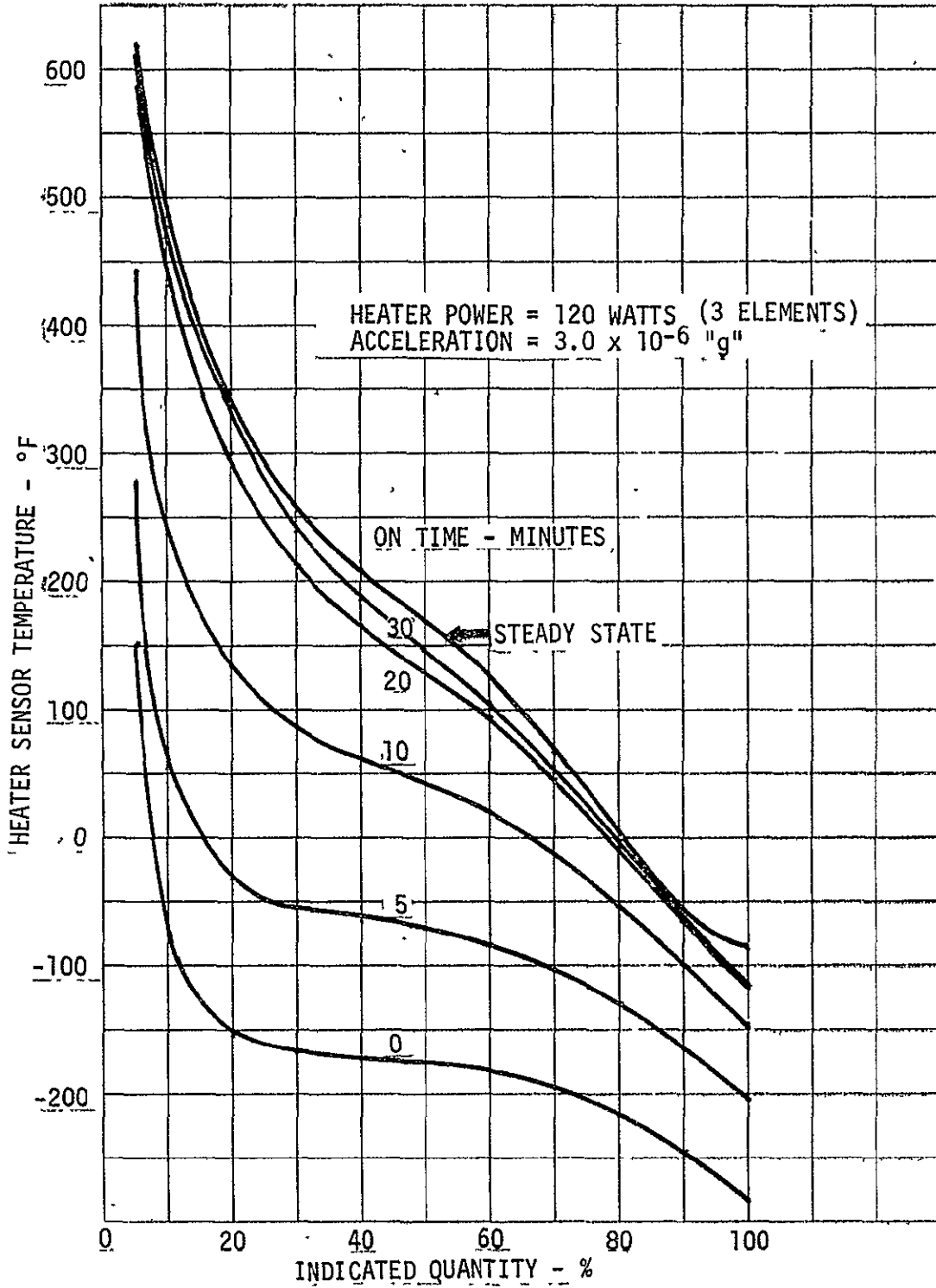


FIGURE 3-34 PARAMETRIC HEATER RESPONSE

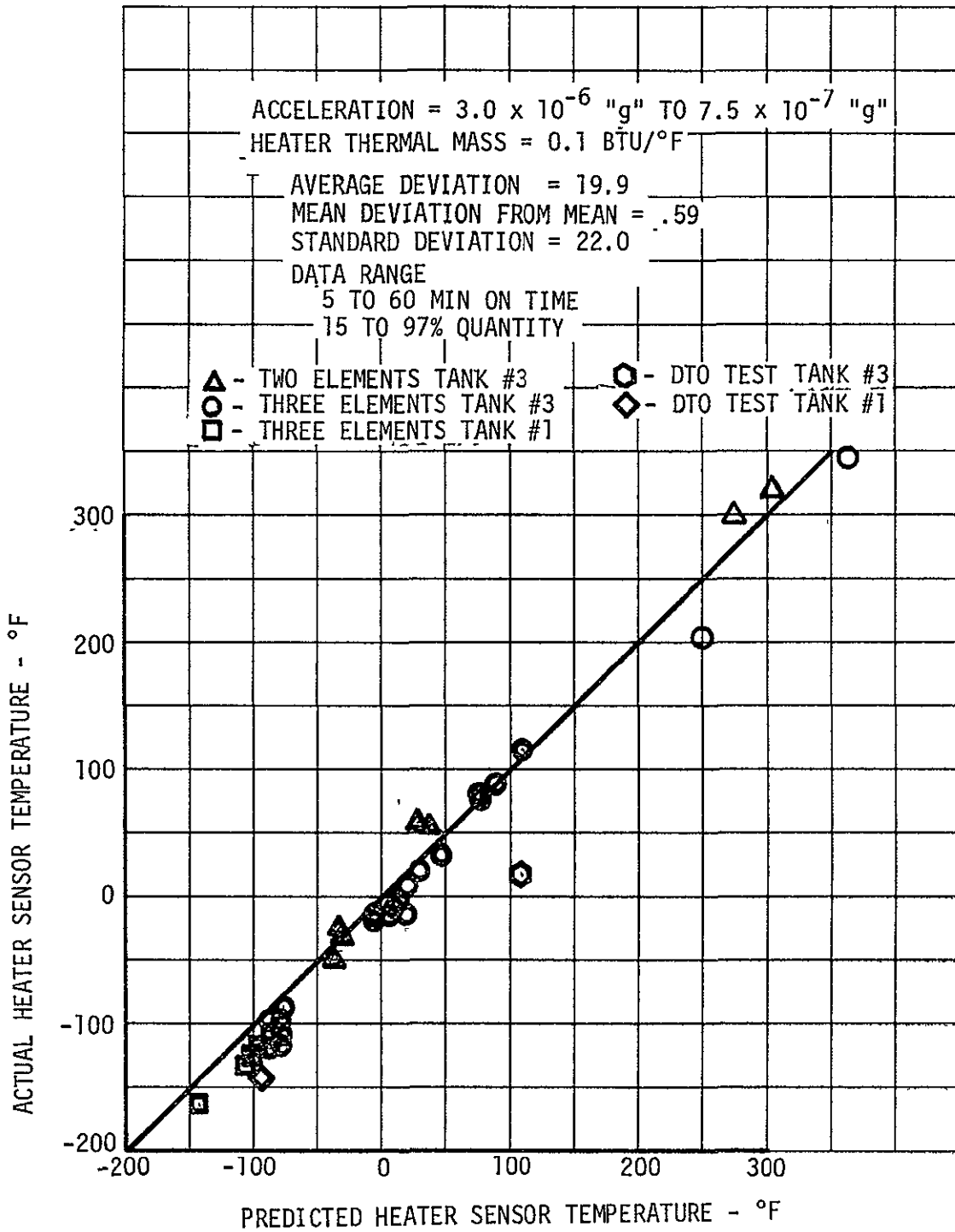


FIGURE 3-35 TEMPERATURE COMPARISONS SUMMARY

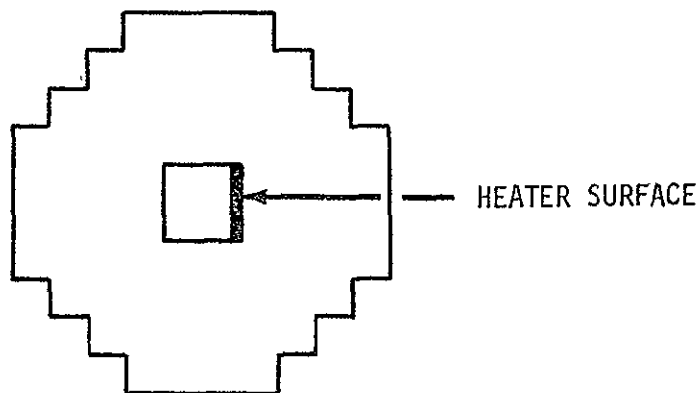
3.4 Task 4 - Fluid Rotation Analysis

The Apollo missions maintain vehicle temperatures by passive thermal control (PTC) rotations about the vehicle longitudinal axis. After a long period of time in the PTC flight mode, the oxygen in the tank will rotate with the tank about the vehicle axis with no relative motion between the oxygen and the tank. At termination of the PTC flight mode, the tank is brought to rest and the fluid inertia causes a continuing rotation of the oxygen relative to the tanks. The relative motion of the fluid and tank causes mixing of the fluid and affects the heater temperatures and the potential pressure decays.

The rotation effects were analyzed with the improved math model (paragraph 3.1) modified to include the relative motion between the tank and fluid. The termination of PTC at AET 30:00 of the Apollo 14 mission was selected for analysis with the concurrence of the Technical Monitor. This Apollo 14 period was selected in lieu of the originally planned Apollo 12 period in order to study effects of fluid rotation on heater temperatures. Heater temperatures were not measured on Apollo 12.

3.4.1 Model Description

The two-dimensional rotation model developed from the improved math model is described in detail by Reference 11. The model uses rectangular geometry to approximate a cylindrical region by a "stair step" grid arrangement as shown below.



The rotating fluid motion in the equatorial plane of a spherical tank is nearly the same as the flow in a cylinder (Appendix C). The heater and quantity probe drag effects were modeled by a square region near the center of the tank with a no-slip boundary condition. The width of the square was taken as 4.8 inches and the right face of the square was approximately the same distance from the center as the heater outer

3.4.1 Model Description (Continued)

surface. The heater is represented by the right side of the square. The fluid rotation was taken in a direction to augment the convection for the flight period analyzed.

The rotation model was checked out with the heater not included by comparing model fluid velocities after spindown with an analytical solution for the flow in a cylinder (Appendix C). The model velocities obtained with a 20 x 20 grid were in good agreement with the analytical spindown solution (Figure 3-36). This grid was not adequate to resolve the boundary layer at the tank wall, but the velocity comparison adequately verified the model capability.

3.4.2 Rotation Effects Simulation

The effects of fluid rotation were most apparent during the Apollo 14 mission for the heater cycle after termination of PTC at AET 30:06. The peak heater temperature for this cycle was -25°F. The peak heater temperature was +42°F for the previous heater cycle during PTC. The 67°F reduction in heater temperature was attributed to residual fluid rotations at the heater surface. A small pressure decay of approximately 8 psi occurred as a result of an acceleration spike caused by the mid-course correction at AET 30:36:36, a few minutes after the heater was turned off (Figure 3-36). The period was simulated with the actual accelerations (2.5×10^{-7} g) both with and without rotation effects and at the PTC acceleration (2.75×10^{-6} g) with no rotation.

The simulation of this period was based on flight data (Reference 12) for rotation rates, accelerations and flow rates. Only the rotation about the vehicle longitudinal axis (parallel to the heater tube) was included due to the two-dimensional limitation of the model. The heater temperatures were decreased by the fluid rotation at the attitude hold acceleration (Figure 3-38). The heater temperature simulated with rotation and the low acceleration condition was higher than the temperature simulated with the PTC acceleration. This is not in agreement with the observed flight data.

The simulated potential pressure decay at the low "g" and with rotation was nearly the same as the pressure decay from the PTC simulation. The pressures resulting from the simulations with no rotation, for low "g" and in PTC "g" were essentially identical (Figure 3-38). Near the top of the cycle the tank pressure with rotation was rising at a slower rate than the other simulations. The rotation reduced the rise rate below the attitude hold rise rate because the potential decay growth was reduced. The rotation rise rate was slower than the PTC rise rate because the heater temperature was higher, which stored thermal energy in the heater mass. The potential pressure decay with rotation was nearly the same as the

3.4.2 Rotation Effects Simulation (Continued)

PTC potential decay, which was in fair agreement with the observed 4-8 psi pressure drop at AET 30:36 of Apollo 14.

The small temperature reduction simulated with rotation was completely different than the large effect observed in the flight data. The guidance data indicated that a vehicle yaw of more than 45° was associated with this termination of PTC. The yaw maneuver caused the ends of the heater and the heater sensor to move into the higher velocity region of the rotation fluid. The relatively high fluid velocities reduced the heater temperature to a much lower value than that obtained in the low velocity region near the center of fluid rotation. The rotation simulation was terminated at approximately the time the flight data indicated the heater turned off. At this time the heater temperature with rotation was nearly the same as the heater temperature at attitude hold. The effects of the yaw maneuver could not be accurately simulated due to the two-dimensional limitation of the model. An approximate simulation of this effect was accomplished by locating the heat source and thermal mass in the high rotational velocity region near the tank wall. This approximate simulation produced heater temperatures approximately 20°F lower than the simulation with the PTC acceleration and approximately 30°F higher than observed in flight (Figure 3-39). This result confirms that the yaw maneuver was a significant factor causing the observed heater temperature reduction below the heater temperature during the PTC flight mode.

The results of the simulations of the heater cycle immediately after the PTC termination indicated that the rotation has a small effect on the heater temperatures and other tank performance parameters if the vehicle axis remains fixed. If the vehicle axis is changed by a yaw or pitch maneuver after the termination of PTC, the heater temperatures and other tank performance variables will be strongly affected. The effects of yaw and pitch maneuvers can be approximately simulated, but the three dimensional flows are not accurately modeled. Thorough evaluation of this effect would require an extensive simulation study to determine effective heater areas and heater(s) locations which would accurately simulate tank response. The rotation effects reduce heater temperatures and potential pressure decays. The model predictions and simulations are, therefore, conservative and additional rotation analyses are not warranted.

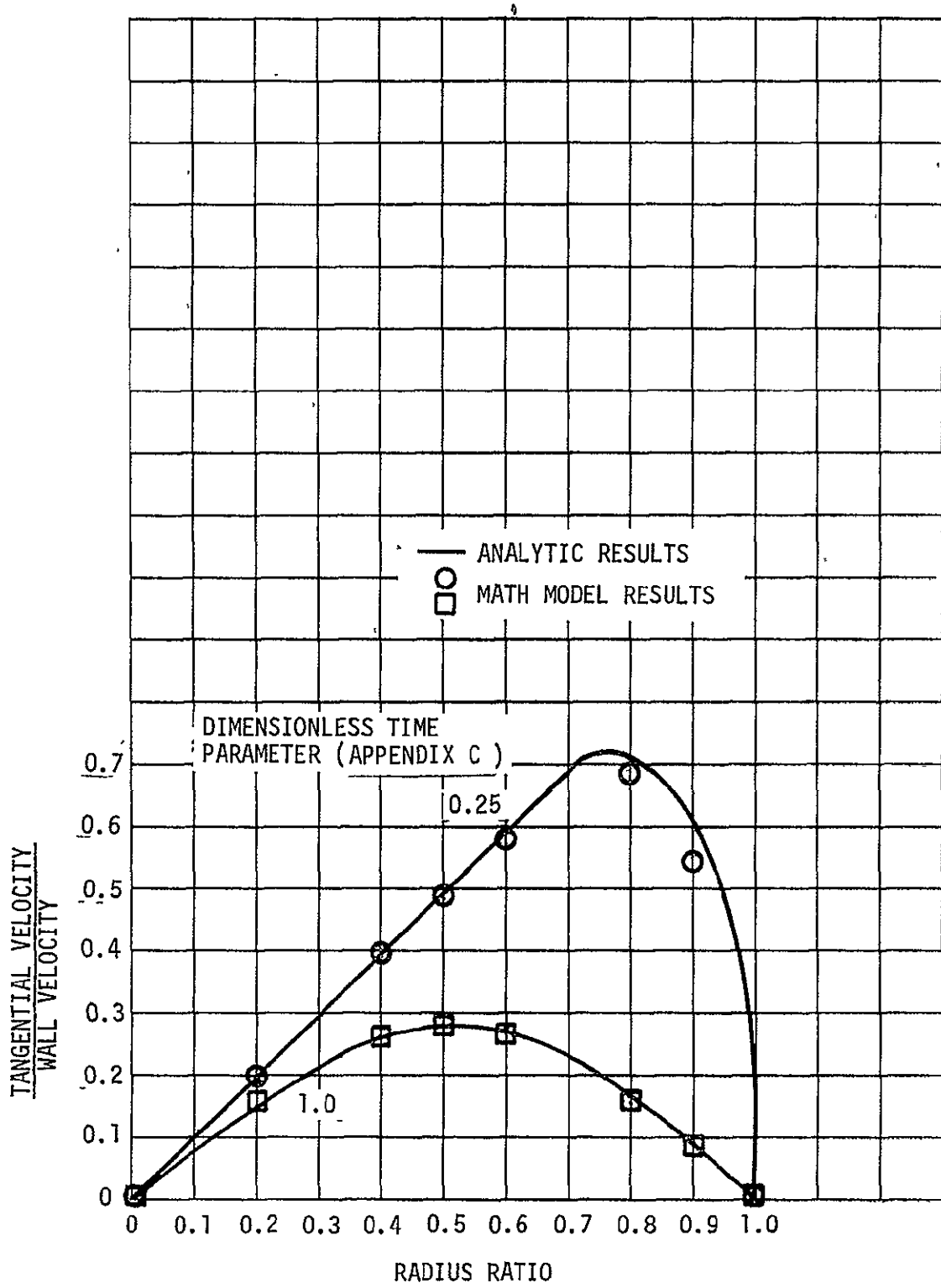


FIGURE 3-36 TRANSIENT VELOCITY PROFILES IN A CYLINDER

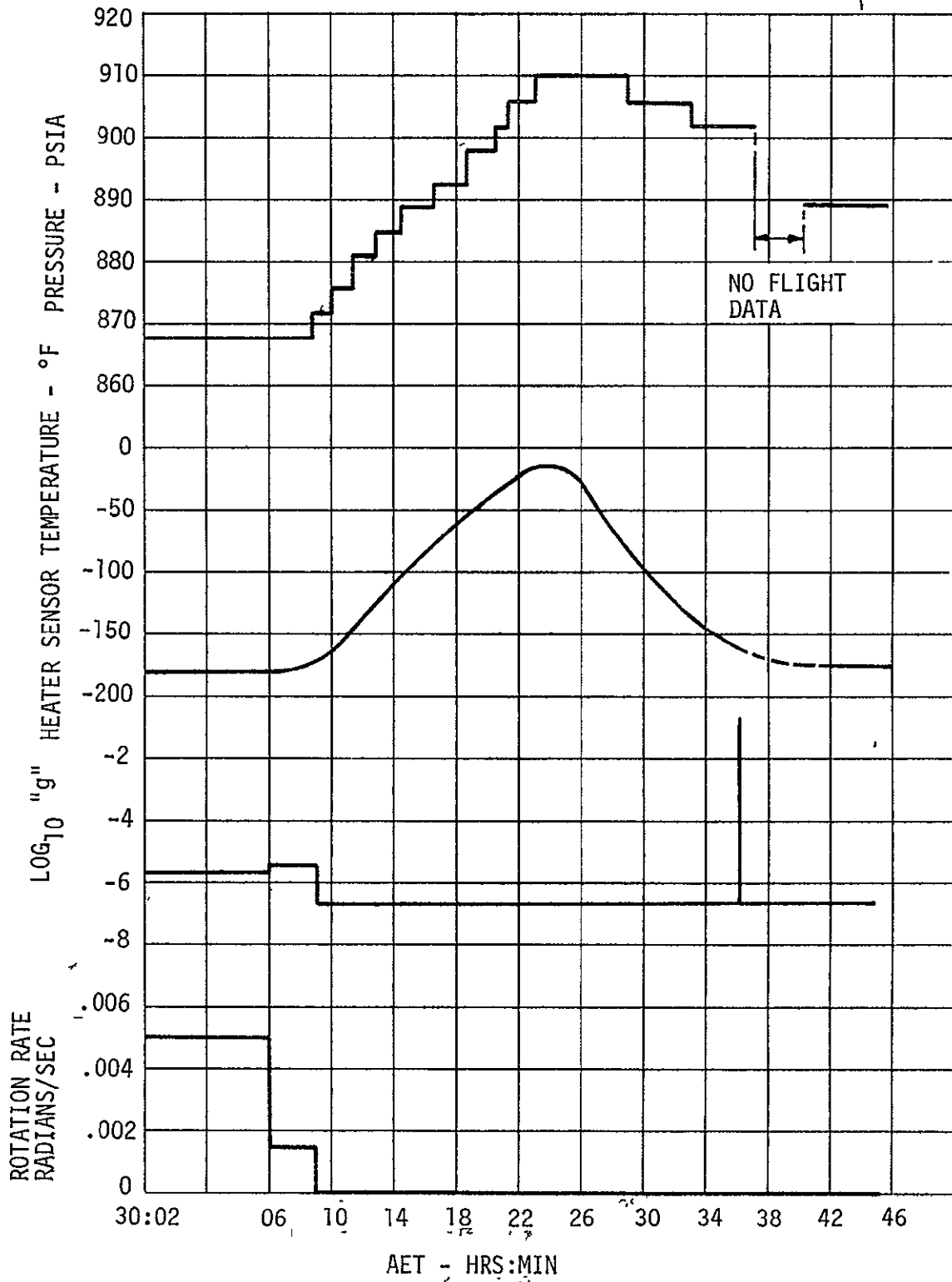


FIGURE 3-37 OXYGEN TANK RESPONSE AFTER PTC TERMINATION

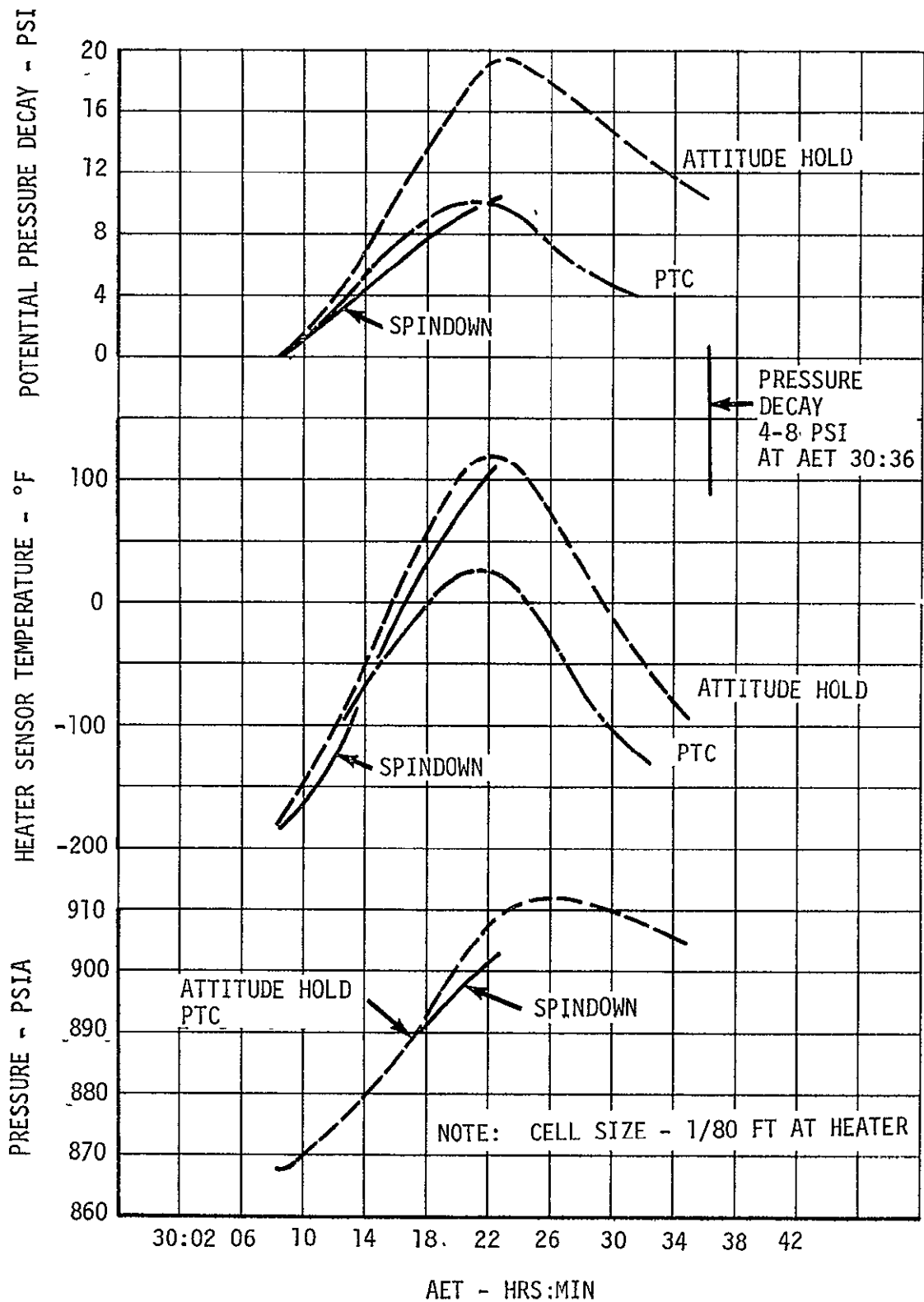


FIGURE 3-38 - RELATIVE ROTATION EFFECT

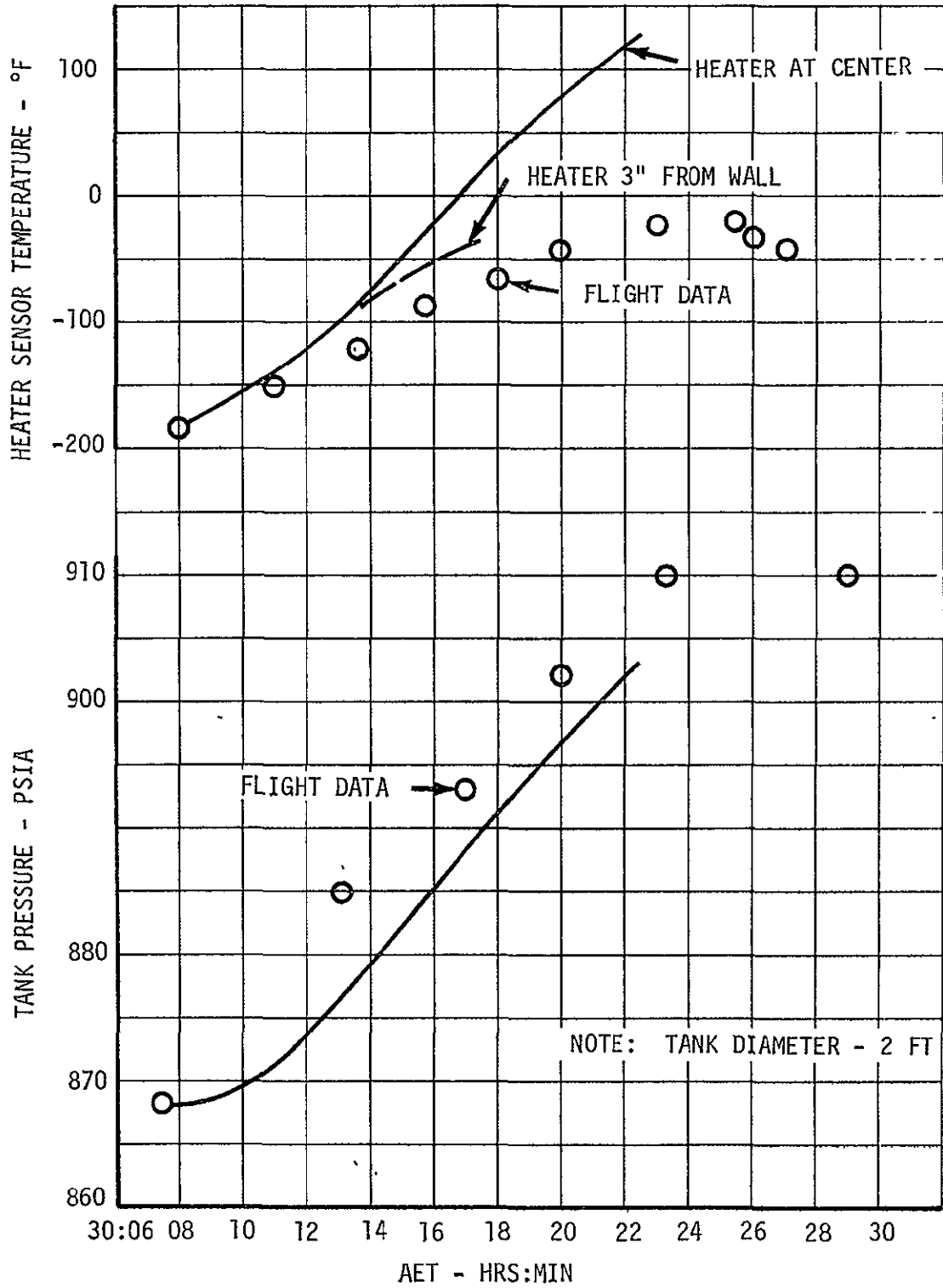


FIGURE 3-39 - ROTATION SIMULATION - FLIGHT DATA COMPARISON

SECTION 4

4.0 CONCLUSIONS AND RECOMMENDATIONS

4.1 Conclusions

Conclusions drawn from the analysis of the Apollo cryogenic oxygen tanks flight performance were:

1. The current design Apollo cryogenic oxygen tank is adequate for known future Apollo mission requirements.
2. Manual management of the heater on time will be required to control heater temperatures at low tank quantities and low accelerations.
3. The stratification math model accurately simulates the oxygen tank flight performance (tank pressure and heater temperature) for all flight conditions with the exception of short periods after termination of PTC.
4. Pitch and yaw maneuvers are associated with the termination of PTC and cause three dimensional flows in the tanks. The two dimensional rotational model does not accurately simulate the effects of vehicle rotation because the three dimensional flows are not modeled.
5. The fluid rotations resulting from initiation and termination of PTC reduce the heater temperatures and potential pressure decays.
6. The simulation accuracy in the absence of rotation effects is primarily limited by the accuracy of the tank flow rates and accelerations.
7. The Apollo 14 high flow oxygen tank tests to demonstrate EVA flow rate capability were conducted with tank accelerations not representative of later mission EVA periods. The atypical accelerations were caused by the oxygen vented during the Apollo 14 test.

4.2 Recommendations

No hardware or operational changes are recommended for the redesigned oxygen tanks which were found to be adequate for known Apollo mission requirements. Additional analyses recommended to improve prediction accuracies and capabilities for future missions are:

4.2 Recommendations (Continued)

1. Perform post-flight analyses of the tanks performance during the Apollo 15 EVA which will duplicate later mission EVA periods more closely than the Apollo 14 simulation tests.
2. Modify the stratification math model to improve the accuracy of the tank flow rate simulation for expected system operating modes.
3. No additional analyses of the effects of fluid rotation are recommended since simulations without rotation are conservative and the three-dimensional model required for accurate predictions is beyond present capabilities.

APPENDIX A - STRATIFICATION MATH MODEL

NOMENCLATURESymbols

C_K	Constant in heater temperature sensor lag equation
\bar{g}	Acceleration in Earth gravity units
MC	Heater thermal mass
Q	Quantity of heat
T	Temperature
T_h	Heater tube temperature
T_s	Heater sensor temperature
t	Time

The stratification math model used for these analyses is based on the General Elliptic Method (GEM) developed by Mr. C. K. Forester of Boeing-Seattle to solve finite difference approximations to the mass, momentum and energy conservation equations (Reference 1). The fundamental assumption of the method is that the pressure terms in the energy and momentum equation are not coupled. This assumption is valid for low velocity flows in which acoustic waves do not contribute significantly to the fluid energy. This assumption permits a much longer time step than is otherwise necessary for stability. The uncoupling is accomplished by using only the global (average) pressure in the energy equation to eliminate the effects of acoustic waves. Other assumptions which have been validated by comparing model results with Apollo 12 flight data are:

1. Two dimensional rectangular geometry (Figure A-1)
2. Viscous energy dissipation and kinetic energies are neglected
3. Radiation heat transfer within the fluid is neglected (radiation from the heater surface is included).
4. Acceleration body forces are constant through the tank.

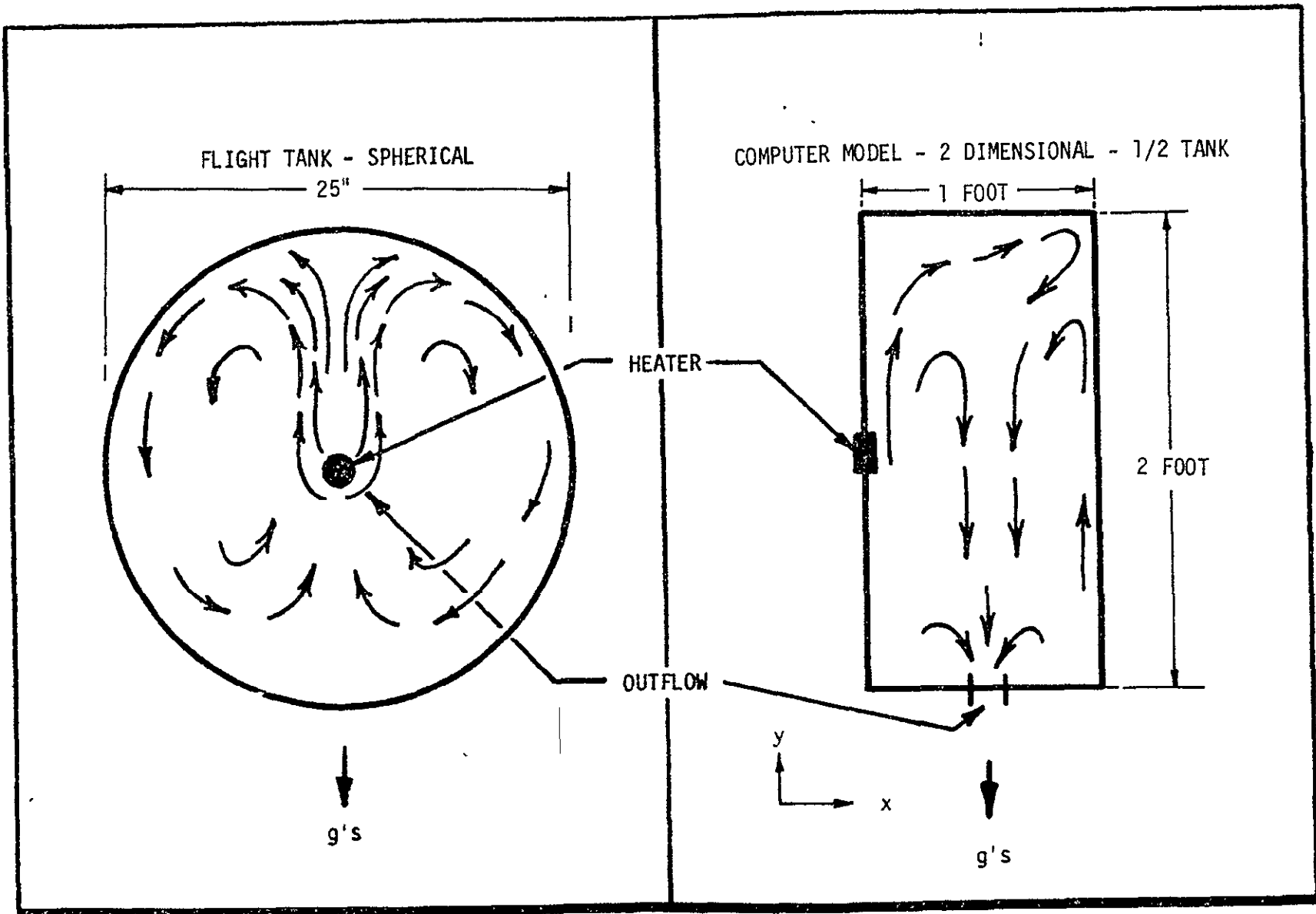


FIGURE A-1 - ANALYTICAL APPROACH - MODEL DESCRIPTION

The difference equations used by the math model are based on the control volume concept. The rectangular flow field region is subdivided into elementary control volumes or cells. The difference equations are formulated with the mass fluxes defined on the cell boundaries, while the fluid properties are defined at the centers of the cells. This formulation results in conservation of mass for each easily defined cell, whereas formulations with fluxes and state properties defined at the same point do not.

The difference equations are solved by extrapolating an initial set of field variables by a time increment. Preliminary field pressure are calculated at the extrapolated time including the effects of the preliminary energy and mass transfers between cells. The preliminary pressures at the extrapolated time are used to revise the energy and mass transfer in the time increment. The extrapolated pressures are revised to account for the new energy and mass transfers, and the extrapolation procedure repeated until satisfactory convergence is obtained. The field variables at the new time are taken as initial conditions for the next time increment. Successive iterative extrapolations are made to describe the fluid state for the simulated time period.

The basic math model was modified to include the effects of heater thermal mass and heater temperature sensor lag. To account for the energy stored in the heater mass, heater temperatures are obtained by numerical integration of the equation,

$$\frac{dT}{dt} = \frac{dQ}{dt} \left(\frac{1}{MC} \right)$$

A heater thermal mass, MC, equal to 0.1 BTU/ F was used to conduct Apollo 14 post flight analyses. To provide a means of direct comparison with flight data, heater temperature sensor lag was included in the integration. The temperature sensor response was determined from:

$$\frac{dT_s}{dt} = C_K (T_h - T_s)$$

The constant, C_K , was estimated to be 0.26 minutes⁻¹.

The difference equations solved by the program are only approximations to the partial differential equations describing the processes in the tank. The quality of this approximate solution improves and approaches the solution of the exact equations as the cell sizes are reduced. The cell

sizes required to obtain an adequate approximation can not be established a priori. The effect of cell size on the model results must be investigated for each tank condition simulated to assure that the approximate solutions are convergent. Separate simulations with at least three different cell sizes or grids are required to test the convergence at the solution for each tank condition. Particular parameters, heater temperature for example, are a function of grid size and are extrapolated to "asymptotic" limits. The asymptotic limit, when obtainable, is the exact solution to the controlling partial differential equations. The extrapolation procedure used in these analyses is based on the parameter differences related to the number of cells in the X direction of the model as shown below.

<u>No of Cells</u>	<u>Parameter-Temperature</u>	<u>Difference</u>
20	60	> 40
40	100	> 20
60	120	> 10
80	130	

The successive differences form a geometric series. The ratio between successive terms is found and the sum of the infinite geometric series determined. The sum of the series of differences is added to the appropriate parameter to obtain the parameter asymptotic limit.

APPENDIX B - HEATER TEMPERATURE CORRELATIONS

NOMENCLATURESymbols

C_K	Constant in heater temperature sensor lag equation
C_p	Specific heat at constant pressure
C_s	Stefan Boltzman constant
C_{ra}	Constant in Rayleigh heat transfer equation (equal to 0.525)
D	Diameter
\bar{g}	Acceleration in Earth gravity units
K	Thermal conductivity
L	Length
MC	Heater thermal mass
Q	Quantity of heat
R_a	Rayleigh number
T	Temperature
T_b	Temperature of the Bulk fluid
T_h	Heater temperature
T_s	Sensor temperature
t	Time
β	Coefficient of thermal expansion
ϵ	Heater emissivity (0.2 assumed)
ρ	Density
μ	Viscosity

Heater temperatures can be determined from the numerical math model, but the computer usage times are excessive for the generation of parametric data and to conduct routine flight analyses. Empirical heat transfer equations were investigated to develop a more convenient tool for heater temperature studies.

The convective heat transfer from a horizontal cylinder is usually determined from a Rayleigh number equation.

$$\frac{dQ}{dt} = \pi L K \Delta T C_{ra} (R_a)^{1/4}$$

The Rayleigh number is determined from:

$$R_a = \frac{D^3 \rho^2 \beta \Delta T C_p}{\mu K}$$

The fluid properties used to evaluate the Rayleigh numbers are usually taken at the mean film temperatures. This convention is based on tests with simple fluids under 1 "g" conditions. Since the properties of supercritical oxygen may vary by an order of magnitude in the boundary layer, the properties in the Rayleigh number were averaged instead of taken at the mean film temperature. The viscosity, conductivity, and density were taken as the average of their values for the bulk temperature and the heater temperature. The specific heat was evaluated as the difference in the enthalpy at the heater, and bulk temperatures divided by the temperature difference. The coefficient of expansion used was,

$$\beta = \frac{-1}{\rho_b} \left(\frac{\rho_h - \rho_b}{T_h - T_b} \right)$$

The radiation from the heater is also significant and was included in the complete heat transfer equation.

$$\frac{dQ}{dt} = \pi L K \Delta T C_{ra} (R_a)^{1/4} + \epsilon C_s (T_h^4 - T_b^4)$$

Heater temperatures were developed as a function of heater-on time by numerical integration of the equation,

$$\frac{dT}{dt} = \frac{dQ}{dt} \left(\frac{1}{MC} \right)$$

where MC is the heater thermal mass of 0.1 BTU/°F. The heater temperature sensor lag was included in the integration to provide a means of comparison with flight data. The temperature sensor response was determined from:

$$\frac{dT_s}{dt} = C_K (T_h - T_s)$$

The constant was estimated as 0.26 minutes⁻¹.

APPENDIX C - SPIN TRANSIENTS FOR A FLUID IN THERMODYNAMIC
EQUILIBRIUM

NOMENCLATURE

Symbol

a	Inner radius of concentric cylinders
a_o	Distance of heater offset (axis to axis)
A	Frontal area
b	Outer radius of concentric cylinders (distance from tank center to inner heater surface)
C_d	Drag coefficient
D	Drag
g_c	Gravitational constant
l	Length
m	Integer
r	Radial position (spherical coordinate)
R	Tank radius
t	Time
T	Torque
u	Velocity in direction of flow
v_ϕ	Velocity in ϕ direction
VOL	Tank volume
x	Direction of flow
y	Direction perpendicular to direction of flow
α	Time constant
η	Similarity parameter
ϕ	Angular position from z axis (spherical coordinate)
μ	Viscosity
ν	Kinematic viscosity
ρ	Density
θ	Angular position from x axis in x-y plane (spherical coordinate)
ω	Angular velocity

C.0 BACKGROUND

Initiation and termination of passive thermal control (PTC) cause spin transients to occur within the Apollo oxygen tanks. These PTC-associated spinups and spindowns can affect the stratification in the oxygen tanks. To investigate these effects equilibrium (non-stratified) fluid dynamics should be analyzed before stratification analyses are undertaken. The equilibrium fluid dynamics can be used as a check or limiting case for the stratification investigation.

C.1 VELOCITY DISTRIBUTION

For a fluid in thermodynamic equilibrium the velocity build-up during spinup and the velocity decay during spindown are similar if the flow remains laminar and pressure gradients are negligible. The only difference is in the frame of reference. If an inertial frame of reference is taken at the tank center, it is apparent that the velocity distribution during spindown is equal to the steady-state velocity distribution minus the velocity distribution during spinup

$$u_{\text{spindown}} = u_{\text{steady state}} - u_{\text{spin up}} \quad (\text{C-1})$$

Because of this similarity only spinup velocity profiles are developed.

To investigate the spin transients created by the spinup of a spherical Apollo oxygen tank (containing a quantity probe and offset heater), various approximations may be used to model the tank. All models assume that the fluid is incompressible with constant viscosity. The models are used to generate transient velocity profiles.

The simplest approximation consists of two parallel plates. One plate represents the tank center, and the other is the tank wall. Effects of the quantity probe-heater assembly are neglected. Initially, both plates are at rest. At some instant, one plate is accelerated to a velocity of $R\omega$, where R is the tank radius and ω is the spin rate. In classical terminology, the problem is called flow formation in Couette motion. The governing equations for this situation are

$$\frac{\partial u}{\partial t} = \nu \frac{\partial^2 u}{\partial y^2} \quad (\text{C-2})$$

$$\begin{array}{l} t \leq 0 \\ t > 0 \end{array} \quad \begin{array}{l} u = 0 \\ u = 0 \end{array} \quad \text{at } y = 0 \quad ; \quad u = R\omega \quad \text{at } y = R$$

C.1 (Continued)

Schlichting (Reference C-1) gives the following solution to these equations

$$\frac{u}{R\omega} = \sum_{m=0}^{\infty} \operatorname{erfc}(2m\eta_1 + \eta) - \sum_{m=0}^{\infty} \operatorname{erfc}[2(m+1)\eta_1 - \eta] \quad (C-3)$$

where $\eta = \frac{R-y}{2\sqrt{vt}}$ and $\eta_1 = \frac{R}{2\sqrt{vt}}$. This solution is plotted in Figure C-1.

Another approximation is to model the Apollo oxygen tank with a spherical tank which contains only fluid. Effects of the quantity probe and heater are again neglected. Initially, the system is at rest. At some instant, the tank wall is spun up to a spin rate of ω . The governing equations of this model are

$$\begin{aligned} \frac{\partial v_{\phi}}{\partial t} = & \frac{\nu}{r^2} \frac{\partial}{\partial r} \left[r^2 \frac{\partial v_{\phi}}{\partial r} \right] + \frac{\nu}{r^2 \sin \theta} \frac{\partial}{\partial \theta} \left[\sin \theta \frac{\partial v_{\phi}}{\partial \theta} \right] \\ & - \frac{\nu v_{\phi}}{r^2 \sin^2 \theta} \end{aligned} \quad (C-4)$$

$$\begin{aligned} t \leq 0 \quad v_{\phi} &= 0 \\ t > 0 \quad v_{\phi} &= 0 \text{ at } r=0 ; v_{\phi} = R\omega \sin \theta \text{ at } r=R \end{aligned}$$

A solution of the form

$$v_{\phi} = r\omega \sin \theta - \frac{u}{x^{3/2}} e^{-\alpha^2 t} \sin \theta \quad (C-5)$$

where

$$x = \alpha r / \sqrt{\nu}$$

is assumed. Substitution of equation (C-5) into equation (C-4) yields

$$x^2 \frac{d^2 u}{dx^2} + x \frac{du}{dx} + \left(x^2 - \frac{9}{4} \right) u = 0 \quad (C-6)$$

This is Bessel's equation which has the following solution

$$u = A J_{3/2}(x) + B J_{-3/2}(x) \quad (C-7)$$

C-4

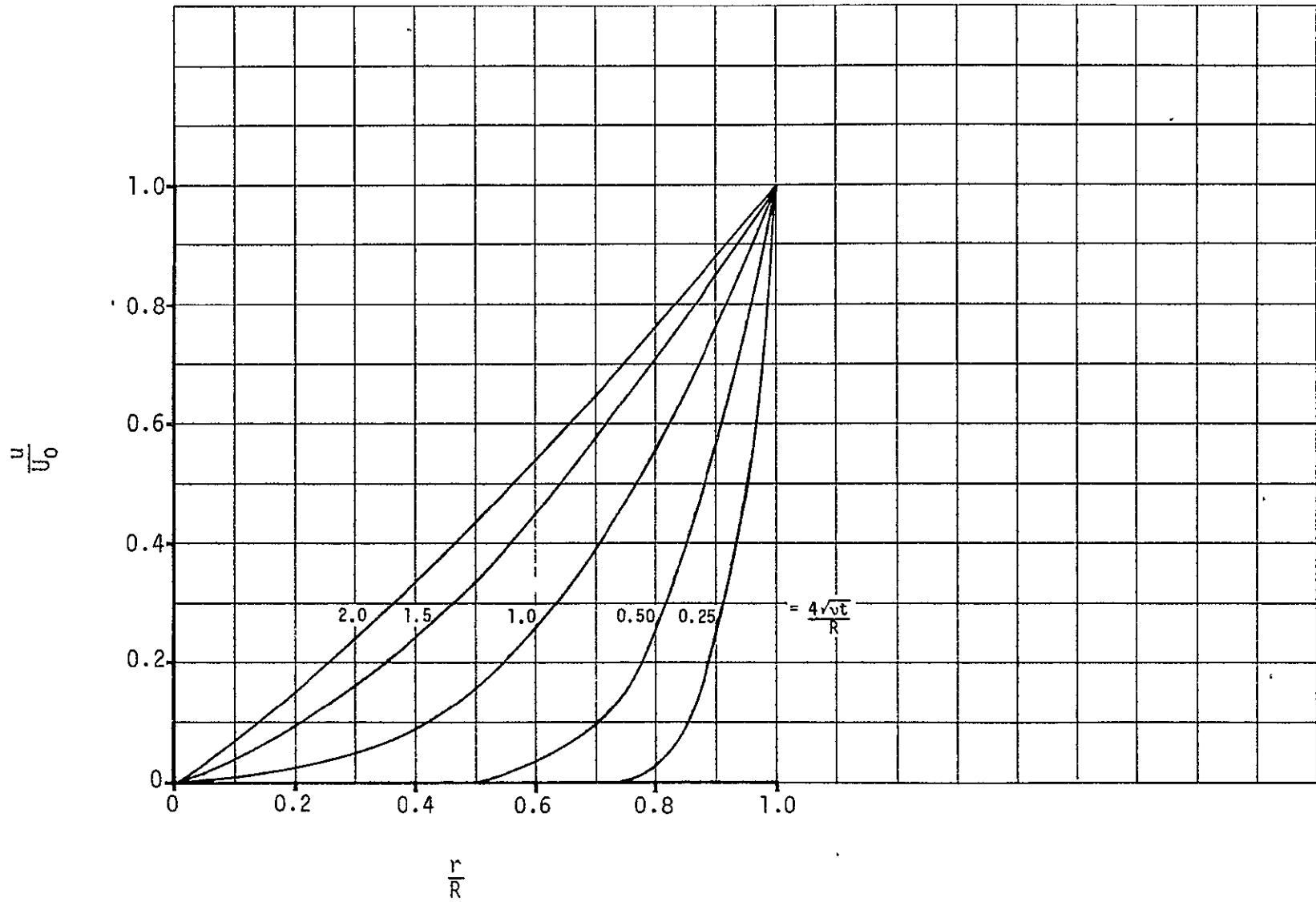


FIGURE C-1 - TRANSIENT VELOCITY PROFILES IN COUETTE FLOW

C.1 (Continued)

B must be zero because of the boundary condition ($u=0$ at $r=0$). Since the spherical Bessel function $j_n(x)$ is defined as (Reference C-2)

$$j_n(x) = \sqrt{\pi/2x} J_{n+1/2}(x) \quad (C-8)$$

the solution to equation (C-4) is

$$v_\phi = r\omega \sin\theta - \sin\theta \sum_{m=1}^{\infty} A_m j_1(\alpha_m r/\sqrt{\nu}) e^{-\alpha_m^2 t} \quad (C-9)$$

To satisfy the boundary conditions $\alpha_m R/\sqrt{\nu}$ are the roots of the following equation

$$j_1(\alpha_m R/\sqrt{\nu}) = 0 \quad (C-10)$$

The initial condition is used to solve for A_m

$$A_m = \frac{2\omega}{\frac{\alpha_m}{\sqrt{\nu}} j_2\left(\frac{\alpha_m R}{\sqrt{\nu}}\right)} \quad (C-11)$$

Thus, equation (C-9) becomes

$$v_\phi = r\omega \sin\theta - 2\omega \sin\theta \sum_{m=1}^{\infty} \frac{j_1(\alpha_m r/\sqrt{\nu}) e^{-\alpha_m^2 t}}{(\alpha_m/\sqrt{\nu}) j_2(\alpha_m R/\sqrt{\nu})} \quad (C-12)$$

Equation (C-12) can be simplified since

$$j_1(x) = \frac{1}{x^2} \sin x - \frac{1}{x} \cos x \quad (C-13)$$

$$j_2(x) = \left(-\frac{1}{x} + \frac{3}{x^3}\right) \sin x - \frac{3}{x^2} \cos x \quad (C-14)$$

C.1 (Continued)

Substituting equations (C-13) and (C-14) into equation (C-12) and noting that equation (C-10) becomes

$$\frac{\alpha_m R}{\sqrt{\nu}} = \tan \left(\frac{\alpha_m R}{\sqrt{\nu}} \right) \quad (\text{C-15})$$

yields

$$\frac{v_\phi}{R\omega \sin \theta} = \frac{r}{R} + 2 \sum_{m=1}^{\infty} \frac{\frac{\sin(\alpha_m r/\sqrt{\nu})}{(\alpha_m r/\sqrt{\nu})^2} - \frac{\cos(\alpha_m r/\sqrt{\nu})}{(\alpha_m r/\sqrt{\nu})}}{\sin(\alpha_m R/\sqrt{\nu})} e^{-\alpha_m^2 t} \quad (\text{C-16})$$

Equation (C-16) is the nondimensionalized solution to equation (C-4). This solution is shown in Figure C-2. Because the heater assembly and quantity probe do not display spherical symmetry, it does not appear possible to modify this solution to include heater-quantity probe effects.

A third model of the Apollo oxygen tank approximates the tank as a cylinder. Initially, the system is at rest. At some instant, the tank wall is spun up to a spin rate of ω . If effects of the quantity probe and heater are neglected, the governing equations are

$$\frac{\partial v_\phi}{\partial t} = \nu \frac{\partial^2 v_\phi}{\partial r^2} + \frac{\nu}{r} \frac{\partial v_\phi}{\partial r} - \frac{\nu}{r^2} v_\phi \quad (\text{C-17})$$

$$\begin{aligned} t \leq 0 & \quad v_\phi = 0 \\ t > 0 & \quad v_\phi = 0 \text{ at } r = 0; \quad v_\phi = R\omega \text{ at } r = R \end{aligned}$$

A solution of the form

$$v_\phi = r\omega - u e^{-\alpha^2 t} \quad (\text{C-18})$$

is assumed. Substitution of equation (C-18) into equation (C-17) yields

$$x^2 \frac{d^2 u}{dx^2} + x \frac{du}{dx} + (x^2 - 1) u = 0 \quad (\text{C-19})$$

where

$$x = \alpha r / \sqrt{\nu}$$

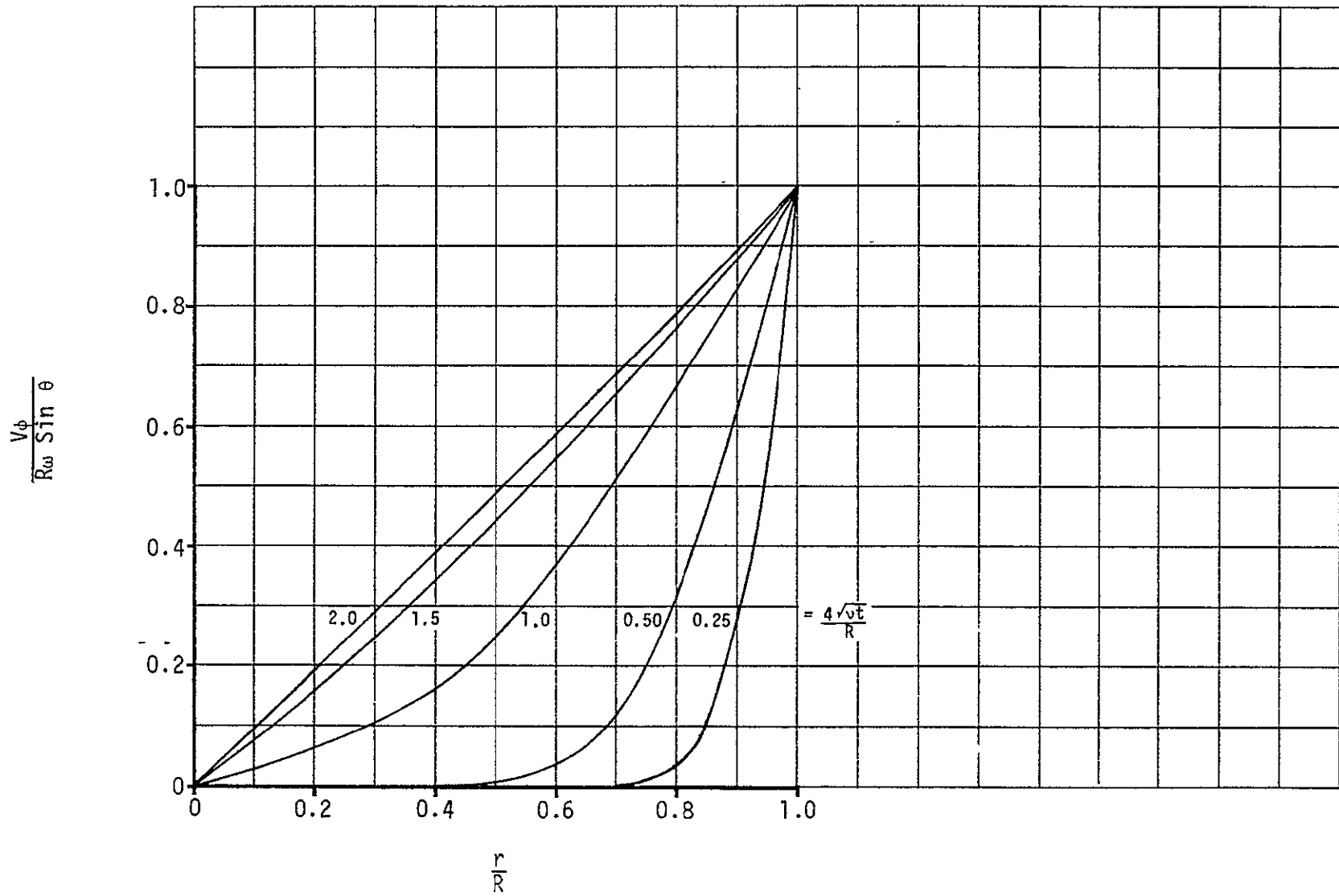


FIGURE C-2 - TRANSIENT VELOCITY PROFILES IN A SPHERE

C.1 (Continued)

This differential equation is Bessel's equation which has the following solution

$$u = A J_1(x) + B Y_1(x) \quad (C-20)$$

B must be zero because of the boundary condition ($u = 0$ at $r = 0$). Thus, the solution to equation (A-17) becomes

$$v_\phi = r\omega - \sum_{m=1}^{\infty} A_m J_1(\alpha_m r / \sqrt{\nu}) e^{-\alpha_m^2 t} \quad (C-21)$$

To satisfy the boundary conditions $\alpha_m R / \sqrt{\nu}$ are roots of the following equation

$$J_1(\alpha_m R / \sqrt{\nu}) = 0 \quad (C-22)$$

The initial condition is used to solve for A_m

$$A_m = \frac{2\omega}{\frac{\alpha_m}{\sqrt{\nu}} J_2\left(\frac{\alpha_m R}{\sqrt{\nu}}\right)} \quad (C-23)$$

Therefore, equation (C-21) becomes

$$\frac{v_\phi}{R\omega} = \frac{r}{R} - 2 \sum_{m=1}^{\infty} \frac{\sqrt{\nu}}{\alpha_m R} \frac{J_1(\alpha_m r / \sqrt{\nu})}{J_2(\alpha_m R / \sqrt{\nu})} e^{-\alpha_m^2 t} \quad (C-24)$$

The velocity profiles resulting from equation (C-24) are shown in Figure C-3. The advantage of the cylindrical model is that it allows the heater and quantity probe to be approximated by a small cylinder that is concentrically located within the tank cylinder. The outer cylinder has a radius of R , and the inner one has a radius of a . The governing equations of the concentric cylinder model are

$$\frac{\partial v_\phi}{\partial t} = \nu \frac{\partial^2 v_\phi}{\partial r^2} + \frac{\nu}{r} \frac{\partial v_\phi}{\partial r} - \frac{\nu}{r^2} v_\phi \quad (C-25)$$

$$\begin{aligned} t \leq 0 & \quad v_\phi = 0 \\ t > 0 & \quad v_\phi = a\omega \text{ at } r = a ; v_\phi = R\omega \text{ at } r = R \end{aligned}$$

C-9

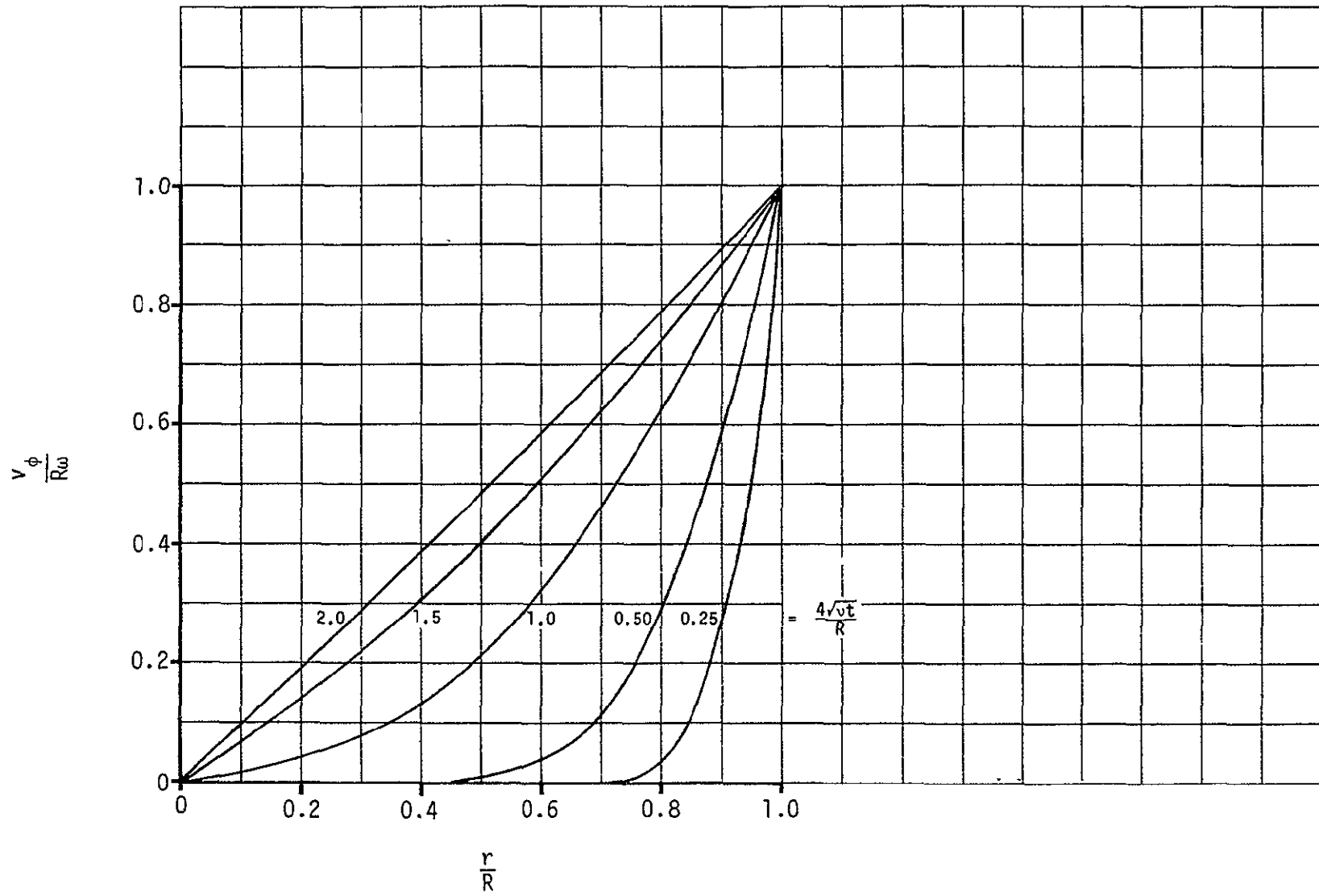


FIGURE C-3 - TRANSIENT VELOCITY PROFILES IN A CYLINDER

D2-118406-1

C.1 (Continued)

A solution of the form

$$v_\phi = r\omega - u e^{-\alpha^2 t} \quad (\text{C-26})$$

is assumed. Substitution of equation (C-26) into equation (C-25) yields

$$x^2 \frac{d^2 u}{dx^2} + x \frac{du}{dx} + (x^2 - 1)u = 0 \quad (\text{C-27})$$

where $x = \alpha r / \sqrt{\nu}$

This is again Bessel's equation which has the following solution

$$u = A \left[J_1 \left(\frac{\alpha r}{\sqrt{\nu}} \right) Y_1 \left(\frac{\alpha R}{\sqrt{\nu}} \right) - J_1 \left(\frac{\alpha R}{\sqrt{\nu}} \right) Y_1 \left(\frac{\alpha r}{\sqrt{\nu}} \right) \right] \quad (\text{C-28})$$

for $a \neq 0$. Therefore, the solution to equation (A-25) is

$$v_\phi = r\omega - \sum_{m=1}^{\infty} A_m \left[J_1 \left(\frac{\alpha_m r}{\sqrt{\nu}} \right) Y_1 \left(\frac{\alpha_m R}{\sqrt{\nu}} \right) - J_1 \left(\frac{\alpha_m R}{\sqrt{\nu}} \right) Y_1 \left(\frac{\alpha_m r}{\sqrt{\nu}} \right) \right] e^{-\alpha_m^2 t} \quad (\text{C-29})$$

To satisfy the boundary conditions $\alpha_m R / \sqrt{\nu}$ are roots of the following equation

$$J_1 \left(\frac{\alpha_m a}{\sqrt{\nu}} \right) Y_1 \left(\frac{\alpha_m R}{\sqrt{\nu}} \right) - J_1 \left(\frac{\alpha_m R}{\sqrt{\nu}} \right) Y_1 \left(\frac{\alpha_m a}{\sqrt{\nu}} \right) = 0 \quad (\text{C-30})$$

The initial condition is used to solve for A_m

$$A_m = \pi \omega J_1 \left(\frac{\alpha_m a}{\sqrt{\nu}} \right) \frac{R J_1 \left(\frac{\alpha_m a}{\sqrt{\nu}} \right) - a J_1 \left(\frac{\alpha_m R}{\sqrt{\nu}} \right)}{J_1^2 \left(\frac{\alpha_m a}{\sqrt{\nu}} \right) - J_1^2 \left(\frac{\alpha_m R}{\sqrt{\nu}} \right)} \quad (\text{C-31})$$

Thus, the nondimensionalized solution to equation (C-25) is

$$\frac{v_\phi}{R\omega} = \frac{r}{R} - \pi \sum_{m=1}^{\infty} J_1 \left(\frac{\alpha_m a}{\sqrt{\nu}} \right)$$

C.1 (Continued)

$$x \frac{R J_1(\alpha_m a/\sqrt{v}) - a J_1(\alpha_m R/\sqrt{v})}{J_1^2(\alpha_m a/\sqrt{v}) - J_1^2(\alpha_m R/\sqrt{v})} \frac{1}{R}$$

$$x \left[J_1\left(\frac{\alpha_m r}{\sqrt{v}}\right) Y_1\left(\frac{\alpha_m R}{\sqrt{v}}\right) - J_1\left(\frac{\alpha_m R}{\sqrt{v}}\right) Y_1\left(\frac{\alpha_m r}{\sqrt{v}}\right) \right] e^{-\alpha_m^2 t} \quad (C-32)$$

Solutions of equation (C-32) are shown in Figures C-4 and C-5.

When spinup is initiated, the offset heater tends to push the fluid in a circular path. If this region described by the inner and outer surfaces of the heater is assumed solid, then the velocity profiles between the outer heater surface and the tank wall and between the quantity probe (which is located along the tank axis) and the inner heater surface can be generated from the concentric cylinder model. The ratio of the distance from the tank center to the outer heater surface to the tank radius is about 0.24 ($a/R = 0.24$). Using this distance ratio, the profiles between the heater and the tank wall are generated from equation (C-32); these profiles are shown in Figure C-4. The ratio of the quantity-probe radius to the distance from the tank center to the inner heater surface is approximately 0.3333 ($a/b = 0.3333$). From this ratio, the velocity profiles between the quantity probe and the heater are determined using equation (C-32), where R is replaced by b ; Figure C-5 shows these profiles. To compare Figure C-4 and C-5 it is necessary to know b/R . This ratio is about 0.12. Thus, from the nondimensional time $4\sqrt{vt}/R$ on Figures C-4 and C-5, it can be seen that the inner region (quantity probe to heater) goes to steady state in about 1/100 of the time required by the outer region (heater to tank wall).

Figure C-6 shows the estimated velocity profiles between the outer heater surface and the spherical tank wall. To make this estimate the spherical spin solution (Figure C-2) was used near the tank wall, and the concentric cylinder solution (Figure C-4) was used near the heater. This method assumes that inner cylinder effects near the tank wall are small. This approximation is essentially true, although these effects cause steady-state to be attained slightly sooner than Figure C-6 indicates.

All velocity profiles in Figures C-1 through C-6 are plotted in nondimensional time, $4\sqrt{vt}/R$. To facilitate converting the data to realtime, Table A-I presents $4\sqrt{vt}/R$ versus time as a function of quantity at 900 psia.

C.2 DRAG

To investigate the effects of the offset heater on spin transients, the torque exerted by the heater on the fluid is of interest. As spinup is initiated, the offset heater exerts drag on the fluid which causes fluid motion. To study these drag effects, it is advantageous to evaluate the drag and torque on the outer heater surface for the concentric cylinder spin solution, on the tank wall, and on the offset heater.

C-12

$\frac{V_\phi}{R\omega}$

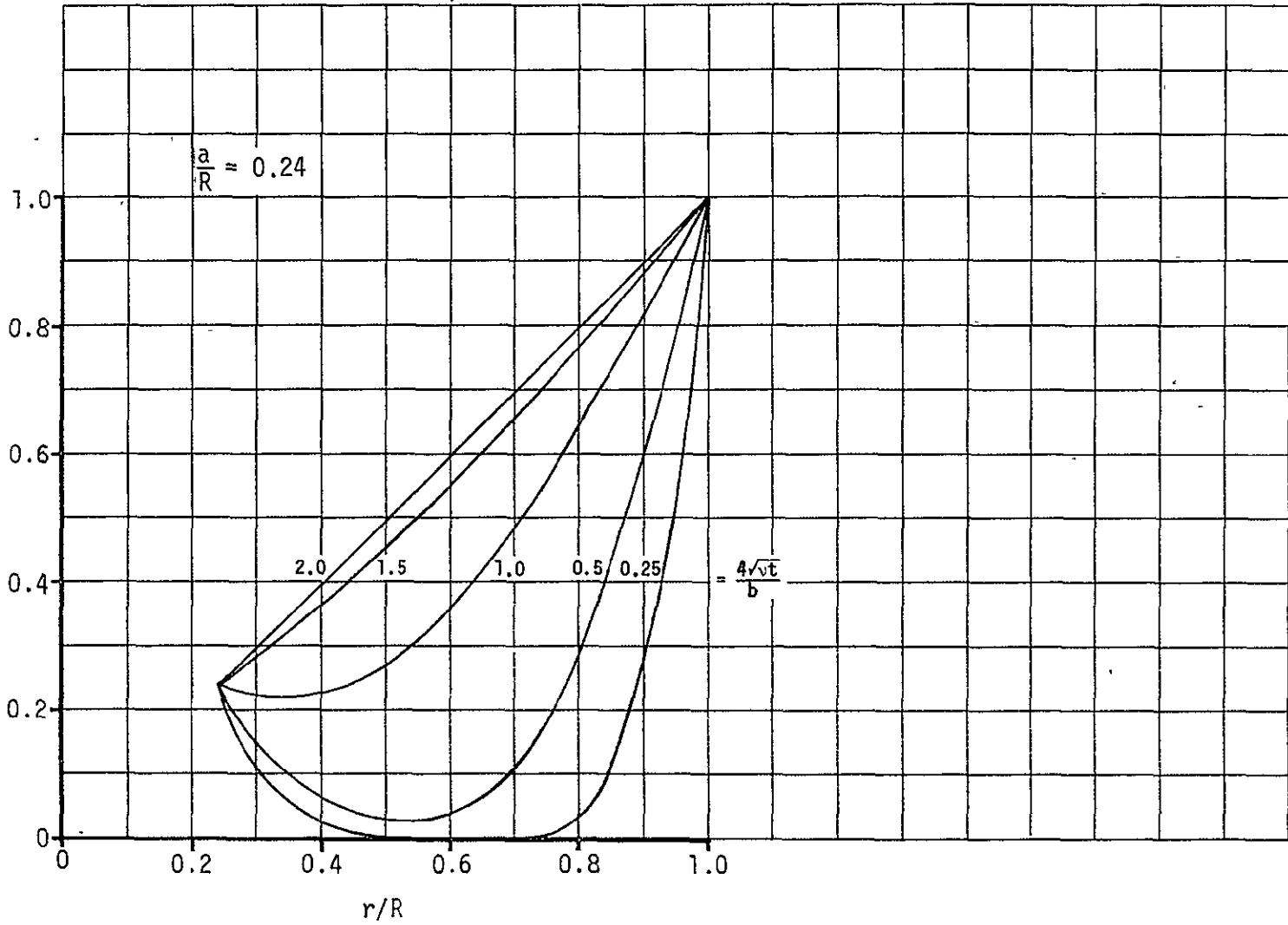


FIGURE C-4 - TRANSIENT VELOCITY PROFILES IN A CYLINDRICAL TANK WITH A HEATER

D2-118406-1

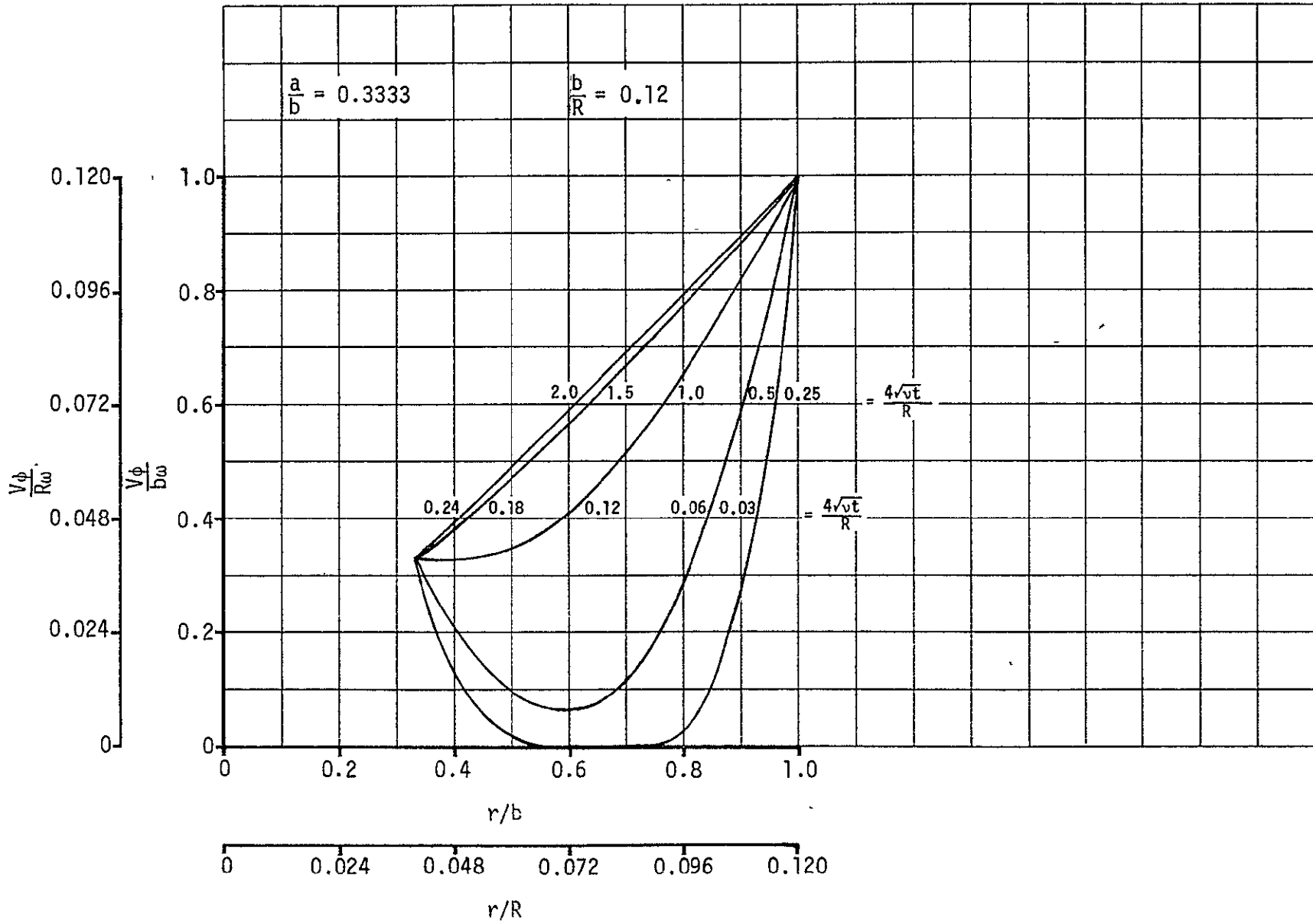


FIGURE C-5 - TRANSIENT VELOCITY PROFILES BETWEEN CYLINDRICAL TANK QUANTITY PROBE AND HEATER

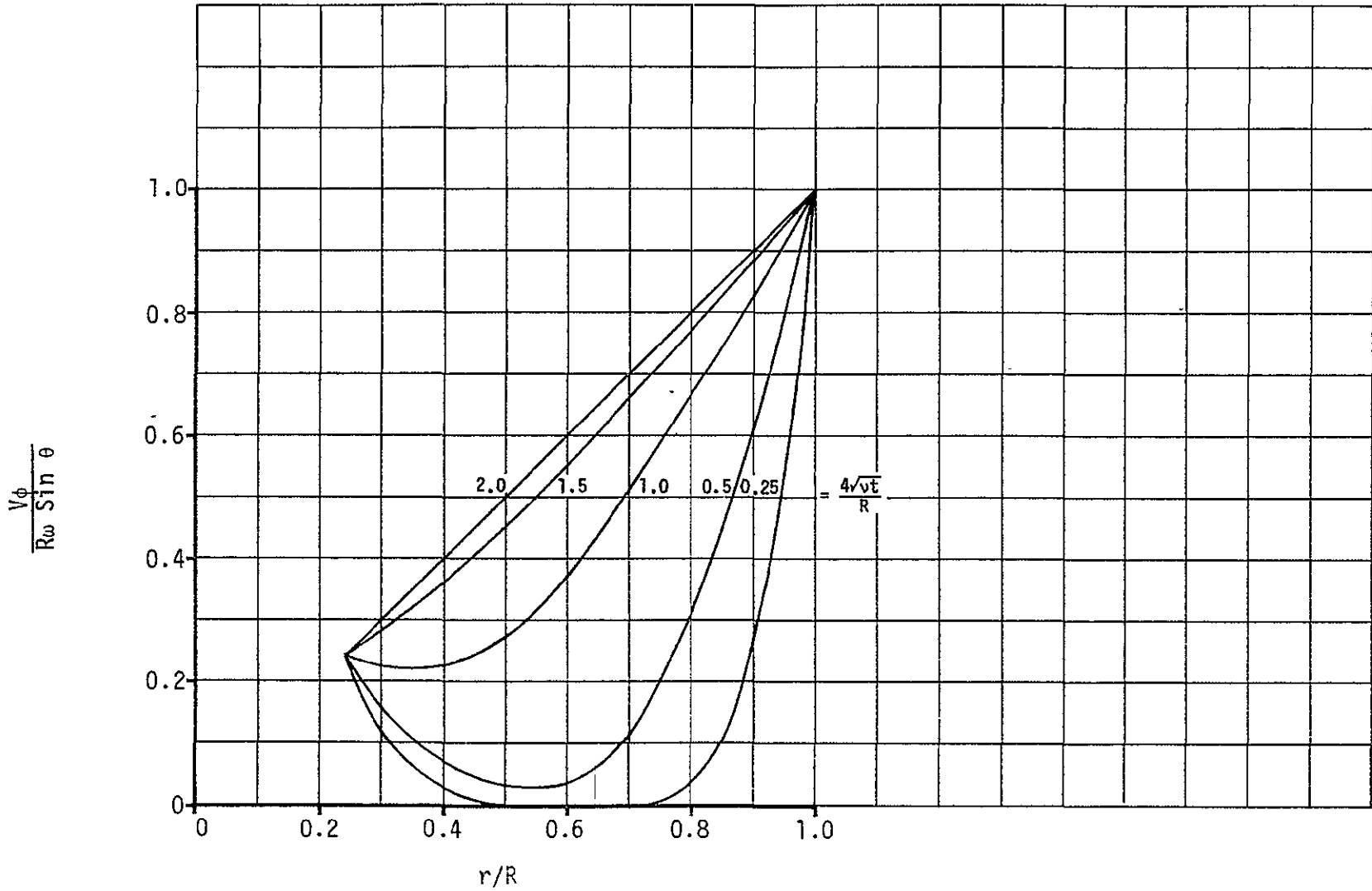


FIGURE C-6 - ESTIMATED TRANSIENT VELOCITY PROFILES BETWEEN SPHERICAL TANK AND HEATER

TABLE C-1 - QUANTITY VERSUS TIME FOR DIMENSIONLESS TIME VARIABLE

QUANTITY (%)	TIME (HOURS)				
	$\frac{4\sqrt{vt}}{R} = 0.25$	0.50	1.00	1.50	2.00
10	0.67	2.67	10.67	24.00	42.67
20	1.11	4.45	17.79	40.02	71.15
30	1.32	5.27	21.09	47.46	84.37
40	1.39	5.57	22.28	50.12	89.12
50	1.43	5.71	22.83	51.36	91.30
60	1.37	5.49	21.95	49.39	87.81
70	1.30	5.19	20.78	46.75	83.11
80	1.21	4.83	19.31	43.45	77.25
90	1.03	4.13	16.54	37.21	66.16
100	0.73	2.90	11.61	26.13	46.45

C.2 (Continued)

The drag on a cylinder rotating about its axis can be determined from

$$D = l\mu \int_0^{2\pi} r^2 \left[\frac{\partial}{\partial r} \left(\frac{v_\phi}{r} \right) \right]_{r=R} d\phi \quad (C-33)$$

The resulting torque is

$$T = RD \quad (C-34)$$

If the inner cylinder is neglected, substitution of equation (C-24) into equation (C-33) yields

$$D = \frac{T}{R} = 4\pi\mu\omega Rl \sum_{m=1}^{\infty} e^{-\alpha_m^2 t} \quad (C-35)$$

For an inner cylinder of radius a , equation (C-32) and equation (C-33) yield

$$\begin{aligned} \text{at } r = a \\ D = \frac{T}{a} = 4\pi\mu\omega a l \sum_{m=1}^{\infty} \frac{R}{a} J_1(\alpha_m R/\sqrt{\nu}) e^{-\alpha_m^2 t} \\ \times \frac{J_1(\alpha_m a/\sqrt{\nu}) - \frac{a}{R} J_1(\alpha_m R/\sqrt{\nu})}{J_1^2(\alpha_m a/\sqrt{\nu}) - J_1^2(\alpha_m R/\sqrt{\nu})} \end{aligned} \quad (C-36)$$

$$\begin{aligned} \text{at } r = R \\ D = \frac{T}{R} = 4\pi\mu\omega R l \sum_{m=1}^{\infty} J_1(\alpha_m a/\sqrt{\nu}) e^{-\alpha_m^2 t} \\ \times \frac{J_1(\alpha_m a/\sqrt{\nu}) - \frac{a}{R} J_1(\alpha_m R/\sqrt{\nu})}{J_1^2(\alpha_m a/\sqrt{\nu}) - J_1^2(\alpha_m R/\sqrt{\nu})} \end{aligned} \quad (C-37)$$

C.2 (Continued)

The drag and torque on a sphere rotating about a diameter can be found from

$$D = \mu \int_0^\pi \int_0^{2\pi} \left[r \frac{\partial}{\partial r} \left(\frac{v_\phi}{r} \right) \right]_{r=R} R^2 \sin \theta \, d\phi \, d\theta \quad (C-38)$$

$$\Gamma = \mu \int_0^\pi \int_0^{2\pi} \left[r \frac{\partial}{\partial r} \left(\frac{v_\phi}{r} \right) \right]_{r=R} R^3 \sin^2 \theta \, d\phi \, d\theta \quad (C-39)$$

Substituting equation (C-16) into equations (C-38) and (C-39) yields

$$D = 2\pi^2 \mu \omega R^2 \sum_{m=1}^{\infty} e^{-\alpha_m^2 t} \quad (C-40)$$

$$\Gamma = \frac{16\pi}{3} \mu \omega R^3 \sum_{m=1}^{\infty} e^{-\alpha_m^2 t} \quad (C-41)$$

The drag at the outer heater surface can be evaluated using equation (C-36). The drag on the fluid at the tank wall can be evaluated from equations (C-35), (C-37), and (C-40) for a spinning cylinder, spinning concentric cylinders, and spinning sphere, respectively. Figure C-7 shows the non-dimensional drag from equations (C-35) and (C-40). Drag from equation (C-37) is about the same as that from equation (C-35) until $4\sqrt{vt}/R > 1.00$; after this equation (C-37) - drag is bracketed by the curves of Figure C-7. Figure C-8 shows the nondimensional torque corresponding to the drag of Figure C-7.

To evaluate drag on the offset cylindrical heater the following equation is used

$$D = \frac{T}{a_o} = c_d \left(\frac{1}{2} \frac{\rho u^2}{g_c} \right) A \quad (C-42)$$

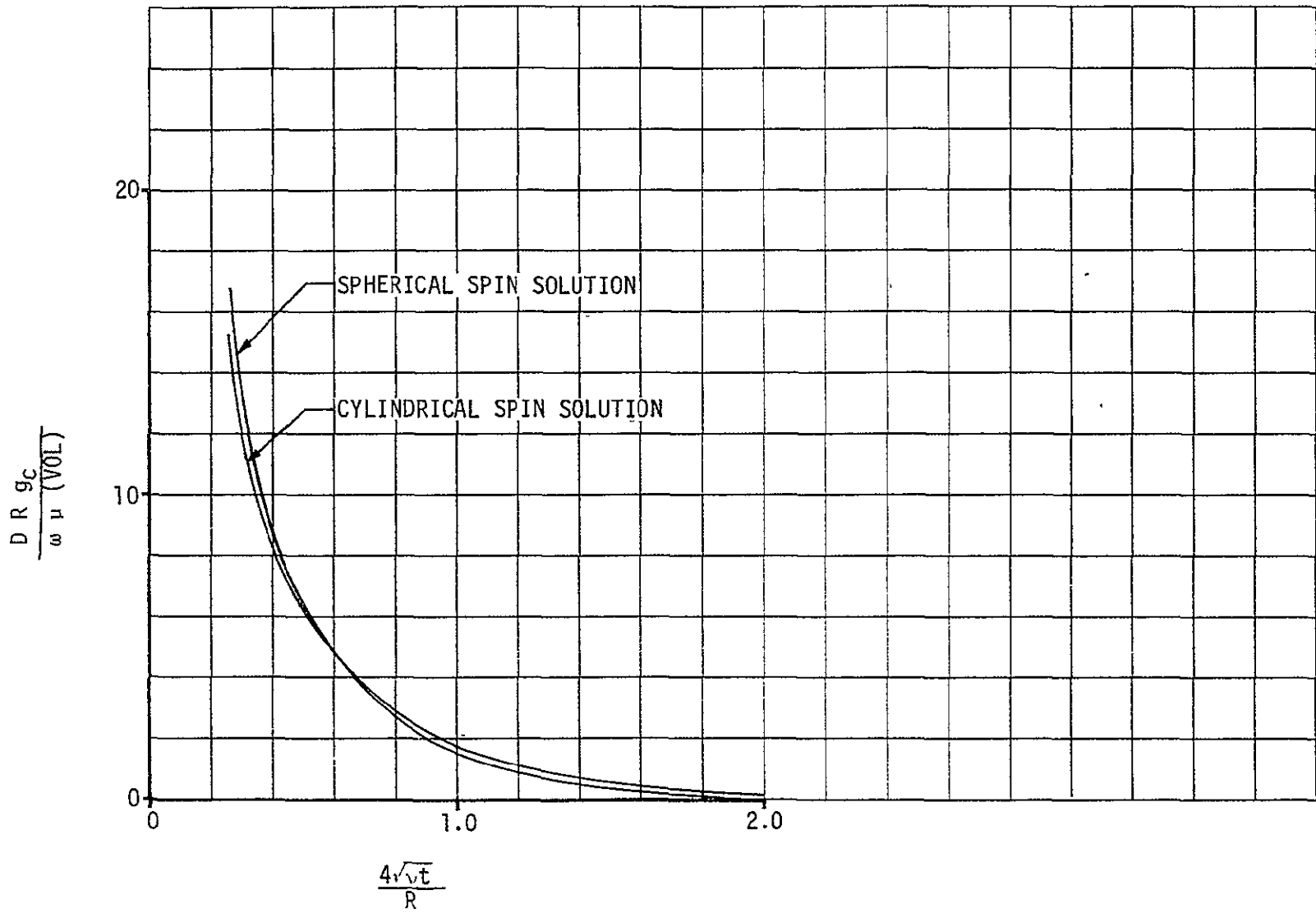


FIGURE C-7 - TANK WALL DRAG

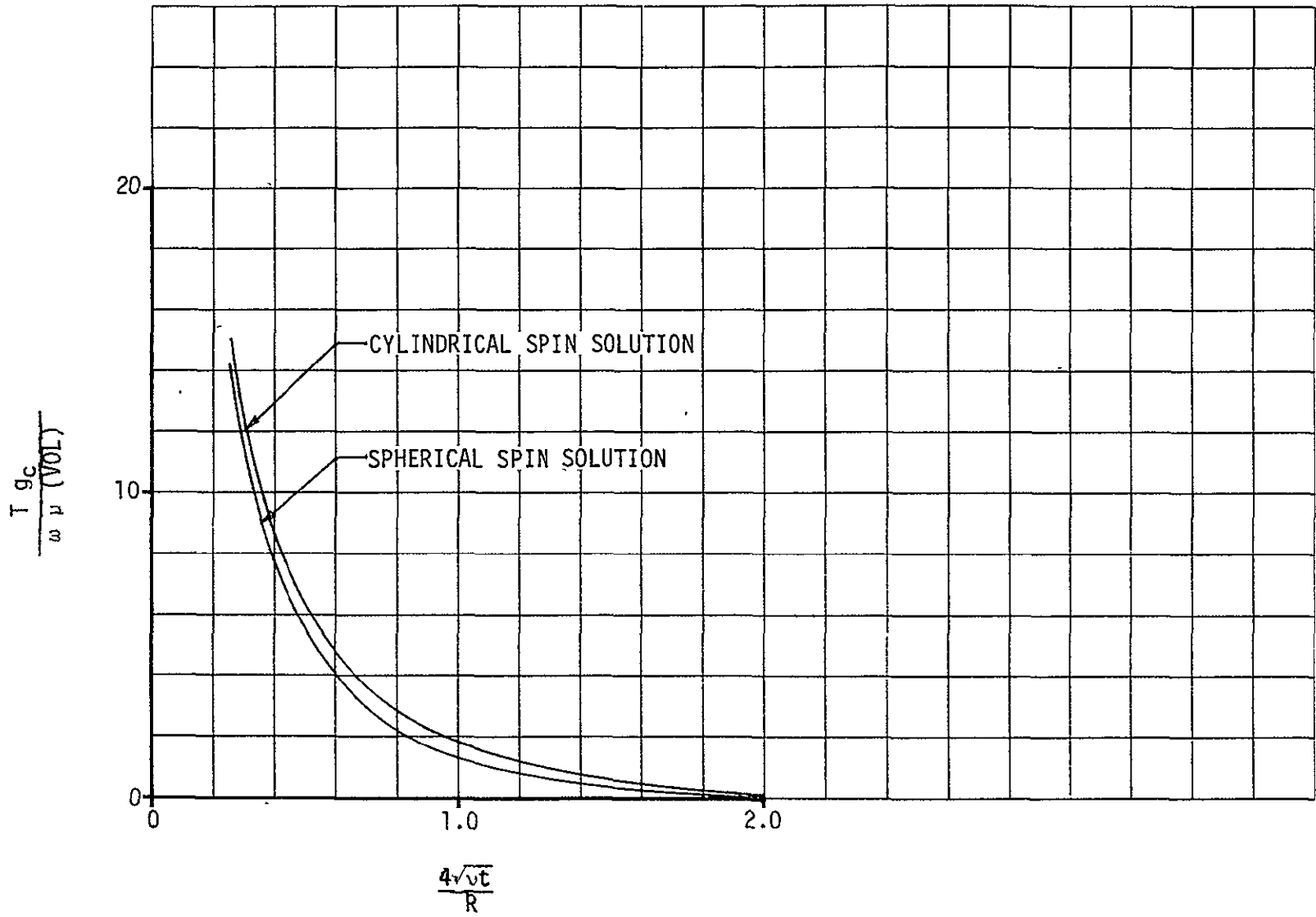


FIGURE C-8 - TANK WALL TORQUE

C.2 (Continued)

The drag coefficient C_d is obtained from Figure C-9 (Reference C-3). The density ρ is a function of tank quantity. The velocity u is assumed to be $a_0\omega$, where a_0 is the distance of heater offset. This velocity is only applicable at the initiation of spin. Therefore, the drag generated from this velocity will be compared with heater outer surface drag and spherical tank wall drag at $4\sqrt{u\tau}/R = 0.25$ since this was the smallest value investigated. Figure C-10 shows these drags, and Figure C-11 shows the corresponding torques as functions of quantity. It is apparent that the torque on the offset cylindrical heater is about three times greater than the heater outer surface torque (concentric cylinder spin solution) and that the tank wall torque is about ten times that on the offset heater. Therefore, the fluid in the Apollo oxygen tank would attain steady state slightly sooner than Figure C-6 indicates.

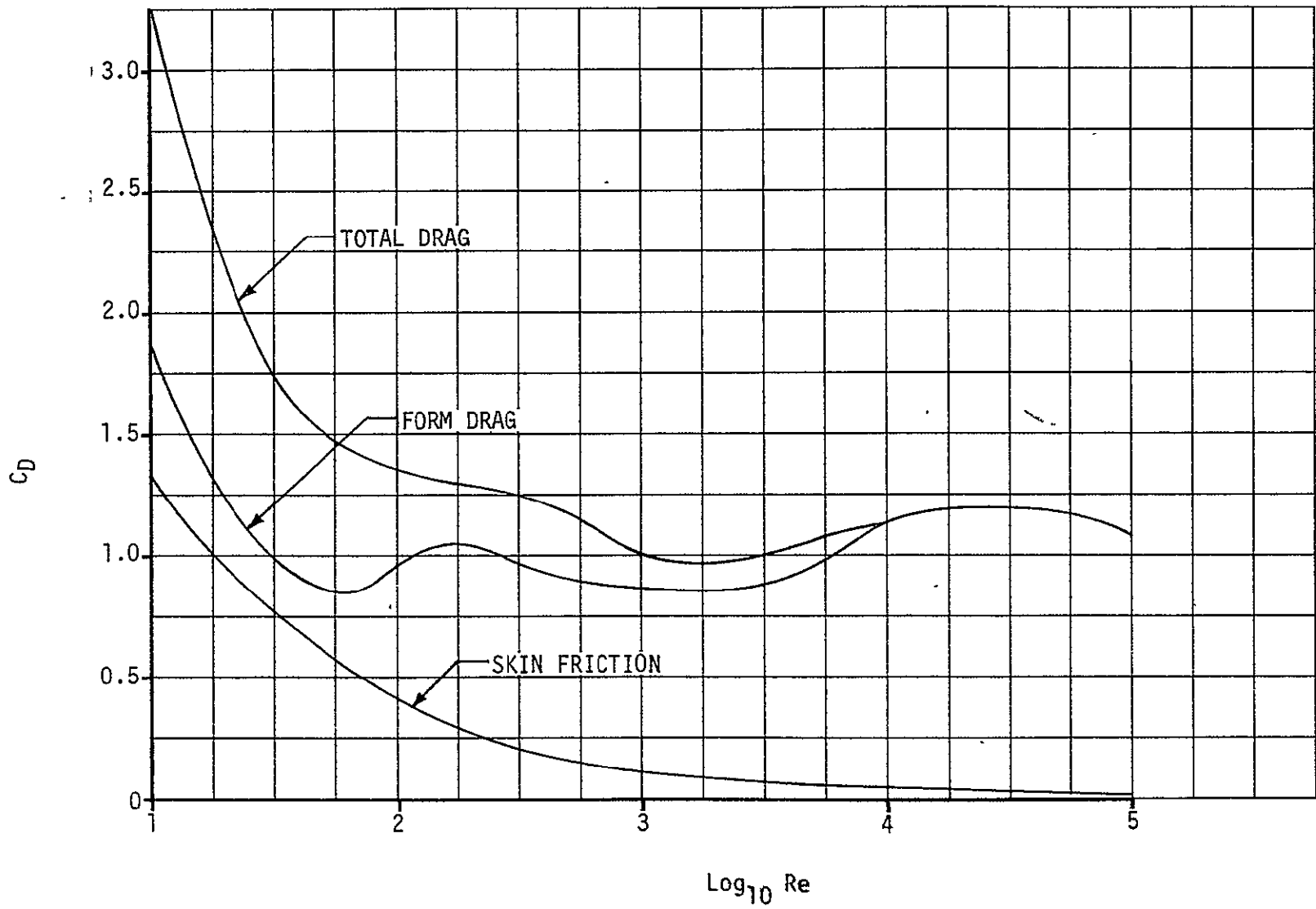


FIGURE C-9 - DRAG COEFFICIENT FOR FLOW OVER CYLINDER

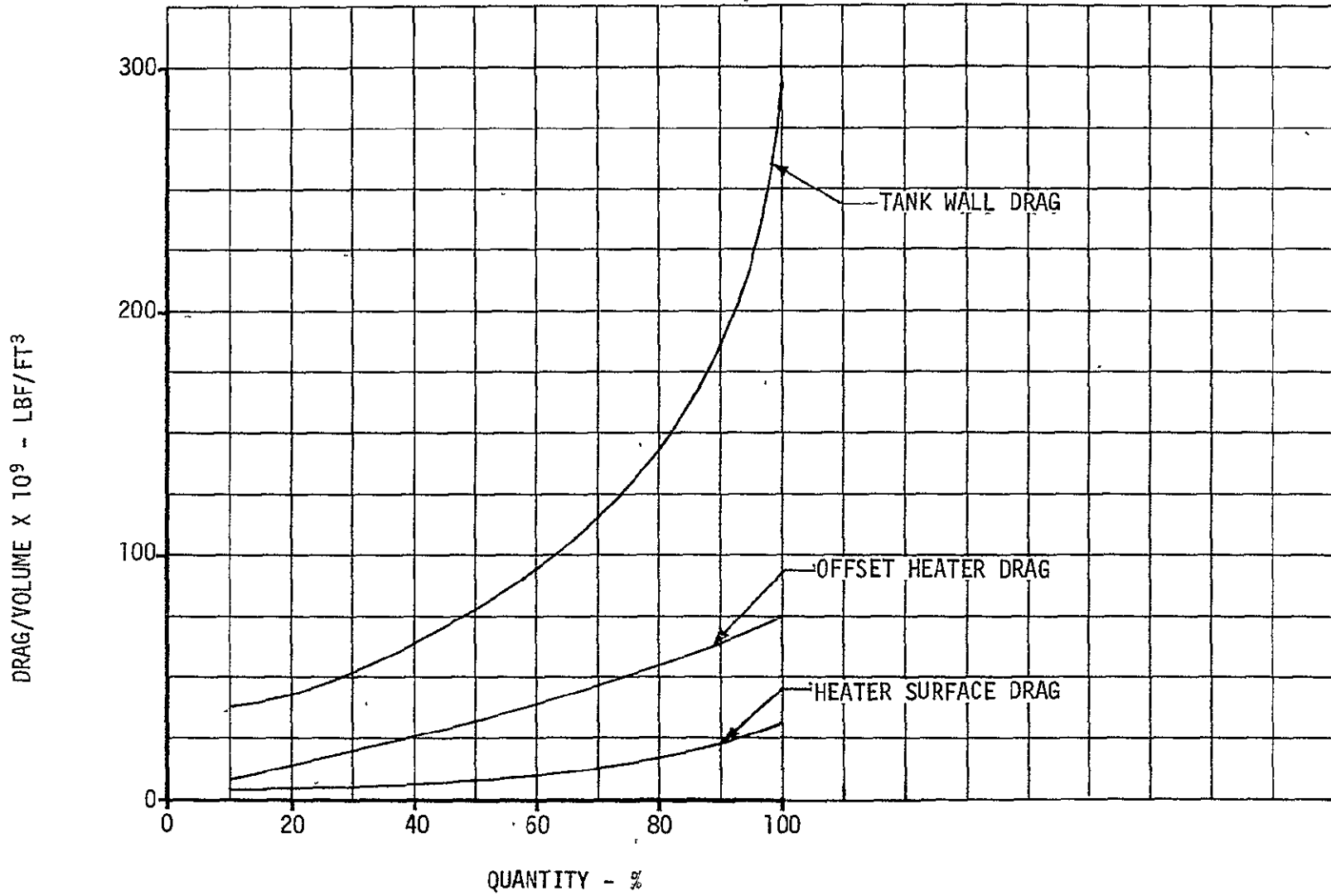


FIGURE C-10 - DRAG AT HEATER AND TANK WALL

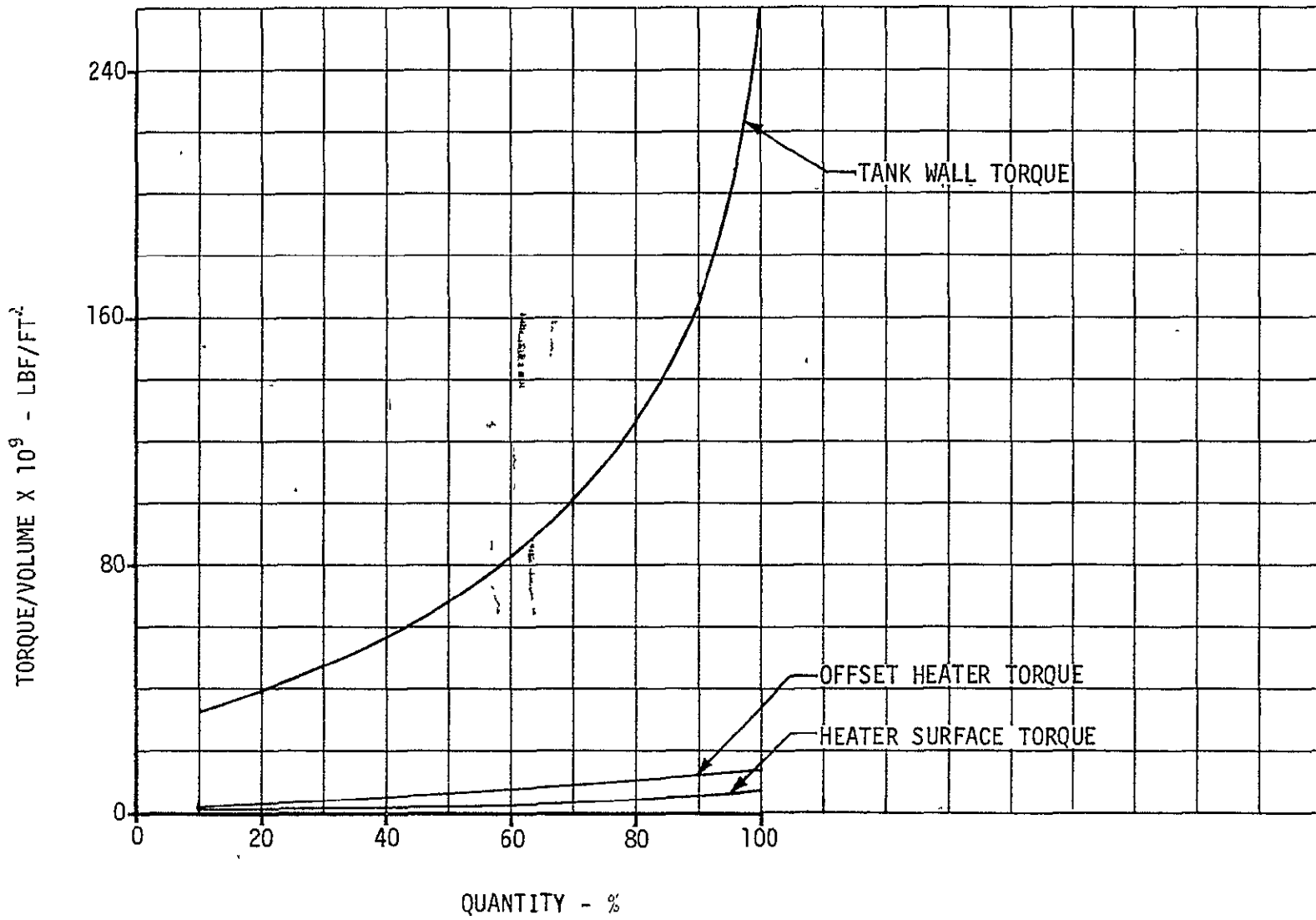


FIGURE C-11 - TORQUE AT HEATER AND TANK WALL

REFERENCES

- C-1) H. Schlichting, Boundary Layer Theory, McGraw-Hill Book Company, Inc., New York, 1960.
- C-2) Handbook of Mathematical Functions, NBS Applied Mathematical Series, June 1964.
- C-3) S. Goldstein, Modern Developments in Fluid Dynamics, Dover Publications, Inc., New York, 1965.